LMSC-HREC TM D496602

LOCKHEED

ASSESSMENT OF ANALYTICAL AND EXPERIMENTAL TECHNIQUES UTILIZED IN CONDUCTING PLUME TECHNOLOGY TESTS 575 AND 593

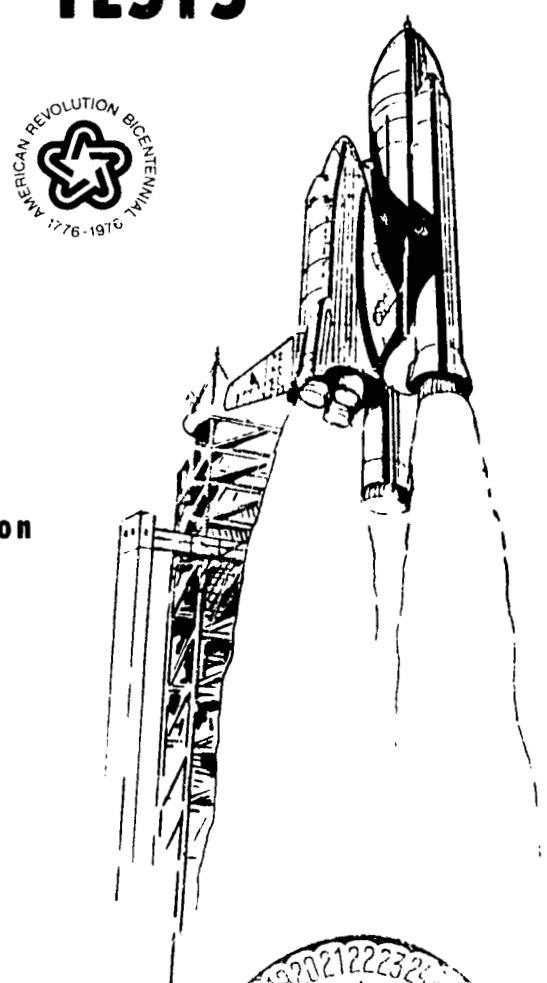

January 1976

Contract NAS9-14517

Prepared for

National Aeronautics and Space Administration
Aerodynamic Systems Analysis Section
Johnson Space Center, Houston, TX 77058

by

L. R. Baker
P. R. Sulyma
J. A. Tevepaugh
M. M. Penny

Lockheed Missiles & Space Company, Inc.
Huntsville Research & Engineering Center
4800 Bradford Drive, Huntsville, AL 35807

N76-21283

(NASA-CR-147530) ASSESSMENT OF ANALYTICAL AND EXPERIMENTAL TECHNIQUES UTILIZED IN CONDUCTING PLUME TECHNOLOGY TESTS 575 AND 593 (Lockheed Missiles and Space Co.) 85 p HC $5.00

CSCL 21H G3/20

Unclas
21591

FOREWORD

This report presents the results of work performed by Lockheed Missiles & Space Company, Inc. Huntsville Research & Engineering Center, under Contract NAS9-14517 for the Engineering Analysis Division, Johnson Space Center (JSC), Houston Texas. The NASA-JSC technical monitor for this contract is Mr. Barney B. Roberts.

CONTENTS

Section 1
INTRODUCTION AND SUMMARY

The interaction of the exhaust plumes, emanating from the Space Shuttle main engines (SSME) and the solid rocket boosters (SRB), with the aerodynamic environment experienced by the Space Shuttle launch vehicle has received considerable attention. Specifically, the exhaust plumes affect vehicle base environment (pressure and heat loads) and the orbiter vehicle aerodynamic control surface effectiveness. The base environment directly impacts the Space Shuttle payload capacity. The more severe the base environment the heavier the base structure and the greater the payload penalty. The exhaust plumes also can induce separation of the boundary layer over the vehicle control surfaces during the launch segment of the vehicle flight trajectory. This interaction reduces the effectiveness of orbiter vehicle aerodynamic control surfaces during the critical launch phase.

An intensive study involving detailed analytical and experimental investigations of the exhaust plume/vehicle interaction has been undertaken as a pertinent part of the overall Space Shuttle development program. Many of the experimental programs are being conducted using scaled launch vehicle configurations with simulated vehicle propulsion systems. One of the items on which the success of these experimental investigation hinges is the degree to which similitude can be achieved between the sub-scale and full-scale exhaust plume characteristics for a particular flight trajectory condition. (Exhaust plume characteristics, as used here, denote plume boundary shape and location.)

Although many investigations have been conducted concerning the simulation of exhaust plumes, very little parametric data in the region of interest to the Space Shuttle have been obtained. Therefore an extensive analytical/

experimental investigation is being conducted to obtain parametric exhaust plume/vehicle interaction data. This program, called the Plume Technology program, has as its objective the determination of the criteria for simulating rocket engine (in particular, Space Shuttle propulsion system) plume-induced aerodynamic effects in a wind tunnel environment.

Correctly simulating the full-scale exhaust plumes during Space Shuttle launch vehicle testing involves some formidable problems. Exhaust plume similitude depends on a complex interaction of the propulsion system flows with the freestream environment (over the full range of the launch trajectory). (The development and implementations of similarity criteria are discussed in detail in Ref. 1 and will not be discussed in this document.) Generally the task of simulating full-scale exhaust plumes is further complicated by model geometry and facility related constraints. Model geometry (configuration, scale, i.e., size) and the test "configuration" (i.e., sting or strut-mounted model) usually dictate the size (i.e., mass flow and/or pressure capacity) of the simulant gas plumbing. In addition, many wind tunnel facilities are restricted to the use of dry room temperature air ("cold gas") as the simulant gas.

To achieve simulation of the prototype plume shape over the full range of trajectory conditions, subject to the above constraints, often results in several scale model nozzles having to be fabricated. Unfortunately at some of the operating pressures required for simulating the prototype exhaust plumes, using room temperature air, liquefaction of the oxygen and nitrogen in the air can occur in the expanding plume. The model plume shape is altered significantly due to this condensation effect. When this occurs, the validity of the test data becomes suspect.

The complexity of the exhaust plume simulation problem, discussed briefly in the previous paragraphs, necessitates a clearer understanding of the interactions of the various geometric, thermodynamic and gasdynamic parameters which affect exhaust plume shape. To better understand the exhaust plume simulation problem, a comprehensive experimental program

was conducted using test facilities at NASA's Marshall Space Flight Center and Ames Research Center. This document reports on a post-test examination of some of the experimental results obtained from NASA-MSFC's 14 x 14-inch trisonic wind tunnel.

This document reports on a study that was conducted to: (1) assess the agreement that could be expected between experimental results and predicted values in future tests; (2) examine in some detail the effectiveness of the various analytical models being employed to generate pretest information and, finally; (3) to specifically recommend analytical and experimental techniques that should be utilized in future tests involving exhaust plume simulation. It is meaningful to note that, although the Space Shuttle application is the driving force behind this study, the results are applicable to other systems employing rocket propulsion.

The following technical discussion begins with a description of the test facility, simulant gas supply system, nozzle hardware, test procedure and test matrix. Nozzle flowfield calculations and comparison of experimental and analytical results are discussed in Section 2.2. Analysis of exhaust plume flow fields and comparison of analytical and experimental exhaust plume data are presented in Section 2.3.

Section 2
TECHNICAL DISCUSSION

2.1 PLUME TECHNOLOGY TEST PROGRAM

- Test Facility

The plume technology test results examined in this study were obtained from test numbers TWT 575 and 593 conducted in the Marshall Space Flight Center's 14 x 14-inch trisonic wind tunnel. The facility is an intermittent trisonic blowdown tunnel which exhausts either to a vacuum system or to atmosphere. The tunnel is capable of producing Mach numbers from 0.2 to 2.5 by utilizing a transonic test section and Mach numbers from 2.74 to 4.96 with a supersonic test section. Reynolds numbers per foot of up to 18,000,000 may be obtained depending upon the test Mach number and tunnel limits. A more detailed description of the facility is presented in the tunnel technical handbook (Ref. 2).

The models for tests TWT 575 and 593 consisted of strut-mounted cone-ogive-cylinder bodies (e.g., Fig. 1) each with six interchangeable nozzles. The models were designed and fabricated by Micro-Craft Inc., Tullahoma, Tenn., (Space Shuttle Plume Technology Model, assembly drawing number LD-520957). The body is made up of the nose section, midbody and afterbody. The midbody is rigidly attached to the strut and is composed of the nozzle plenum chamber and upper and lower removable skin panels which cover the plenum chamber. The nose section is attached to the midbody at the forward bulkhead and the afterbody at the aft bulkhead. Figure 2 shows the cone-ogive-cylinder model installed in the wind tunnel.

The model support consists of the strut and sting as shown in Fig. 1. The strut and sting shown in Fig. 1 are used not only to support the model but

also to supply the simulant gas to the model. The pressure tubing was routed through the leading and trailing edges of the strut and along the lower and upper surfaces of the sting. The sting adapter was rigidly attached to the sting and was fitted into the tunnel main chuck.

Forty-nine static pressure orifices are located on the model and are distributed as follows:

- Nose 5
- Midbody 19
- Afterbody 25

The model plenum chamber is equipped with a total pressure probe, a static pressure orifice and a total temperature probe. In addition, five thermocouples were used to measure skin temperature at various points on the model. The location and numbering system for all of the pressure orifices and thermocouples are shown in Figs. 3, 4 and 5.

- Gas Heater/Reservior

A high pressure (2000 psia maximum), electrically heated (600°F), gas reservior system was used to supply the simulant gas to the test model. The heater/reservior system is capable of supplying a gas flow of up to 4.0 lb/sec (at maximum temperature and pressure) for a period of 10 seconds and was designed for use with either air or carbon tetraflouride (CF_4).

A one-inch outside diameter heated and insulated steel pipe was used to connect the heater to the model. The pipe was attached to the heater discharge valve and routed through the side of the tunnel, up through the tunnel floor and attached to the sting.

A more detailed description of the heater and its operating characteristics is presented in Ref. 3.

- Nozzle Hardware

During the TWT 575 tests, three single exhaust nozzle configurations and one triple nozzle were flowed with heated air. In addition, one single and one triple nozzle were flowed with CF_4 as the simulant gas. All of the nozzles were conical and ranged in area ratio from 3.5 to 8.0 with nozzle lip angles of 15 to 35 degrees. Figure 6 shows typical single and triple nozzle. Geometry data for the nozzles used in the TWT 575 test are presented in Table 1. Two single nozzle configurations and four triple nozzle configurations were utilized in the TWT 593 tests. Geometric data for these nozzles are given in Table 2.

- Test Procedure

Exhaust plume data were obtained for both quiescent and wind-on tunnel ambient conditions. For the quiescent condition the basic test procedure involved: (1) evacuating the wind tunnel test section to a prescribed pressure; (2) setting desired conditions on gas heater reservior (and waiting until heater conditions stabilized); initiation of nozzle flow and data acquisition. The wind-on procedure differed in the fact that the tunnel air flow was initiated prior to the nozzle flow initiation. Test data recorded included model surface and base static pressure, tunnel freestream conditions, nozzle plenum pressure and temperature and schlieren photographs. A more detailed description of the basic test procedure is available in Ref. 4.

- Test Parameter Matrix

Parameters varied during test numbers TWT 575 and 593 included: freestream Mach number, nozzle area ratio, conical nozzle divergence angle, nozzle plenum total pressure, nozzle plenum total temperature and the simulant gas (either air or CF_4). The investigation reported on in this document has examined only the test data obtained with quiescent tunnel conditions (M = 0.) This approach was taken since the plume/vehicle interaction was not studied during the effort reported in this document. Data from these tests are documented in Ref. 5 for TWT 575 and in Ref. 6 for TWT 593.

2.2 INVISCID NOZZLE FLOW CALCULATIONS

Post-test nozzle flowfield characteristics were defined using the Lockheed Method-of-Characteristics (MOC) computer code described in Ref. 7. Utilization of this code required that thermochemical data be generated to describe the simulant gas property behavior and the formulations of mathematical models of the nozzle wall geometry.

Tests numbers TWT 575 and 593 were conducted in part with heated air and in part with heated carbon tetrafluoride (CF_4). The thermochemical gas property data describing the behavior of the air and CF_4 for use in this analysis were generated using two computer codes which are described in Ref. 8. Air thermodynamic behavior was modeled using the form of the Beattie-Bridgeman equation of state given in Ref. 9. Carbon tetrafluoride (CF_4) gas thermodynamic behavior was modeled using the Martin-Hou equation of state also given in Ref. 9. Thermodynamic data for the air and CF_4 were prepared in tabular form for use as input to the MOC computer code. Pressure variations as well as temperature variations are reflected in the gas property data. Additional discussion of the equation of state models and the application of these thermochemical data codes is presented in the plume technology program pretest analysis document, Ref. 9.

Mathematical models based on measured (actual) nozzle dimensions, presented in Refs. 5 and 6, were used in this analysis. These data have been reproduced in this document for ease of references in Table 1 for TWT 575 and Table 2 for TWT 593.

For the purposes of this investigation a minimum of two calibration test points were selected from the Plume Technology Test Run Log of Ref. 5 for each of the nozzles (with the exception of nozzle 4 for which the accuracy of the test data was suspect). An additional set of calibration data was obtained for two of the nozzles from the test run log of Ref. 6. (Note: "Calibration" denotes quiescent or M = 0 wind tunnel environment conditions.) The actual nozzle plenum conditions used in the analysis were then obtained from the

tabulated test data (Appendix A, Ref. 5, and Appendix B, Ref. 6). The nozzle plenum conditions used in the analysis correspond to the data "frame" at which the schlieren photographs of the exhaust plume were taken for each test point. Table 3 summarizes the test points examined in this investigation.

The basic analytical procedure employed to generate the inviscid nozzle flowfield characteristics involved the following steps: (1) specification of nozzle geometry and test condition; (2) generation of thermochemical gas property data; (3) formulation of the mathematical nozzle models; and (4) calculations of the nozzle and exhaust plume flowfields. This procedure was used in generating the analytical data discussed in the remainder of this document.

- Test Data Quality

The quality of the experimental data can be assessed by examining the dimensional accuracy of the model hardware and the accuracy employed in making the test data measurements. Deviation of model hardware dimensions from design values can adversely affect the anticipated agreement between predicted and measured nozzle gasdynamic characteristics. Some obvious results of poor model dimensional accuracy would be changes in nozzle wall angle (or contour), nozzle area ratio, and the relative location of pressure orifices. A detailed dimensional inspection of the model nozzle hardware was made during the course of this study. Dimensional data resulting from the inspection were presented in Refs. 5 and 6 and are reproduced in this document for ease of refeference. (See Table 1 for TWT 575 and Table 2 for 593.)

Both design and measured nozzle dimensions are given in Tables 1 and 2. Examination of these data did not reveal any gross deviations of measured nozzle dimensions from the design values. However, differences between design and measured dimensions were large enough to warrant using the measured data as the basis for mathematically modeling the model nozzle geometry.

Pressure orifice locations used in comparing experimental and analytical data were also obtained from the inspection results. These data, presented

in Tables 1 and 2, were obtained by measuring the distance from the center (average of fore and aft port edge location) of the pressure port to the nozzle exit plane and subtracting this value from the overall measured nozzle throat to exit plane length. As indicated a minimum of three measurements are required to locate a pressure tap. At this point it should be noted that the inspection data is also bounded by some tolerance range. The inspection tolerance range, although not defined, was assumed small enough so as to not be a significant influence on accuracy of the inspection data.

In considering the overall model dimensional influence on the test data quality it was noted that the diameter of the pressure orifices (or taps) exceeded 10% of the nozzle overall length for many of the nozzles. Ports of this relative size can induce considerable flow disturbance which could adversely affect the quality of the nozzle gasdynamic data. However, in surveying the experimental results no specific data agreement problem could be attributed to the relative size of the pressure orifices. This is not to say that the relative size of the pressure orifice is not an important consideration. It indicates only that the influence of pressure orifice size in this program may have been overshadowed by other stronger influences.

- Comparison of Experimental and Analytical Results

Agreement between experimental and post-test analytically predicted nozzle performance was assessed by comparing experimentally determined and calculated nozzle wall static pressure distributions. The influence of test data acquisition accuracy, pressure tap size, and analytical models on the degree of agreement achieved was investigated.

Nozzles 1, 2 and 4 of test TWT 575 were operated in the single nozzle configuration illustrated in Fig. 6. Comparison of experimental and calculated nozzle wall pressure distributions for these nozzles are presented in Figs. 7 through 14. Nozzles 5 and 6 of test TWT 575 were operated in the triple nozzle configuration shown in Fig. 6. Calculated and experimental nozzle wall pressure distributions for nozzles 5A, 5B and 5C are compared in Figs. 15 through

23 and for nozzles 6A, 6B and 6C are compared in Figs. 24 through 29. Nozzles 4 and 4A of test TWT 593 were operated in the single nozzle configuration. The experimental and calculated nozzle wall pressure distributions for these nozzles are compared in Figs. 30 through 37 for various operating conditions.

An important consideration of any analytical/experimental data comparison involving pressure measurements is the transducer accuracy. Transducer data accuracy information for TWT 575 (Ref. 5) and for TWT 593 (Ref. 6) are presented in Tables 4, 5 and 6, respectively. As indicated, the transducer instrumentation was changed between TWT 575 and TWT 593 with a significant improvement in the overall transducer accuracy. The non-dimensionalized nozzle wall static pressure was utilized to compare measured and predicted results. This quantity is a function of two measured values, each subject to transducer accuracy. It was desirable, therefore, to assess the accuracy of the experimental values of P_C and P_W being used to compare the two sets of data.

The absolute uncertainty in the experimental data can be assessed by applying the following relation:

$$\delta z = \frac{\delta x}{y} + \frac{x}{y^2} \delta y$$

where z is the non-dimensionlized nozzle wall pressure; x is the model plenum pressure; and y is the nozzle wall static pressure. This technique is outlined in greater detail in the Appendix. Applying the above relations for the experimental data from TWT 575 and 593 resulted in absolute uncertainty values for the non-dimensionalized nozzle wall static pressures. This information is presented in Table 7 for TWT 575 and Table 8 for TWT 593. As shown, the absolute uncertainty in the non-dimensionalized nozzle wall static pressure values ranges from slightly greater than 10% to less than 1% depending on the particular transducer arrangement utilized and the magnitude of the model plenum pressure. The data presented in Figs. 10 through 13 has

been utilized to indicate graphically the influence of the absolute uncertainty on the plotted data. The absolute uncertainty ranges from ±9.4% in Fig. 10 to ±2.7% in Fig. 13. The decrease in the magnitude of the absolute uncertainty is due to the ranges of transducers utilized in the data aqusition system. The influence of transducer accuracy on the quality of the test data and correspondingly the quality of the measured and predicted data comparison is readily shown in Figs. 10 through 13.

- Simulant Gas Thermochemical Model Influence

The influence of the thermochemical model used for the simulant gas was readily apparent. Both the air and CF_4 models were not applicable over the complete range of test data considered. Deficiencies were noted particularly for nozzle plenum conditions of high pressures (greater than ≈ 1000 psia) in conjunction with low temperature (less than ≈ 250°F). This trend was evident in the data obtained for nozzle 1 flowing CF_4 (Figs. 8 and 9); for nozzle 2 flowing air (Figs. 10 through 13); and nozzle 6 flowing air (Figs. 23 through 28).

The data shown in Fig. 11 (P_C = 1889 psia, T_C = 513°F) indicate excellent agreement between measured and calculated nozzle wall static pressure distribution. However, where the total temperature of the CF_4 gas in the model plenum chamber is decreased to 190.9°F (with increase of P_C to 2026 psia) the agreement between calculated and measured data is poor, as shown in Fig. 9. Additional calculations made using an "ideal" gas model for CF_4 (γ = 1.217) gave better agreement (Fig. 9), but the results were still not satisfactory.

The same trend in the degree of agreement achieved between calculated and measured data was exhibited for air. Figures 10 through 13 show data for nozzle 2. The data shown in Fig. 10 were obtained for relatively low model plenum pressure and temperature conditions and agreement was excellent. As the model plenum air pressure was increased and temperature decreased (to approximately room temperature level) the agreement achieved between calculated and measured data deteriorates significantly, as shown in Figs. 11, 12 and 13. Calculations made using an "ideal" gas model for air (γ = 1.4)

yielded good agreement between calculated and measured data for all of the test conditions presented in Figs. 10 through 13.

The origin of the deficiences in both the air and CF_4 thermochemical data appears to lie in the applicable pressure and temperature range for the coefficients used in the equation of state model. Therefore, as a result of this study, the thermochemical data generated using the computer codes of Ref. 8 do not appear to be reliable for model plenum conditions corresponding to total pressures greater than 1000 psia in conjunction with total temperatures less than 200 ^{o}F. It should be realized, however, that these are "rule-of-thumb" limits to guide potential users of these techniques.

- Assessment of Transonic Effects on Data Comparisons

The method-of-characteristic (MOC) calculation of rocket nozzle flow fields typically uses a one-dimensional startline at the nozzle throat with a constant Mach number from the nozzle wall to the nozzle centerline. Actually, the transition from subsonic to supersonic flow is more appropriately modeled by a curved or two-dimensional line in the nozzle throat region. To assess the effect of this difference in transonic start lines on the analytical and experimental data comparisons, a transonic start line was caluclated for nozzle 4 of TWT 575. Operating conditions were for test point 114 with P_C = 1830.28 psia and T_C = 550^{o}F.

A computer code for calculating transonic flow fields in rocket motors (Ref. 11) was used to calculate a transonic startline in the nozzle throat region. The transonic startline was then used to initiate a method-of-characteristic nozzle calculation using the VOFMOC computer code. The results of the nozzle calculation initiated with a transonic startline were compared with the results of the nozzle calculation initiated with a straight startline. In Fig. 38 the non-dimensional nozzle wall static pressure ratio is plotted for the nozzle calculations generated with both startlines. Use of the transonic startline produced only slightly better agreement with the experimental pressure data.

- Effect of Boundary Layer Growth on Data Comparisons

A boundary layer is present along a nozzle contour while the nozzle is flowing a working fluid. The displacement effect of the boundary layer can cause changes in the pressure distribution as compared to inviscid flow predictions. Viscous effects in the boundary layer can also influence the thrust coefficient of a nozzle and impact convective heat transfer rates to the nozzle wall. Of particular interest in this study is the effect of boundary layer displacement on nozzle wall static pressure distributions.

To investigate the effect of boundary layer displacement on the comparison of experimental and analytical nozzle wall pressure distributions, test point 114 of TWT 575 was selected for a boundary layer analysis. The geometry point 4 and operating conditions for test point 114 (P_C = 1830 psia and T_C = 550°F) were input to Hoenig's boundary layer computer code (Ref. 12). Boundary layer characteristics were calculated from the nozzle throat to the nozzle exit. The calculated boundary layer displacement thickness was subtracted from the local nozzle radius along the length of the nozzle. The nozzle contour with no boundary layer is compared in Fig. 39 with the nozzle contour modified by boundary layer displacement thickness.

The modified nozzle geometry was input to the MOC computer code with the corresponding operating conditions. A nozzle flow field was calculated using a straight startline and real gas thermodynamics for air. The resulting non-dimensional nozzle wall static pressure distribution is compared in Fig. 40 against the experimental static pressure measurements and the pressure distribution calculated with a nozzle unmodified by boundary layer displacement thickness.

From Fig. 40 it is evident that the boundary layer displacement effect on the nozzle wall static pressure distribution was minimal. Including the effect of boundary layer displacement thickness in the analysis did not have a significant effect on the comparison of the analytical and experimental data.

It was concluded that boundary layer growth in the nozzles did not have any significant effect on data comparisons for the nozzle geometries and operating conditions under investigation.

2.3 EXHAUST PLUME ANALYSIS

Simulation of full-scale exhaust plumes with subscale nozzle exhaust plumes requires that the exhaust plume boundary shapes be matched. Analytical exhaust plume boundaries and internal boundary shock shapes were compared with these characteristics on schlieren photographs of the subscale nozzle exhaust plumes. The degree of agreement between the analytical calculations and the experimental results provided a measure of how well the subscale nozzle exhaust plume could be predicted by the analytical techniques employed in the analysis.

- Exhaust Plume Calculation Procedure

Analytical exhaust plume boundaries and internal boundary shock shapes were calculated with an inviscid MOC computer code. Transonic effects had been shown previously to have a negligible effect as the comparison of analytical and experimental nozzle wall pressure data. Therefore, the nozzle plume solutions were initiated with a straight startline with a Mach number of 1.01. Previous analysis had shown that boundary layer growth had an insignificant effect on data comparisons. The measured nozzle geometry was input to the MOC code without being modified to account for boundary layer growth. Two MOC calculations were performed for each operating condition investigated. Real gas thermodynamics from the Beattie-Bridgeman equations were input for one calculation and ideal gas thermodynamics were input for the other calculation. Each analytical calculation was expanded to a back pressure equal to the ambient test cell pressure of the corresponding experimental data point. The MOC solutions were carried out to an axial location at least five nozzle exit diameters downstream of the nozzle exit plane.

- Experimental Data Acquisition Procedure

Experimental exhaust plume boundaries and internal boundary shocks were obtained by use of a schlieren photograph system. Schlieren photographs of the nozzle exhaust plumes were obtained at discrete time intervals during each run.

The schlieren system is the most widely used optical method of recording nozzle exhaust plumes on photographic plates. Light from a uniformly illuminated line source of small width is collimated by a lens or mirror and then passed through the test section in which the nozzle is located. The light is then brought to a focus by another lens or mirror and projected on a screen (or photographic plate). At the focal point of the focusing lens or mirror, where an image of the source exits, a knife edge is introduced which cuts off part of the light. With no flow in the test section, the knife edge is usually adjusted to intercept half of the light from the source and the screen is uniformly illuminated by the portion of the light escaping the knife edge. When flow is established in the nozzle and/or test section, any light ray passing through a region in which there is a density gradient normal to the light direction will be deflected as though it has passed through a prism. Depending on the orientation of the knife edge with respect to the density gradient and on the algebraic sign of the denisty gradient, more or less of the light passing through each part of the test section will escape the knife edge and illuminate the screen. Thus a schlieren system makes density gradients visible in terms of intensity of illumination. A photographic plate at the viewing screen would record density gradients in the test section as different shades of gray. The schlieren system in the MSFC facility employs a horizontal knife edge orientation. A horizontal knife edge orientation (knife edge parallel to the direction of flow) detects density gradients perpendicular to the flow direction.

The internal boundary shock appears on the schlieren photographs as a sharp well defined line which is easily interpreted. A viscous shear layer of measurable thickness is present at the boundary of the exhaust plume and the ambient environment.

The inviscid MOC solution of the exhaust plume flow field does not account for the viscous shear layer thickness in the calculation of the exhaust plume boundary. The results of a previous analysis (Ref. 10) indicate that the MOC plume boundary is located along a line which evenly divides the shear layer visible on schlieren photographs. For the purpose of comparing experimental and analytical plume boundaries, the experimental plume boundaries were assumed to lie along a line which evenly divided the shear layer visible on each schlieren photograph.

- Comparison of Experimental and Analytical Results

Comparison of analytical and experimental exhaust plumes was accomplished by two methods. For some test points, the calculated exhaust plume boundaries and boundary shock locations were converted to the schlieren coordinate system and superimposed on the corresponding schlieren photographs. For other test points, the coordinates of the experimentally determined exhaust plume boundary and boundary shock were located with respect to the nozzle exit plane and nozzle centerline. These axial and radial coordinates were nondimensionalized by the nozzle exit radius and plotted with the corresponding calculated values of plume boundary and boundary shock location.

The effect on exhaust plume structure of different thermochemical models in the calculated flow fields is illustrated in Fig. 41 for test number 575, nozzle 1 and test point 511. The exhaust plume calculated with an ideal gas thermochemical model exhibits relatively good agreement with the experimental exhaust plume structure displayed on the schlieren photograph. The exhaust plume calculated with a real gas thermochemical model exhibited poor agreement. In Figs. 42 through 45 experimental exhaust plume boundary and boundary shock locations are compared (using method 2) with calculated values using real and ideal gas thermodynamics. Comparisons are presented for test number 575, nozzle 2 and test points 382, 383, 384 and 385, respectively. The nozzle wall static pressure distributions are presented in Figs. 10 through 13.

The corresponding exhaust plumes for test points 383, 384 and 385 did not expand enough to match the experimental exhaust plume boundaries. This

is demonstrated more clearly in Figs. 47, 48 and 49 in which the exhaust plume structure calculated with real gas thermodynamics is superimposed on the corresponding schlieren photograph. The experimental and calculated exhaust plumes for test point 382 show good agreement in Figs. 42 and 46. For test point 382, nozzle 2 was operating at a relatively low chamber pressure (517 psia) and a relatively high chamber temperature (156^{o}F). These conditions are considered to be within the operating range for which the real gas thermochemical models are applicable. For test points 383, 384 and 385, the plume calculations generated with ideal gas thermodynamics compared favorably with the experimental exhaust plume structures (see Figs. 43, 44 and 45) for several nozzle exit radii downstream of the nozzle exit.

It was concluded that experimental exhaust plume structures can be modeled analytically using either ideal gas or real gas thermochemical models for relatively low chamber pressures in conjunction with relatively high temperatures. For higher pressures in conjunction with lower temperatures, calculations using ideal gas thermodynamics produce better agreement with experimental exhaust plume boundary and boundary shock locations for several nozzle exit radii downstream of the nozzle exit plane. For the higher chamber pressures in conjunction with lower chamber temperatures illustrated in Figs. 43, 44 and 45, analytical calculations with both thermochemical models failed to compare favorably with the experimental exhaust plume boundaries beyond several radii downstream of the nozzle exit plane. The experimental exhaust plume boundaries in Figs. 43, 44 and 45 expand to a larger diameter than predicted analytically. This condition is indicative of exhaust plumes in which a gaseous species is condensing (Ref. 13). As the nozzle or exhaust plume expands, the local pressure and temperature decrease and may cross the saturated vapor curve for a particular specie (CO_2, H_2O, etc.). Continued expansion of the plume will cause a large portion of the gaseous species in the flow to condense. Condensation of a relatively large mass of a gaseous species adds a significant amount of energy to the remaining flow reducing the Mach number and increasing the pressure. If the flow is still in the nozzle, condensation will be evidenced by a significant change in the nozzle wall pressure distribution slope. With condensation present, the nozzle wall pressure will be significantly higher than predicted and the P_C/P_W ratio is

significantly lower. If condensation occurs in the exhaust plume, it will be evidenced by a significantly larger plume than predicted.

For the nozzle geometries and operating conditions investigated in this study, the experimental nozzle wall pressure distributions did not deviate sufficiently from the best analytical calculation to indicate the presence of condensing species in the nozzle. The overexpanded experimental exhaust plumes of Figs. 43, 44 and 45 did indicate however, the presence of condensing species in the nozzle exhaust plumes for some operating conditions.

Section 3
CONCLUSIONS

The following conclusions were reached during the course of this study.

- The nozzles used in TWT 575 and TWT 593 did not exhibit any gross physical deviations from the nozzle design parameters (page 8).
- The large diameter of the pressure orifices relative to the overall nozzle length did not have a primary influence on the agreement of analytical and experimental data (page 9).
- Transducer accuracy had a modest effect on the quality of the experimental nozzle wall pressure data and the comparison of experimental data with the calculated pressure data (page 10).
- The air and CF_4 thermochemical models were not applicable over the complete range of test conditions. Particularly poor agreement was noted between real gas analytical calculations and experimental data for chamber pressures greater than 1000 psia in conjunction with chamber temperatures lower than 250°F (page 11).
- Transonic effects had an insignificant influence on analytical and experimental data comparisons (page 12).
- Boundary layer growth in the nozzle had an insignificant effect on analytical and experimental data comparisons (page 13).
- Analytical and experimental exhaust plume characteristics compared well at lower chamber pressures in conjunction with higher chamber temperatures using both ideal and real gas thermochemical models (page 16).
- Analytical and experimental exhaust plume characteristics for higher chamber pressure in conjunction with higher chamber temperatures compared favorably for analytical data calculated with a real gas thermochemical model for CF_4 (page 17).
- No instances were noted where the lack of agreement between the predicted and experimental nozzle wall pressure distributions (flowing air) could be attributed to the presence of condensing species in the nozzles (page 17).
- Condensing species were suspected, however, to be present in the exhaust plumes of nozzles operating at high chamber to ambient pressure ratios and low chamber temperatures. Condensation in the exhaust plume causes the local pressure in the plume to increase thereby yielding a larger plume than is predicted using single phase analytical models (page 18).

- The accuracy with which the exhaust plume boundaries could be predicted was strongly affected by the adequacy of the thermochemical model for the working fluid. Chamber conditions for which agreement between predicted and experimental nozzle wall pressure distribution was poor also resulted in poor exhaust plume boundary agreement.

Section 4
RECOMMENDATIONS

1. Predictions of exhaust nozzle and plume flowfield characteristics for systems using air as the working fluid should utilize an equilibrium chemistry (standard equation of state) or ideal gas thermochemical model for the air.
2. Predictions of exhaust nozzle and plume flowfield characteristics for systems using CF_4 as the working fluid should generally utilize the real gas model of Ref. 8 for the CF_4. It should be noted, however, that this model does not adequately treat test conditions involving high chamber pressures (> 1000 psia) in conjunction with low chamber (i.e., total) temperatures (< 250°F).
3. Additional investigations should be made to establish an applicable CF_4 gas model for the test conditions not adequately treated if deemed necessary by the experimental program requirements.
4. Transonic effects and boundary layer growth can be neglected for nozzles of the size range considered in this program when operating in the same (or larger) Reynolds number range.
5. The accuracy of the transducers used to assess nozzle performance should be maintained at a high and consistent level over the range of test conditions.
6. Consideration should be given to the size of the pressure ports in the nozzle walls. The ports should be kept small relative to nozzle length.
7. Future tests should include near field pitot pressure surveys in the exhaust plumes to correlate with optical data. These additional data will aid in more accurately determining exhaust plume characteristics.
8. Calculations made to predict nozzle wall pressure distributions and exhaust plume shapes should utilize nozzle dimensional inspection data in forming the mathematical models of the nozzles.

REFERENCES

1. Baker, L. R., M. M. Penny and R. W. McCanna, "Design and Calibration of Model Nozzles for Use in Gasdynamic Simulation of the Space Shuttle Propulsion System Exhaust Plumes," LMSC-HREC TR D306555, Lockheed Missiles & Space Company, Huntsville, Ala., April 1973.

2. Simon, Erwin, The George C. Marshall Space Flight Center's 14 x 14-Inch Trisonic Wind Tunnel Handbook, NASA TM X-64624, November 1971.

3. Cooper, C. E., "Updated Operational Procedures of the NASA-MSFC High Pressure Gas Heating System," LMSC-HREC TN D306709, Lockheed Missiles & Space Company, Huntsville, Ala., March 1974.

4. Andrews, C. D., and C. E. Cooper, "Pretest Report for a Plume Technology Test Program in the MSFC 14 x 14-inch Trisonic Wind Tunnel," LMSC-HREC TM D306631, Lockheed Missiles & Space Company, Huntsville, Ala., May 1973.

5. Andrews, C. D., and C. E. Cooper, "A Transonic and Supersonic Investigation of Jet Exhaust Plume Effects on the Afterbody and Base Pressures of a Body of Revolution," LMSC-HREC TM D306909, Lockheed Missiles & Space Company, Huntsville, Ala., March 1974.

6. Andrews, C. D., "A Subsonic and Transonic Investigation of Triple Nozzle Jet Exhaust Plume Effects on the Base Pressure of a Body of Revolution," LMSC-HREC TM D390200, Lockheed Missiles & Space Company, Huntsville, Ala., May 1974.

7. Ratliff, A. W., S. D. Smith and M. M. Penney, "Rocket Exhaust Plume Computer Program Improvement - Volume I - Final Report," LMSC-HREC D162220 - I, Lockheed Missiles & Space Company, Huntsville, Ala., January 1972.

8. Tevepaugh, J. A., M. M. Penny and L. Ray Baker, "Input Guide for Computer Programs to Generate Thermodynamic Data for Air and Freon (CF_4)," LMSC-HREC TM D390169, Lockheed Missiles & Space Company, Huntsville, Ala., March 1974.

9. Baker, L. Ray, M. M. Penny, and J. A. Tevepaugh, "Plume Simulation Technology Experimental Program Pretest Analysis," LMSC-HREC TM D309610, Lockheed Missiles & Space Company, Huntsville, Ala., December 1973.

10. Tevepaugh, J. A., and M. M. Penny, "Interpretation of Schlieren Photographs of Model Nozzle Supersonic Flow Fields," LMSC-HREC TM D390280, Lockheed Missiles & Space Company, Huntsville, Ala., July 1974.

11. Stephens, J. T., "Analytical Results for Transonic Flow Fields in Rocket Motors," LMSC-HREC TM 54/20-157, Lockheed Missiles & Space Company, Huntsville, Ala., October 1967.

12. Hoenig, R. J., "LMSC/HREC Boundary Layer Computer Program Theory," LMSC/HREC A782405, Lockheed Missiles & Space Company, Huntsville, Ala., March 1967.

Table 1

PLUME TECHNOLOGY TEST MODEL NOZZLE GEOMETRY (TWT 575)

Nozzle No.	Gas	Nozzle Config.	A/A* (in.)	θ_{lip} (deg)	A (in.)	B (in.)	C (in.)	D (in.)	E (in.)
1	CF_4*	Single	(8.0)† 7.90	(15) 14.92	0.247	0.695	(.750)	0.978	(.312)
2	Air	Single	(3.5)† 3.51	(25) 23.22	0.372	0.698	(.750)	0.513	(.312)
4	Air	Single	(6.5)† 6.52	(35) 34.77	0.273	0.697	(.500)	0.471	(.312)
4A	Air	Single*	(3.5)† 3.45	(35) 34.77	0.375	0.697	(.188)	0.282	(.312)
5	CF_4	Triple	(8.0)†	(15)			(.375)		(.312)
		Nozzle A	8.21	15.10	0.143	0.404		0.523	
		Nozzle B	8.17	15.12	0.141	0.403		0.518	
		Nozzle C	8.05	15.08	0.143	0.404		0.525	
6	Air	Triple	(4.0)†	(25)			(.400)		(.312)
		Nozzle A	4.06	24.85	0.200	0.404		0.322	
		Nozzle B	4.01	24.58	0.201	0.402		0.328	
		Nozzle C	4.03	24.83	0.199	0.400		0.335	

Built during test from a A/A = 6.5, $\theta_{lip} = 35^{\circ}$ air single nozzle

†(design dimension)
Actual Dimension

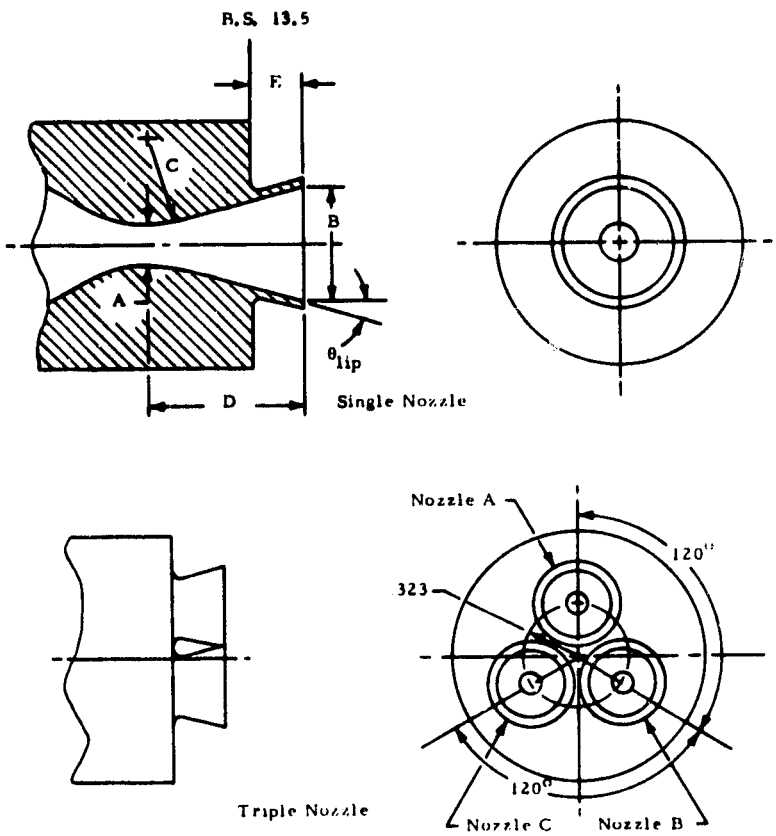

Table 2
PLUME TECHNOLOGY TEST MODEL NOZZLE GEOMETRY (TWT 593)

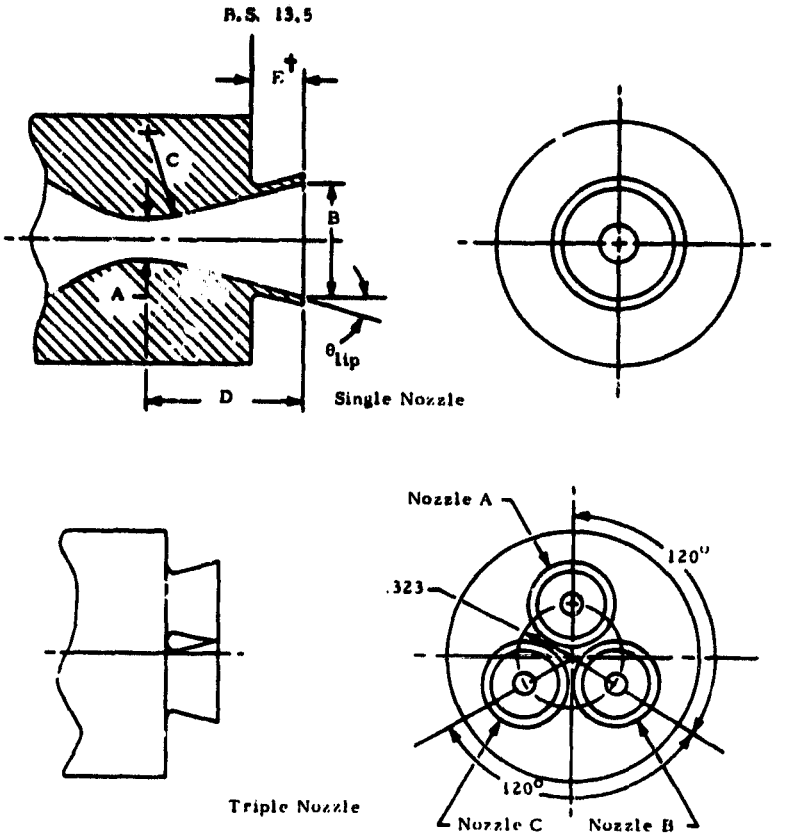

Nozzle No.	Gas	Nozzle Config	A/A*	θ_{lip} (deg)	A (in.)	B (in.)	C (in.)	D (in.)
4A	Air	Single	(3.5)° 3.51	(35) 34.92	(0.3742) 0.3726	(0.700) 0.6985	(0.188) 0.190	(0.282) 0.289
4	Air	Single	(6.5) 6.59	(35) 35.08	(0.2745) 0.2770	(0.700) 0.6984	(0.500) 0.505	(0.462) 0.4655
5	Air	Triple Nozzle A Nozzle B Nozzle C	(8.0) 8.30 8.31 8.33	(15) 14.83 15.03 15.10	(0.1429) 0.1421 0.1410 0.1407	(0.4042) 0.4094 0.4064 0.4061	(0.375) 0.385 0.390 0.390	(0.537) 0.5395 0.5374 0.5375
7	Air	Triple Nozzle A Nozzle B Nozzle C	(6.0) 5.90 5.85 5.85	(35) 35.16 34.75 35.43	(0.1650) 0.1636 0.1636 0.1636	(0.4042) 0.3974 0.3956 0.3957	(0.330) 0.310 0.330 0.310	(0.275) 0.2755 0.2750 0.2765
8	Air	Triple Nozzle A Nozzle B Nozzle C	(4.0) 4.06 4.00 3.97	(10) 10.12 10.00 10.11	(0.202) 0.1990 0.1999 0.2008	(0.4042) 0.4010 0.3999 0.4001	(0.400) • • •	(0.605) • • •
9	Air	Triple Nozzle A Nozzle B Nozzle C	(5.29) 5.29 5.31 5.32	o o o o	(0.1758) 0.1742 0.1751 0.1753	(0.4042) 0.4024 0.4034 0.4044	o o o o	(0.648) 0.6402 0.6385 0.6467

† The dimension is a constant equal to 0.312 in. for all nozzles

• Irregularity in Nozzle No. 8 geometry; refer to Fig. 12 for exact dimensions

° Contoured geometry nozzle; dimensions not applicable; see Table 2 for exact dimensions.

°° (Design dimension)
Actual Dimension

Table 3

TEST POINTS INVESTIGATED

Test No.	Nozzle No.	Test Points (Figure No.)*
575	1	505(7), 509(8), 511(9, 41)
	2	382(10, 42, 46), 383(11, 43, 47), 384(12, 44, 48), 385(13, 45, 49)
	4	107(14), 114(38, 40)
	5	603(15-17), 604(18-20), 606(21-23)
	6	401(24-26), 405(27-29)
593	4A	2(30), 7(31), 12(32), 17(33)
	4	161(34), 167(35), 172(36), 176(37)

*Data for the indicated test point appear on the on the figure indicated in parentheses.

Table 4

DATA ACCURACY TEST NUMBER TWT 575

The estimated accuracy of the data is as follows:

- **Tunnel Conditions**

Freestream total pressure	$\pm$0.05 psia
Freestream static pressure	$\pm$0.015 psia

- **Model Surface and Base Pressures**

M_∞ = 0.9, 1.2 and 1.46	$\pm$0.113 psia
M_∞ = 3.48	$\pm$0.038 psia

- **Nozzle Internal Pressures**

Air Single Nozzle, A/A^* = 6.5, all nozzle orifices $\pm$0.227 psia

Air Single Nozzle, A/A^* = 3.5, all nozzle orifices $\pm$1.13 psia

Air Triple Nozzle, A/A^* = 4.0, all nozzle orifices $\pm$1.13 psia

CF_4 Single Nozzle, A/A^* = 8.0, orifice 44 ~ $\pm$3.75 psia, orifices 45, 46 and 47 ~ $\pm$0.227 psia, orifice 48 ~ $\pm$1.125 psia

CF_4 Triple Nozzle, A/A^* = 8.0, all nozzle orifices $\pm$0.227 psia

- **Model Plenum Chamber Conditions**

Total and static pressures	$\pm$18.75 psia
Total temperature	$\pm 2^\circ F$

Table 5

DATA ACCURACY TEST NUMBER TWT 593

The estimated accuracy of the data is as follows:	
● Tunnel Conditions	
Freestream total pressure	±0.05 psia
Freestream static pressure	±0.015 psia
● Model Surface and Base Pressures	
M_∞ = 0.5, 0.7, 0.9, 1.2 and 1.46	±0.022 psia
● Nozzle Wall Static Pressures	
See Tables 5 and 6	
● Model Plenum Chamber Conditions	
Total and static pressures	
$0 < p \leq 150$	±0.225 psia
$150 < p \leq 500$	±0.750 psia
$500 < p \leq 2000$	±3.000 psia
Total temperature	±2°F
● Model and Hardware Static Temperatures	
Model skin temperatures	±2°F
Pipe and sting temperatures	±2°F

Table 6

NOZZLE WALL STATIC PRESSURE ACCURACY
TEST NUMBER TWT 593

Nozzle	Chamber Pressure (psia)	Orifice No.					
		44	45	46	47	48	49
		Accuracy in psia					
Single $A/A^* = 3.5$ $\theta_{lip} = 35^\circ$	600	±.225	±.045	±.045	±.045	±.225	—
	1000 to 2000	±.225	±.225	±.225	±.225	±.225	—
Single $A/A^* = 6.5$ $\theta_{lip} = 35^\circ$	1000 to 1500	±.045	±.045	±.045	±.045	±.045	—
	2000	±.225	±.225	±.225	±.225	±.225	—
Triple $A/A^* = 8.0$ $\theta_{lip} = 15^\circ$	0 to 500	—	—	—	±.045	±.045	—
	1000 to 2000	—	—	—	±.225	±.225	—
Triple $A/A^* = 6.0$ $\theta_{lip} = 35^\circ$	250	±.045	±.045	±.045	±.045	±.045	±.045
	1000	±.045	±.045	±.045	±.045	±.045	±.045
Triple $A/A^* = 4.0$ $\theta_{lip} = 10^\circ$	0 to 500	±.045	±.045	±.045	±.045	±.045	±.045
	1000 to 2000	±.225	±.225	±.225	±.225	±.225	±.225
Triple $A/A^* = 5.3$ $\theta_{lip} = 6^\circ$	0 to 500	—	±.045	±.045	±.045	±.045	—
	1000 to 2000	—	±.225	±.225	±.225	±.225	—

Table 7

ABSOLUTE UNCERTAINTY VALUES FOR THE NON-DIMENSIONALIZED NOZZLE WALL STATIC PRESSURES FOR TEST NUMBER TWT 575

Nozzle No.	Run No.	P_c (psia)	Tap Number 44 $\frac{P_c}{P_{wall}}$	±	45 $\frac{P_c}{P_{wall}}$	±	46 $\frac{P_c}{P_{wall}}$	±	48 $\frac{P_c}{P_{wall}}$	±
1	505	1937	8.184	0.209	85.974	1.698			31.578	0.885
1	509	1889	5.829	0.125	46.401	0.719			18.805	0.397
1	511	2026	5.821	0.117	48.866	0.720			18.790	0.370
2	382	517	26.445	2.490						
2	383	933	26.957	1.422						
2	384	1376	27.161	0.976						
2	385	1841	27.780	0.756						
4	107	1706	56.063	1.035	101.487	1.983			83.668	1.851
4	114	1830	56.152	0.966	101.711	2.326			83.945	1.734
5	603	558	41.892	2.122	39.351	1.952				
5	604	1067	41.501	1.096	39.271	1.018				
5	606	1813	42.359	0.663	39.533	0.605				
6	401	1654			25.015	0.711	30.343	0.973		
6	405	1888	26.685	0.691	25.291	0.634	30.719	0.870		

Table 8

ABSOLUTE UNCERTAINTY VALUES FOR THE NON-DIMENSIONALIZED NOZZLE WALL STATIC PRESSURES FOR TEST NUMBER TWT 593

Nozzle No.	Run No.	P_c (psia)	Tap Number 44 $\frac{P_c}{P_{wall}}$	±	46 $\frac{P_c}{P_{wall}}$	±	47 $\frac{P_c}{P_{wall}}$	±	48 $\frac{P_c}{P_{wall}}$	±
4A	2	1036	20.179	0.147	35.262	0.372	35.035	0.368	28.306	0.256
4A	7	996	20.141	0.152	35.095	0.384	34.935	0.380	28.311	0.266
4A	12	938	19.847	0.158	34.548	0.397	34.472	0.395	27.908	0.276
4A	17	1689	20.937	0.096	20.484	0.247	36.361	0.241	29.333	0.167
4	161	1453	63.588	0.758			113.782	2.238	87.583	1.368
4	167	1460	64.516	0.755			114.062	2.238	87.740	1.366
4	172	1492	63.979	0.746			114.241	2.197	87.971	1.344
4	176	1989	66.924	0.607			118.322	1.763	91.029	1.074

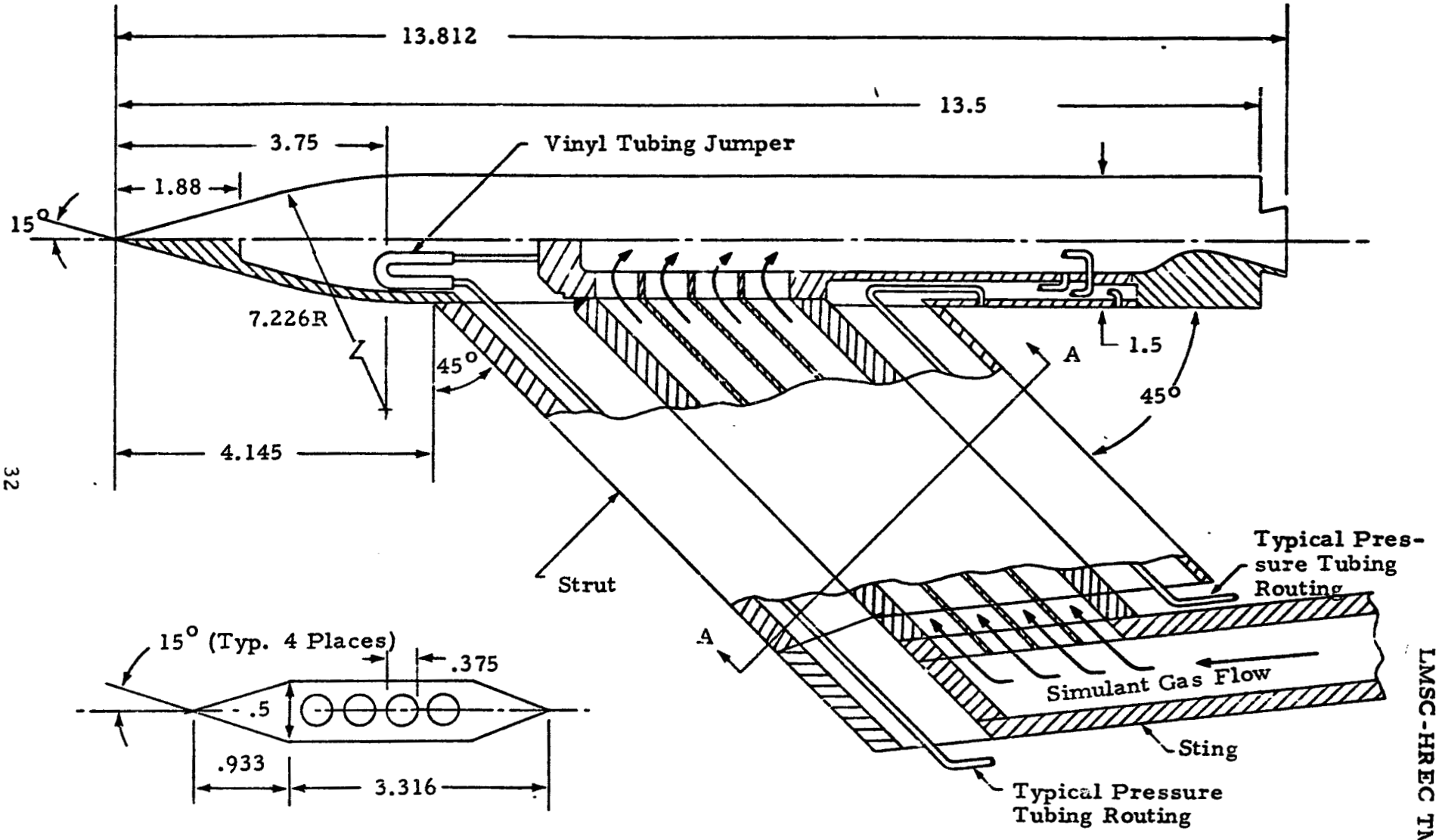

Fig. 1 - Sketch of Model Used in Plume Technology Study

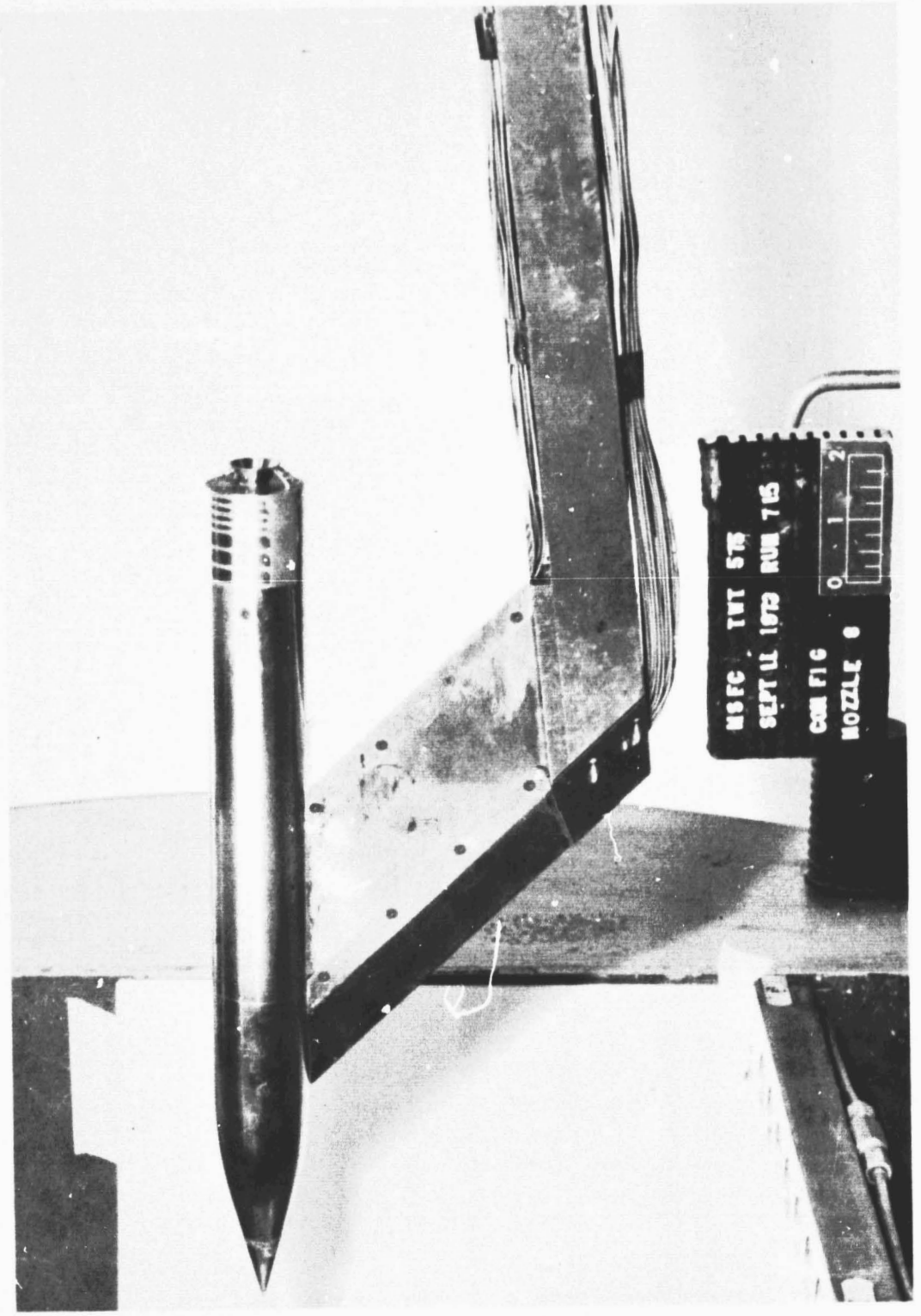

Fig. 2 - Cone-Ogive-Cylinder Model Installed in the Supersonic Test Section

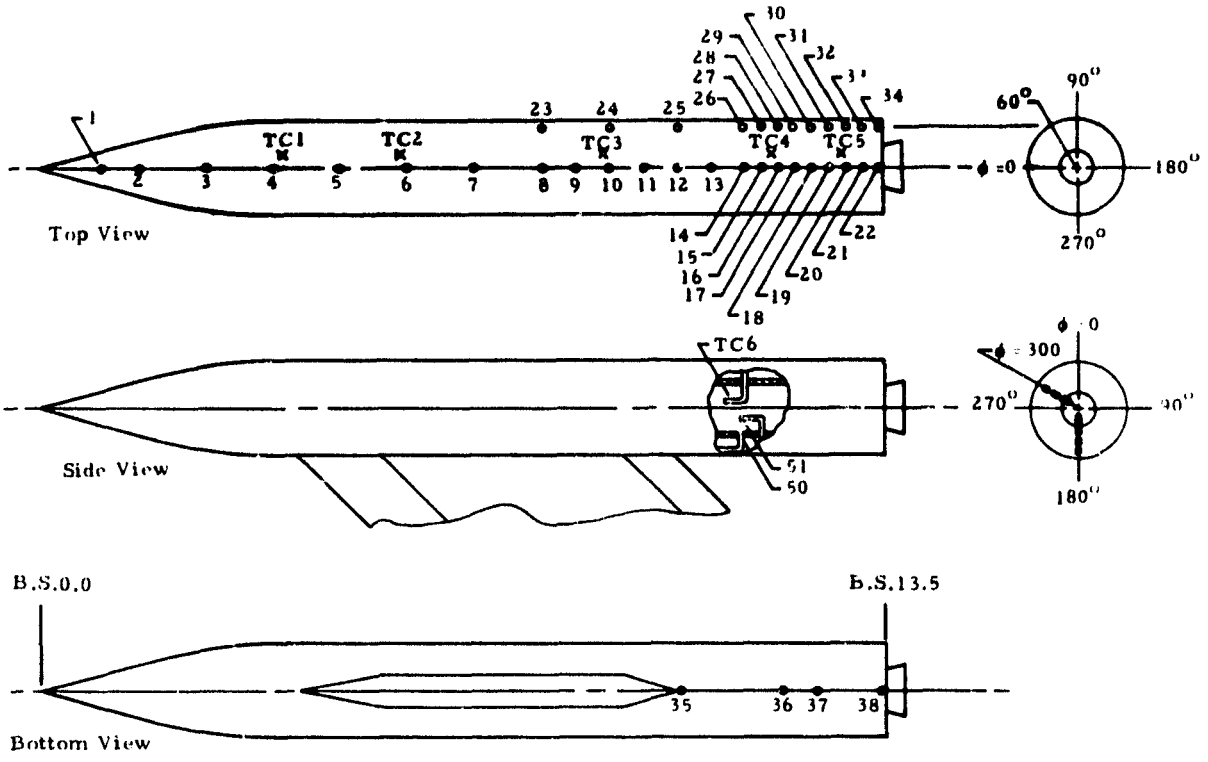

Model Surface Pressure Orifice Locations

Orifice No.	Body Station (in.)	Angular Orientation ϕ (deg)
1	1.011	0
2	1.631	
3	2.700	
4	3.778	
5	4.809	
6	5.880	
7	6.959	
8	8.038	
9	8.582	
10	9.119	
11	9.663	
12	10.202	
13	10.743	
14	11.284	
15	11.555	
16	11.824	
17	12.094	
18	12.363	
19	12.631	0

Model Surface Pressure Orifice Locations

Orifice No.	Body Station (in.)	Angular Orientation ϕ (deg)
20	12.904	0
21	13.172	0
22	13.443	0
23	8.043	60
24	9.125	
25	10.205	
26	11.283	
27	11.554	
28	11.825	
29	12.096	
30	12.366	
31	12.636	
32	12.906	
33	13.176	
34	13.446	60
35	10.206	180
36	11.826	
37	12.366	
38	13.466	180

Model Surface Temperature Thermocouple Locations

No.	Body Station (in.)	Angular Orientation ϕ (deg)
TC1	3.9	15
TC2	5.8	15
TC3	9.1	15
TC4	11.7	15
TC5	12.8	15

Model Chamber Pressure and Temperature Instrumentation Location

Type	No.	Body Station (in.)	Angular Orientation ϕ (deg)
Static Pressure	50	11.188	180
Total Pressure	51	11.188	180
Total Temperature	TC6	10.938	300

Fig. 3 - Model Surface and Chamber Pressure Orifice and Thermocouple Locations

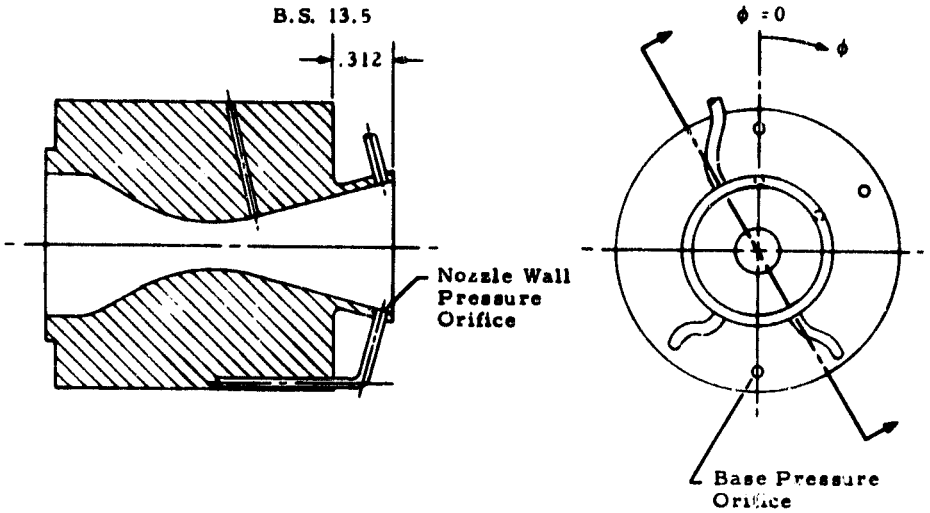

Single Nozzle Wall Pressure Orifice Locations

Nozzle Config.	Gas	Orifice No.	Dist. from Throat (in.)	Angular Orientation ϕ (deg)
$A/A^* = 6.5$ $\theta_{lip} = 35^o$	Air	44*	0.327	330
		45*	0.429	330
		46	0.430	150
		47	0.430	210
		48*	0.379	30
$A/A^* = 3.5$ $\theta_{lip} = 35^o$	Air	46	0.241	150
		47	0.241	210
$A/A^* = 3.5$ $\theta_{lip} = 25^o$	Air	44*	0.348	330
		45*	0.467	330
		46	0.471	150
		47	0.471	210
		48*	0.407	30
$A/A^* = 8.0$ $\theta_{lip} = 15^o$	CF_4	44*	0.259	335
		45*	0.934	330
		46	0.936	150
		47	0.934	210
		48*	0.588	30

* Tube routed outside the nozzle.

Model Base Pressure Orifice Locations for All Single Nozzles

Orifice No.	Body Station (in.)	Radius (in.)	Angular Orientation (deg)
39	13.499	0.63	0
40	↓	0.39	0
41	↓	0.63	60
42	↓	0.39	60
43	13.499	0.63	180

Fig. 4 - Single Nozzle Wall and Model Base Pressure Orifice Locations

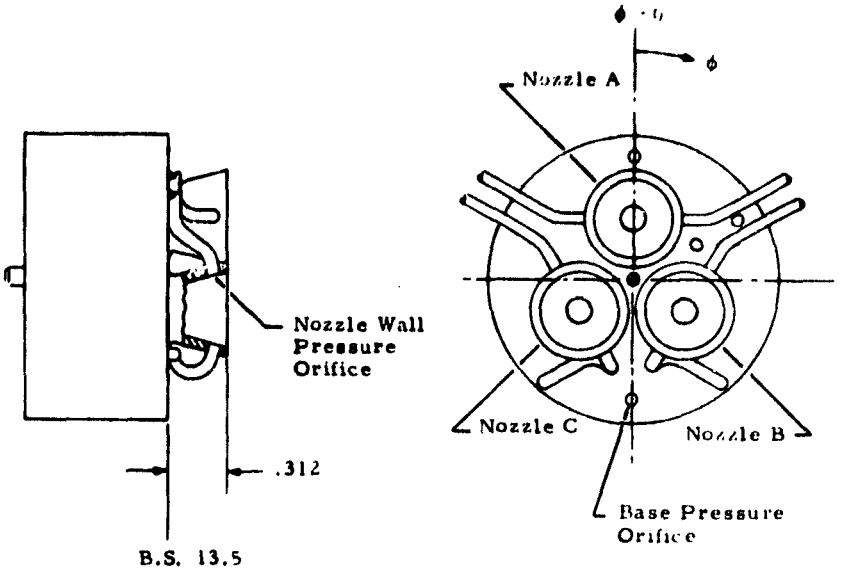

Triple Nozzle Wall Pressure Orifice Locations

Nozzle Config.	Gas	Orifice No.	Nozzle	Dist. from Throat (in.)	Angular Orientation ϕ (deg)
A/A* = 4.0 $\theta_{lip} = 25^{o}$	Air	44*	A	0.269	270
		45*	A	0.268	90
		46*	B	0.275	30
		47	B	0.275	210
		48	C	0.281	150
		49*	C	0.281	330
A/A* = 8.0 $\theta_{lip} = 15^{o}$	CF_4	44*	A	0.465	270
		45*	A	0.463	90
		46*	B	0.461	30
		47	B	0.461	210
		48	C	0.468	150
		49*	C	0.469	330

* Tube routed outside the nozzle.

Model Base Pressure Orifice Locations for All Triple Nozzles

Orifice No.	Body Station (in.)	Radius (in.)	Angular Orientation (deg)
39	13.499	0.63	0
40		0.0	0
41		0.63	60
42		0.39	60
43	13.499	0.63	180

Fig. 5 - Triple Nozzle Wall and Model Base Pressure Orifice Locations

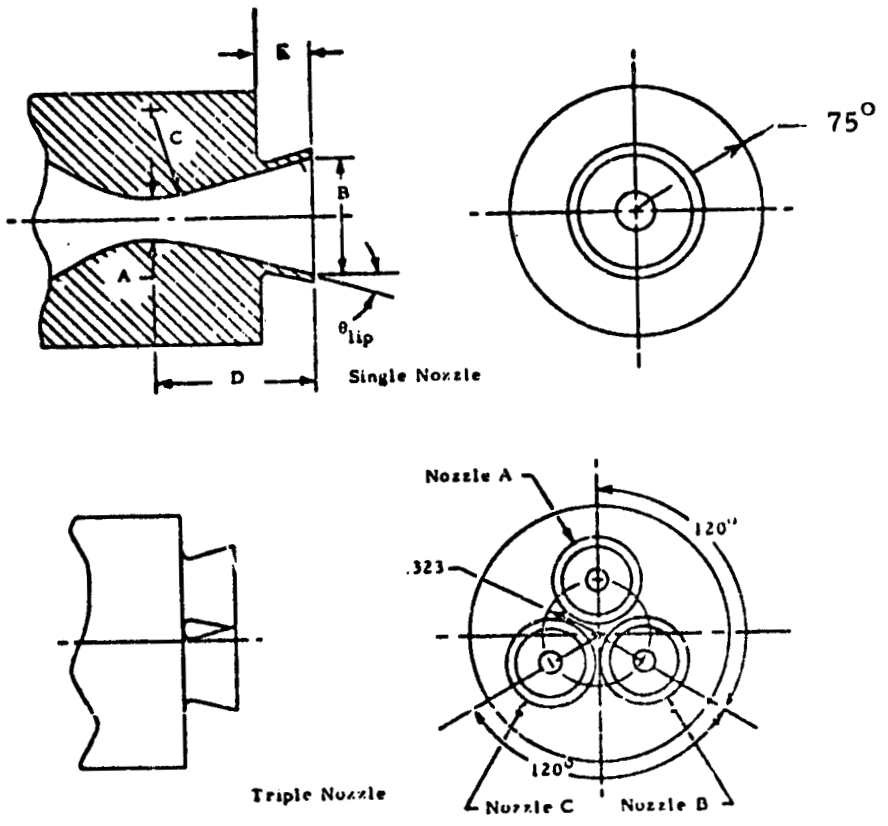

Fig. 6 - Plume Technology Test Model Nozzle Geometry

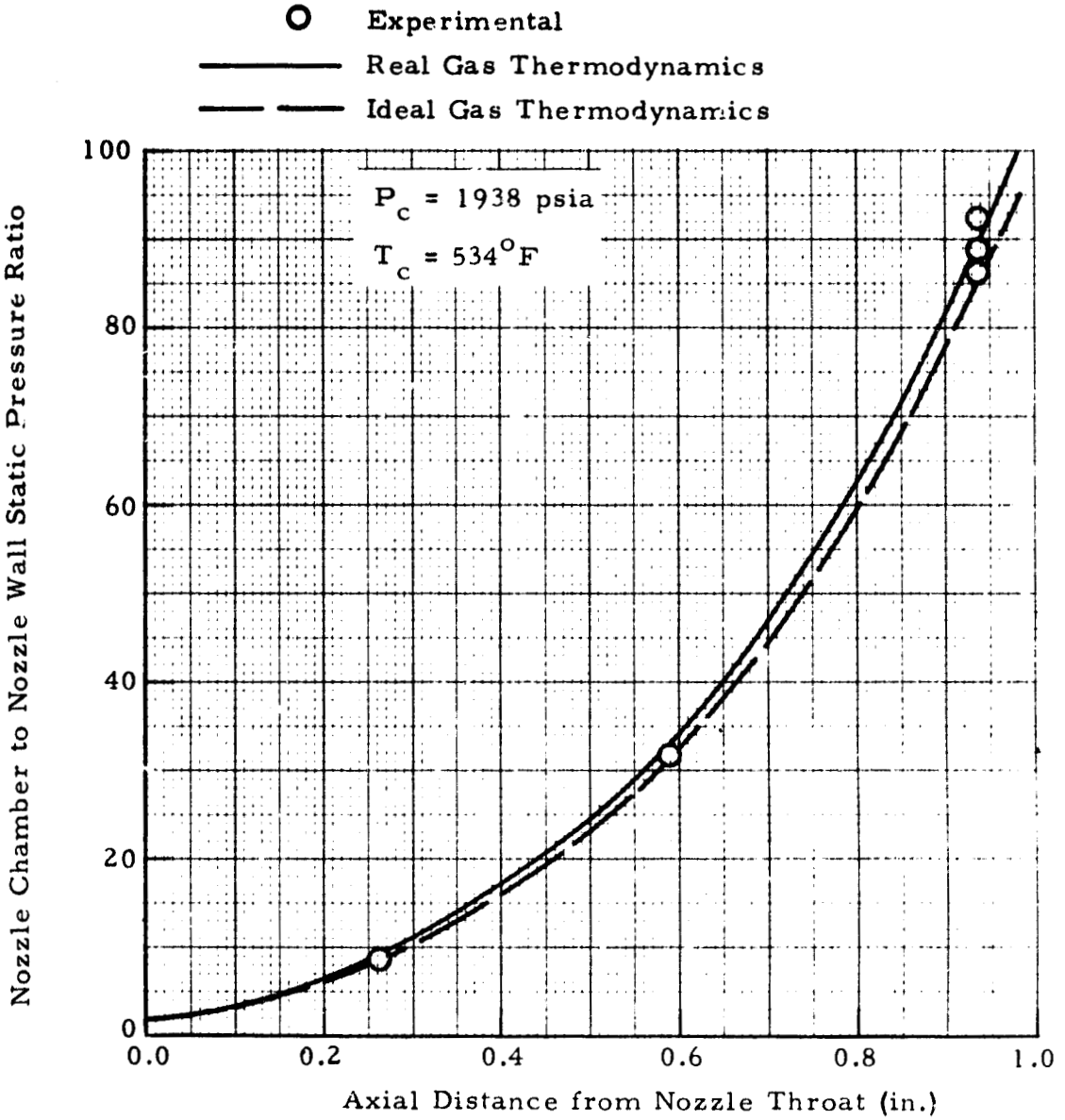

Fig. 7 - Non-Dimensional Nozzle Wall Static Pressure Distributions for Test Number TWT 575 and Nozzle 1 Flowing Air at Test Point 505

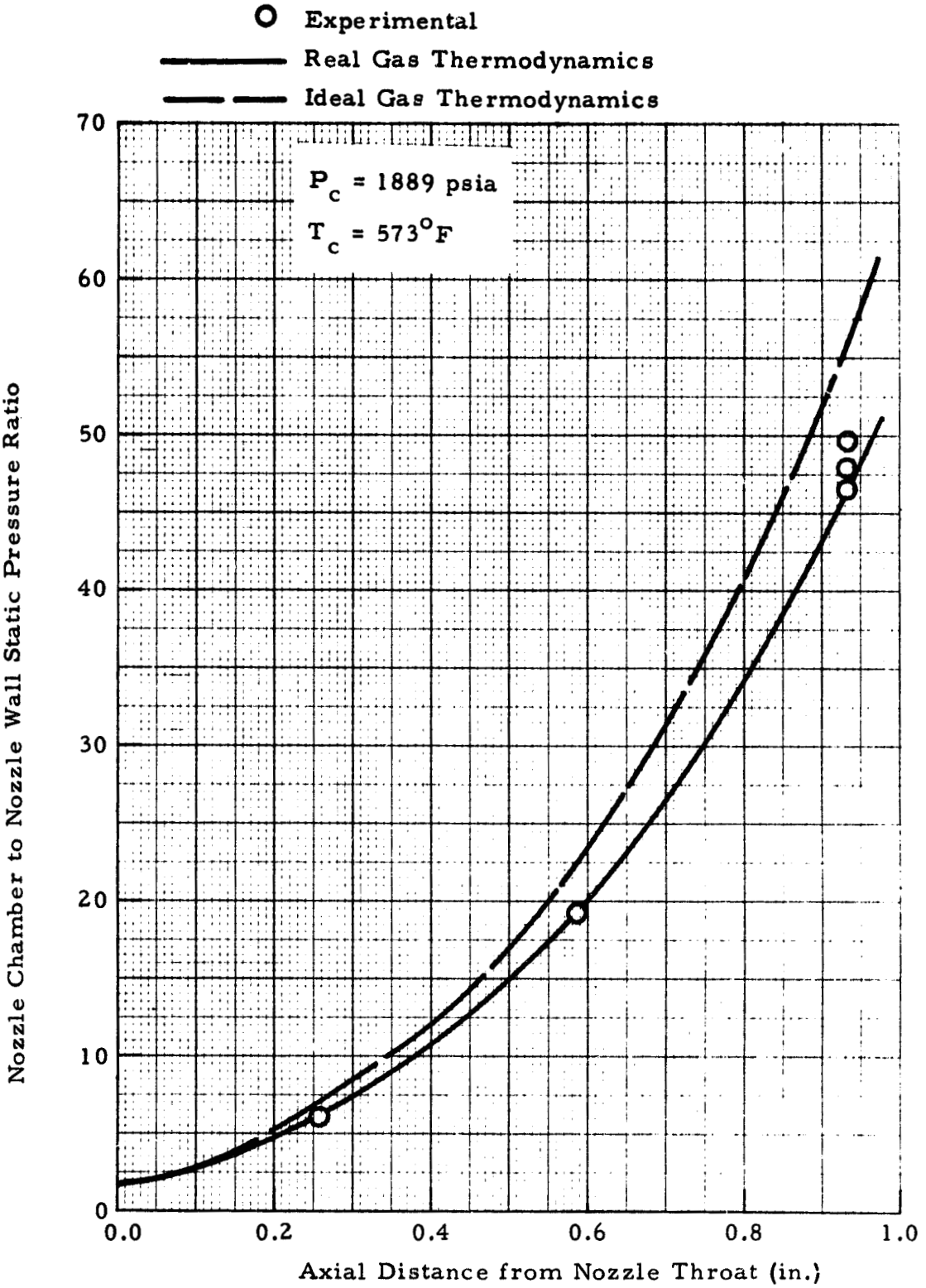

Fig. 8 - Non-Dimensional Nozzle Wall Static Pressure Distributions for Test Number TWT 575 and Nozzle 1 Flowing CF_4 at Test Point 509

Fig. 9 - Non-Dimensional Nozzle Wall Static Pressure Distributions for Test Number TWT 575 and Nozzle 1 Flowing CF_4 at Test Point 511

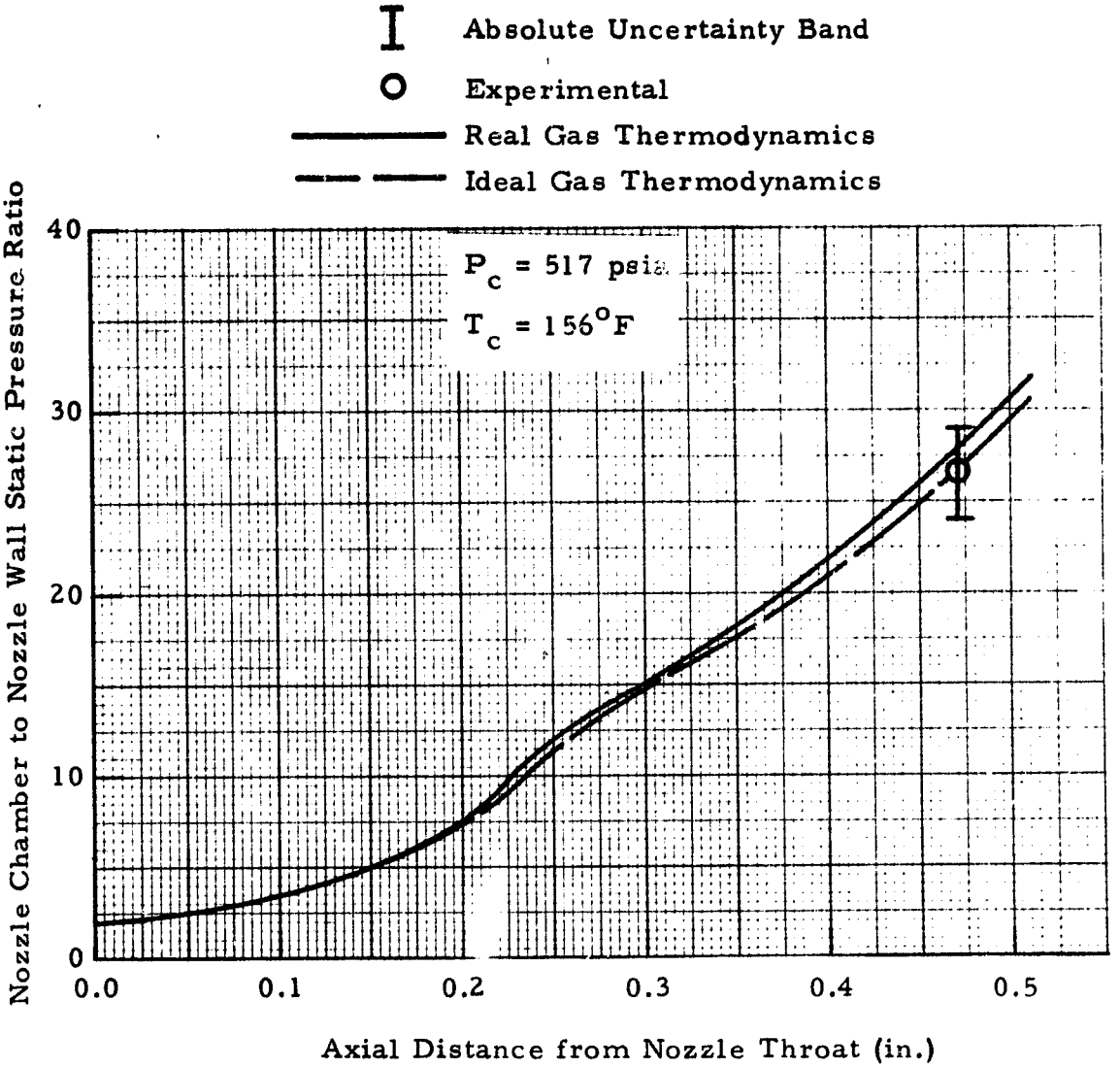

Fig. 10 - Non-Dimensional Nozzle Wall Static Pressure Distributions for Test Number TWT 575 and Nozzle 2 Flowing Air at Test Point 382

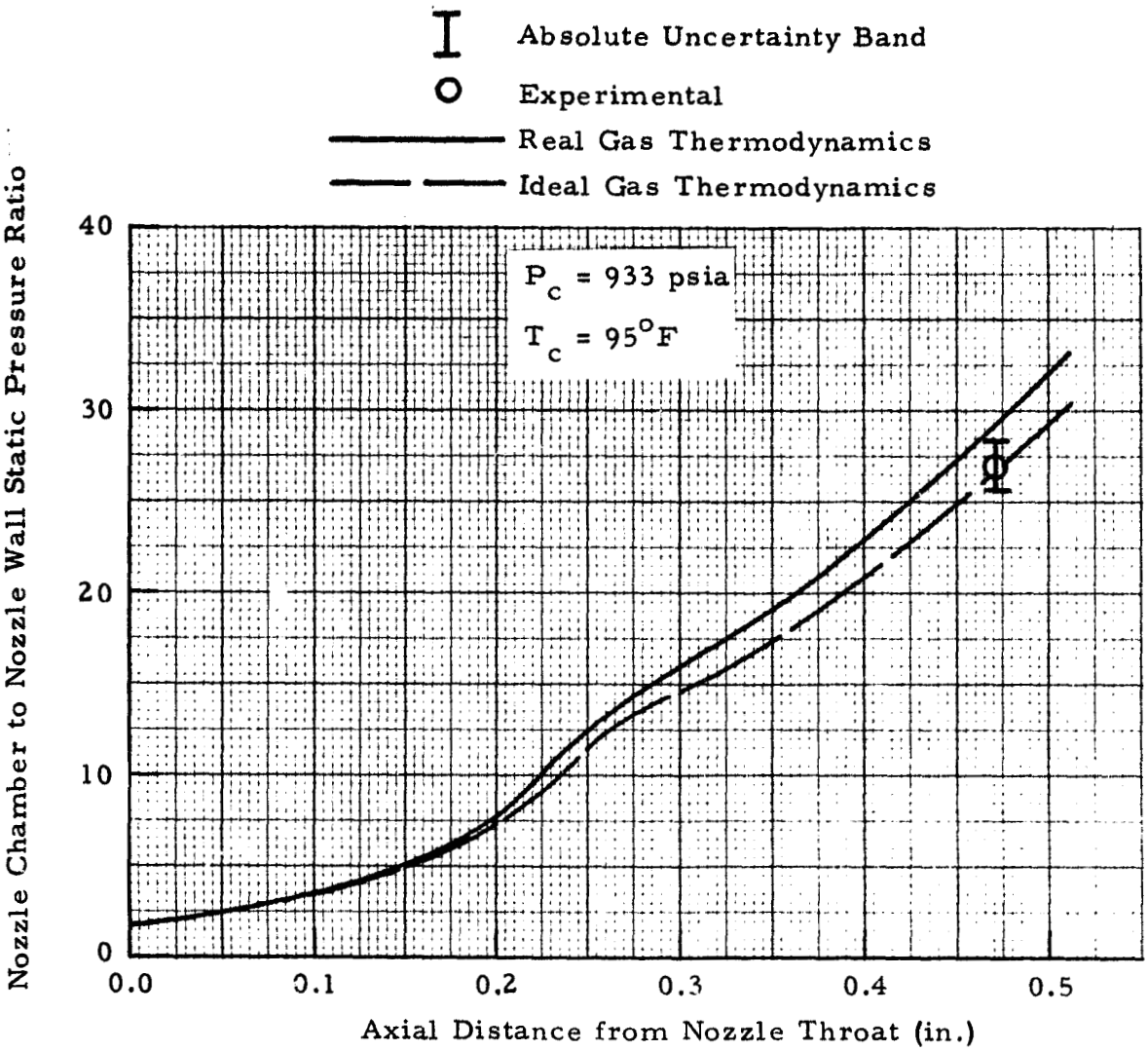

Fig. 11 - Non-Dimensional Nozzle Wall Static Pressure Distribution for Test Number TWT 575 and Nozzle 2 Flowing Air at Test Point 383

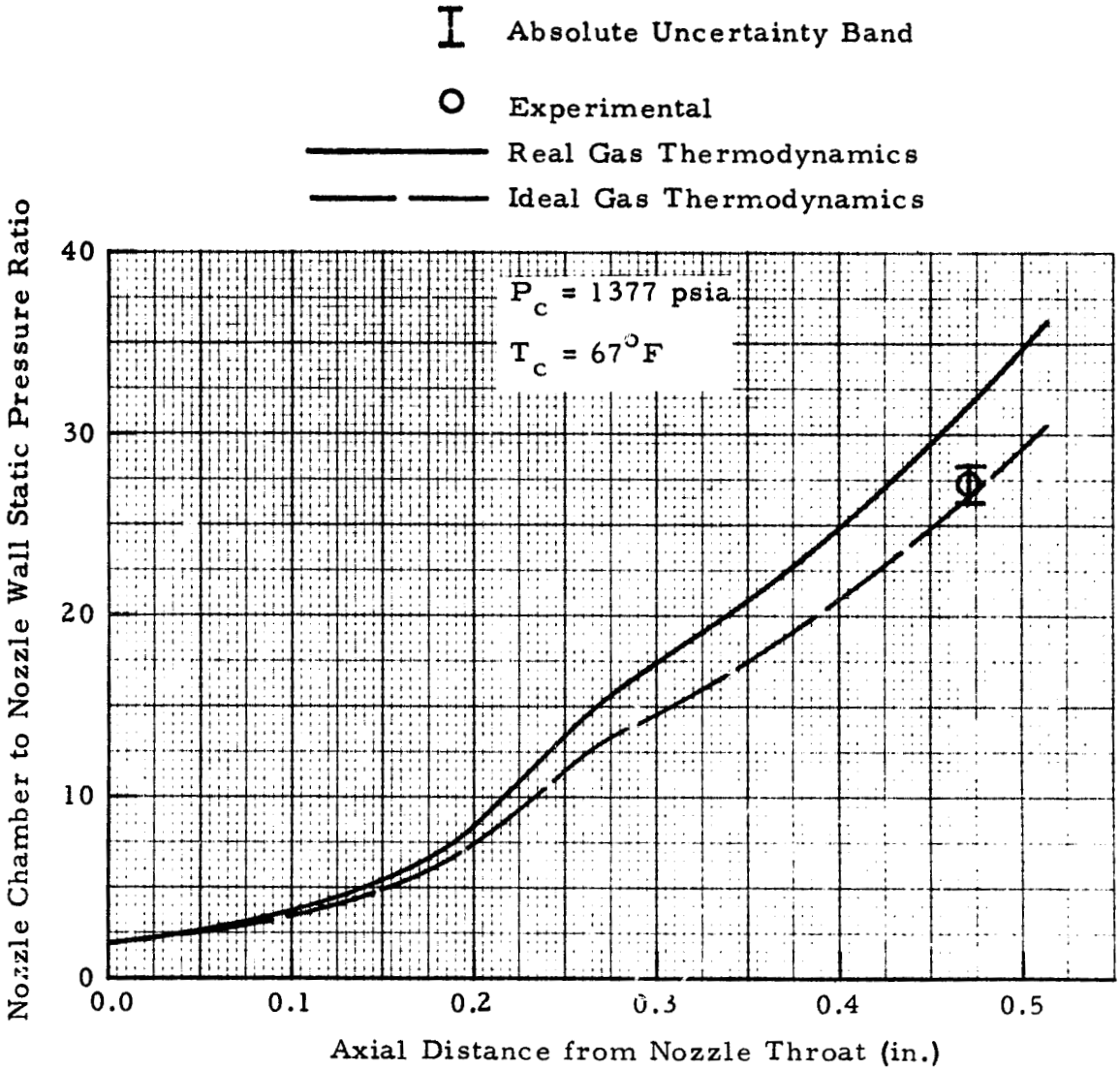

Fig. 12 - Non-Dimensional Nozzle Wall Static Pressure Distributions for Test Number TWT 575 and Nozzle 2 Flowing Air at Test Point 384

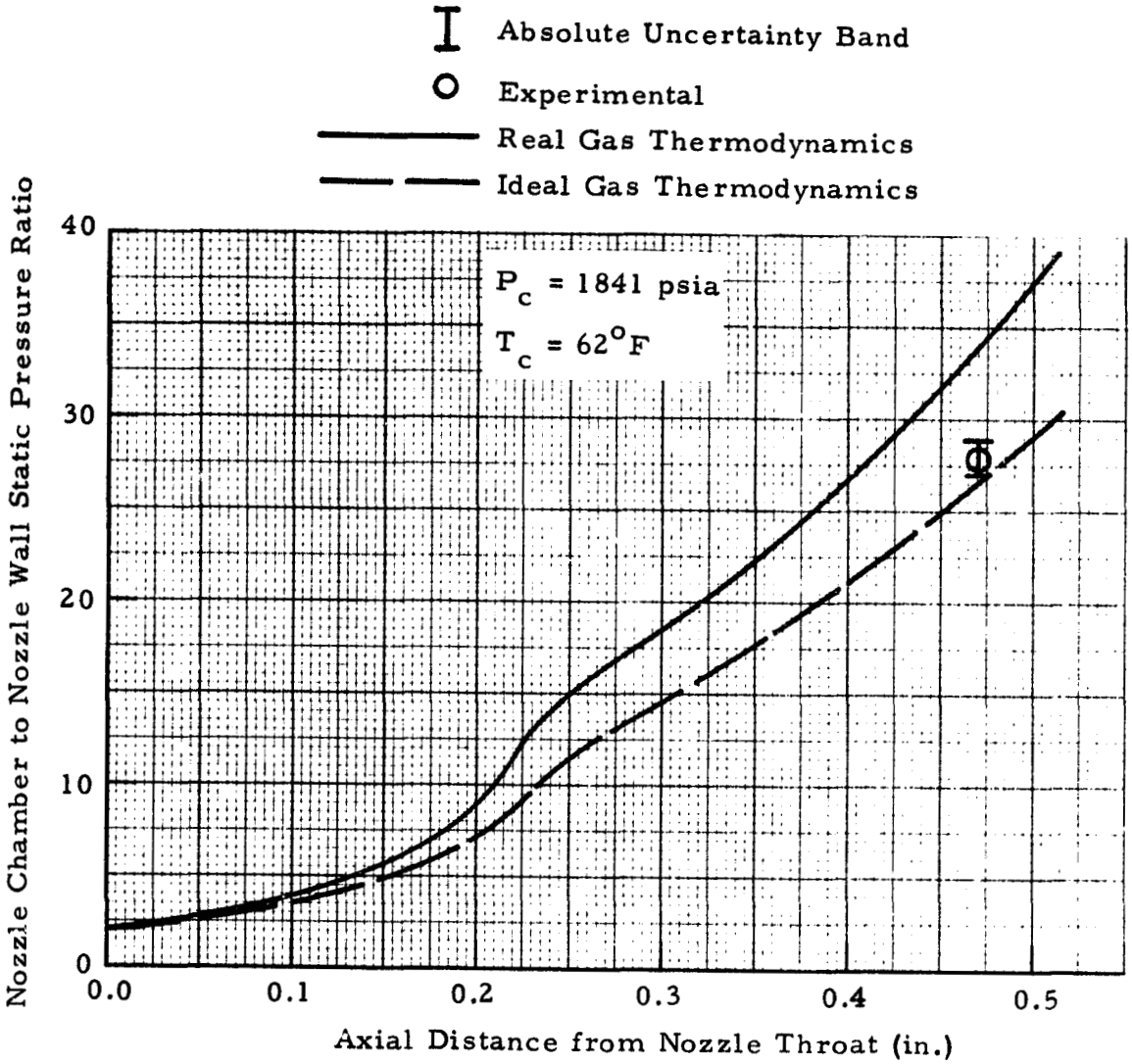

Fig. 13 - Non-Dimensional Nozzle Wall Static Pressure Distributions for Test Number TWT 575 and Nozzle 2 Flowing Air at Test Point 385

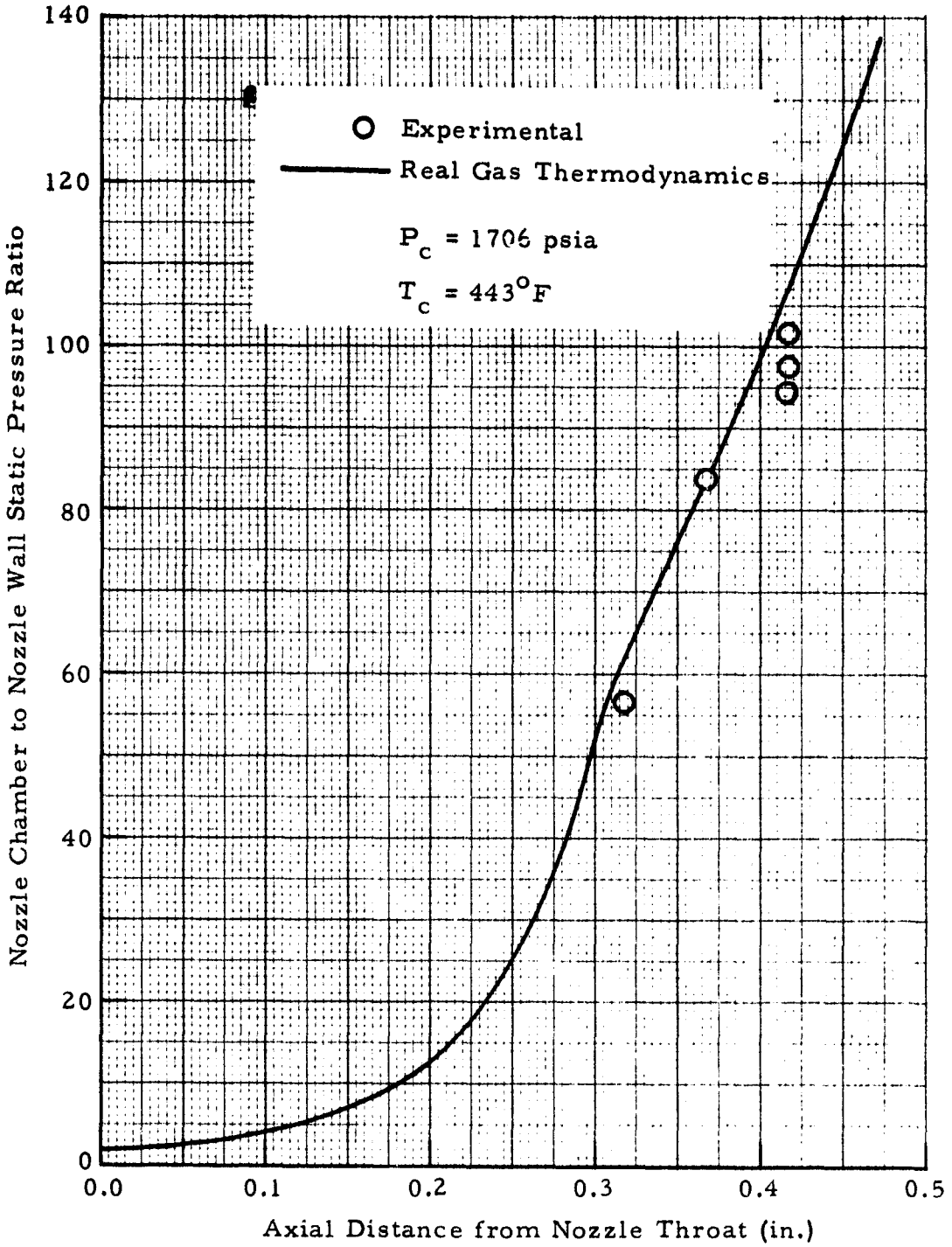

Fig. 14 - Non-Dimensional Nozzle Wall Static Pressure Distributions for Test Number TWT 575 and Nozzle 4 Flowing Air at Test Point 107

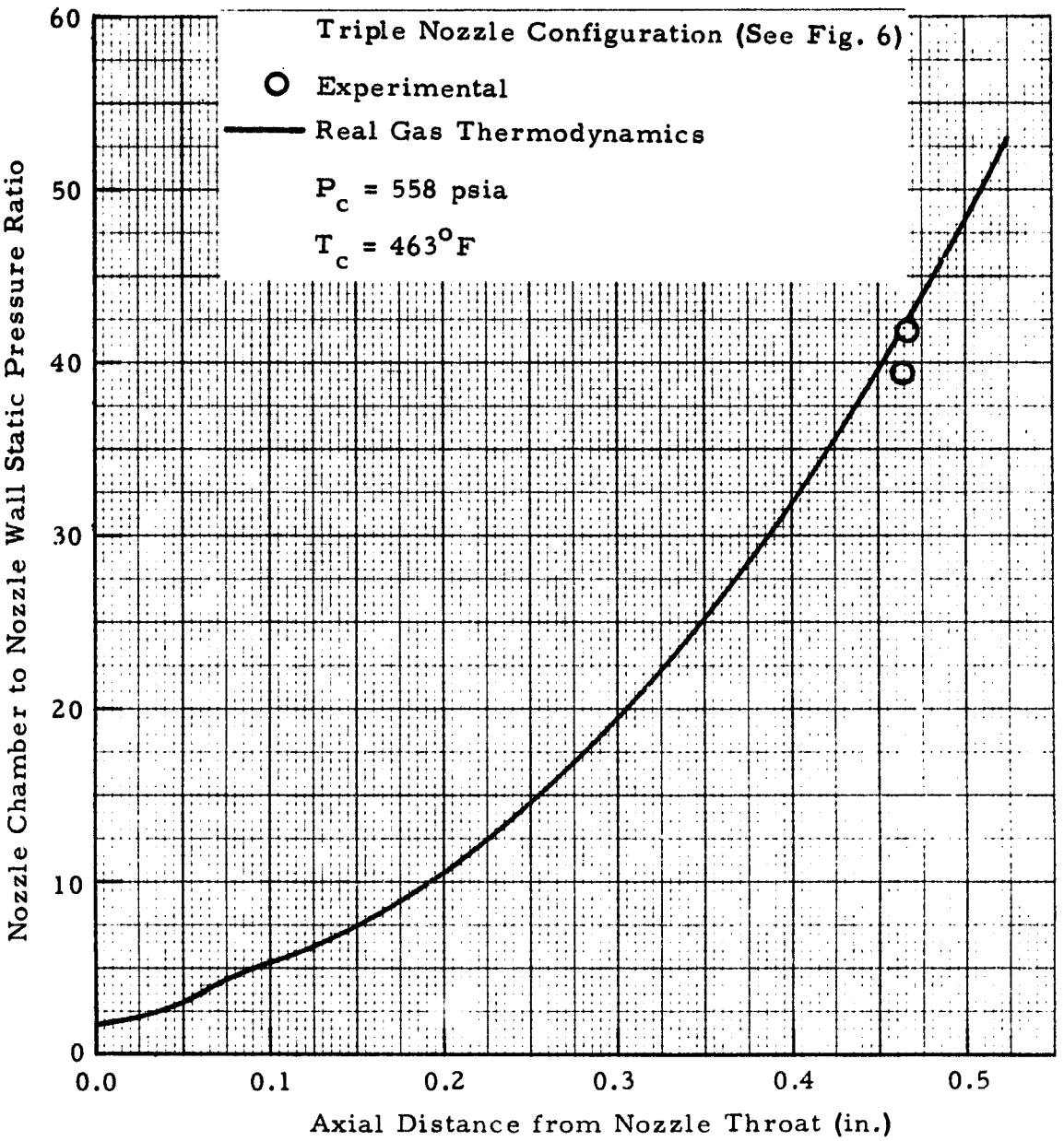

Fig. 15 - Non-Dimensional Nozzle Wall Static Pressure Distributions for Test Number TWT 575 and Nozzle 5A Flowing CF_4 at Test Point 603

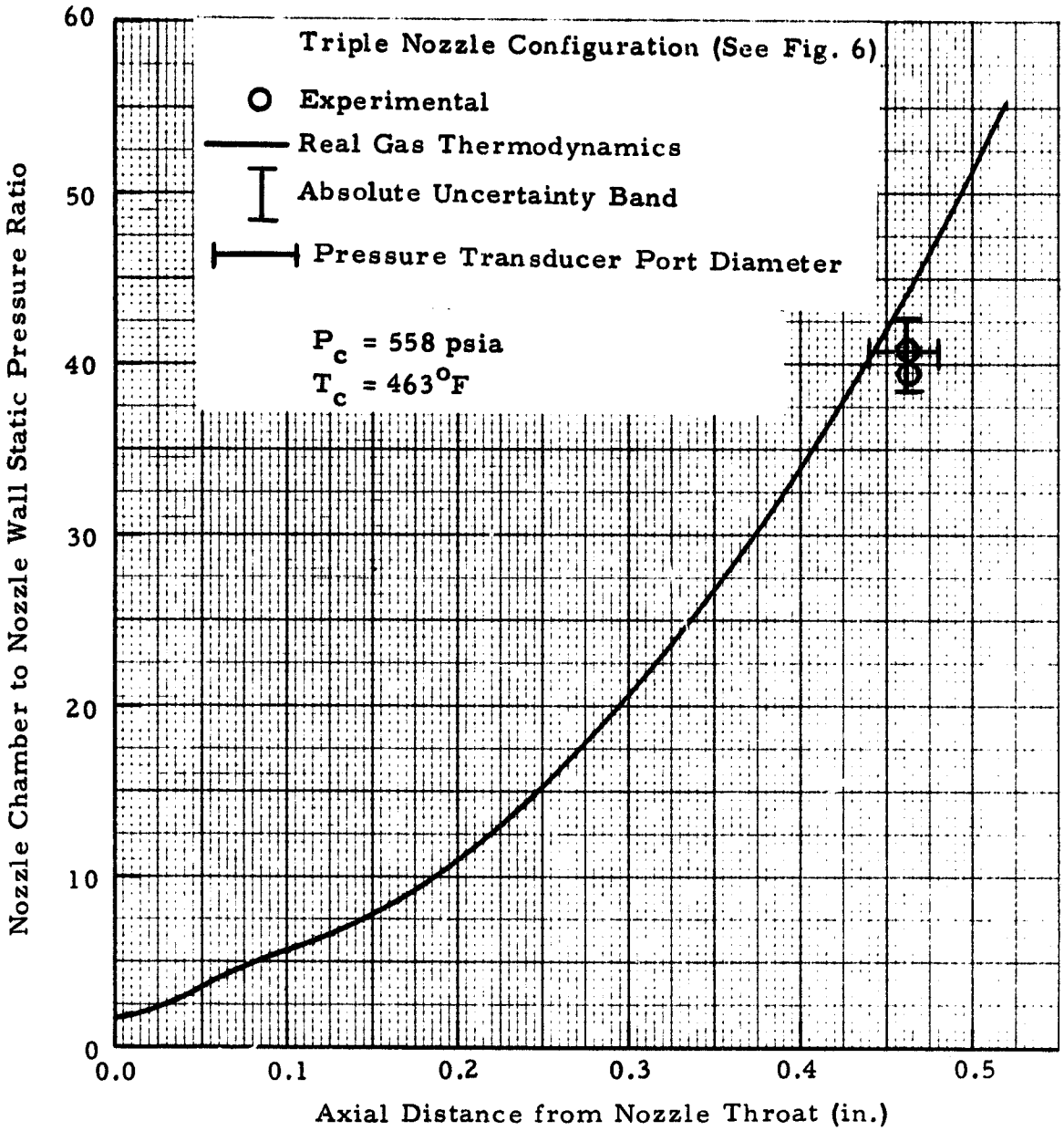

Fig. 16 - Non-Dimensional Nozzle Wall Static Pressure Distributions for Test Number TWT 575 and Nozzle 5B Flowing CF_4 at Test Point 603

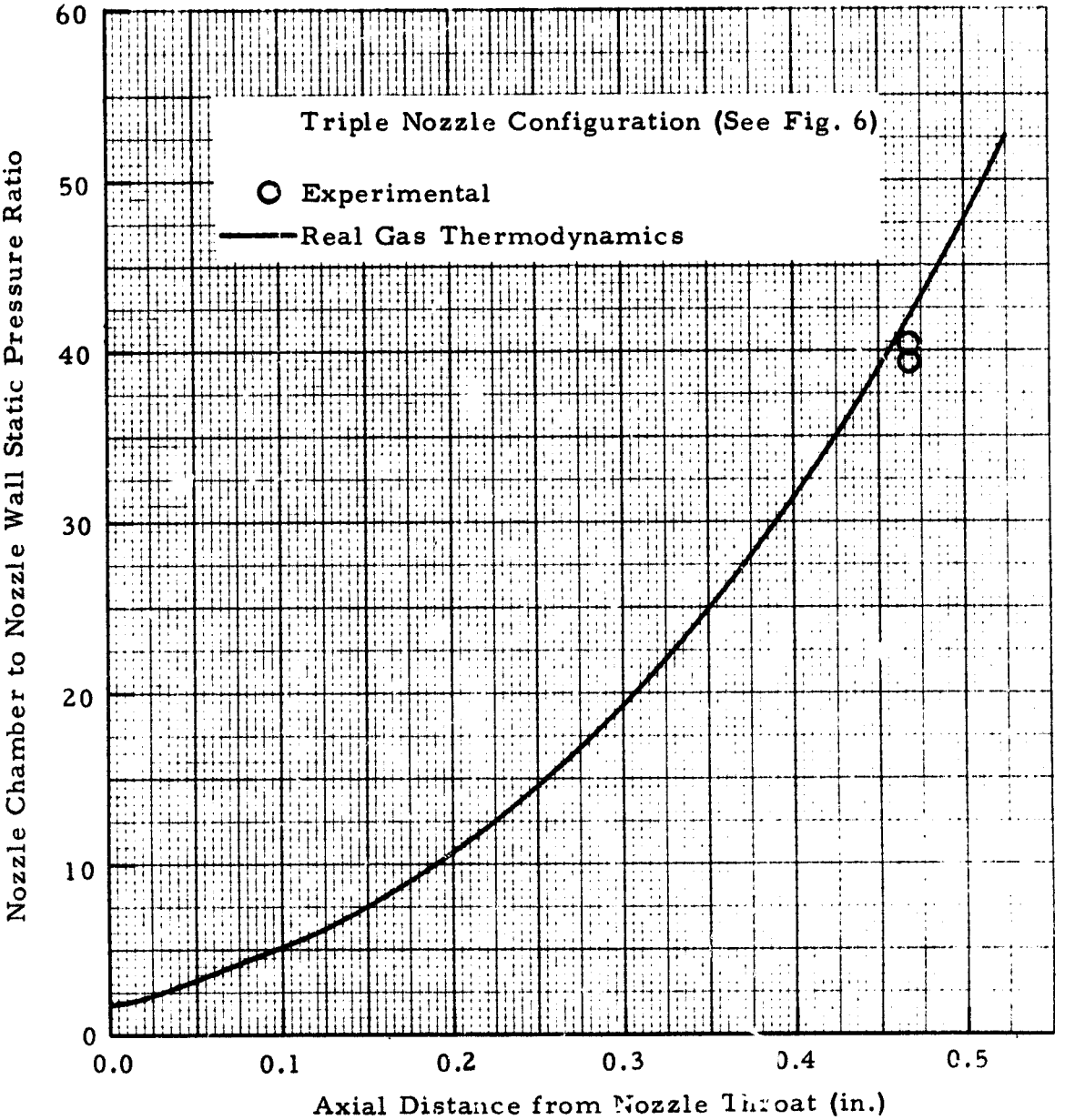

Fig. 17 - Non-Dimensional Nozzle Wall Static Pressure Distributions for Test Number TWT 575 and Nozzle 5C Flowing CF_4 at Test Point 603

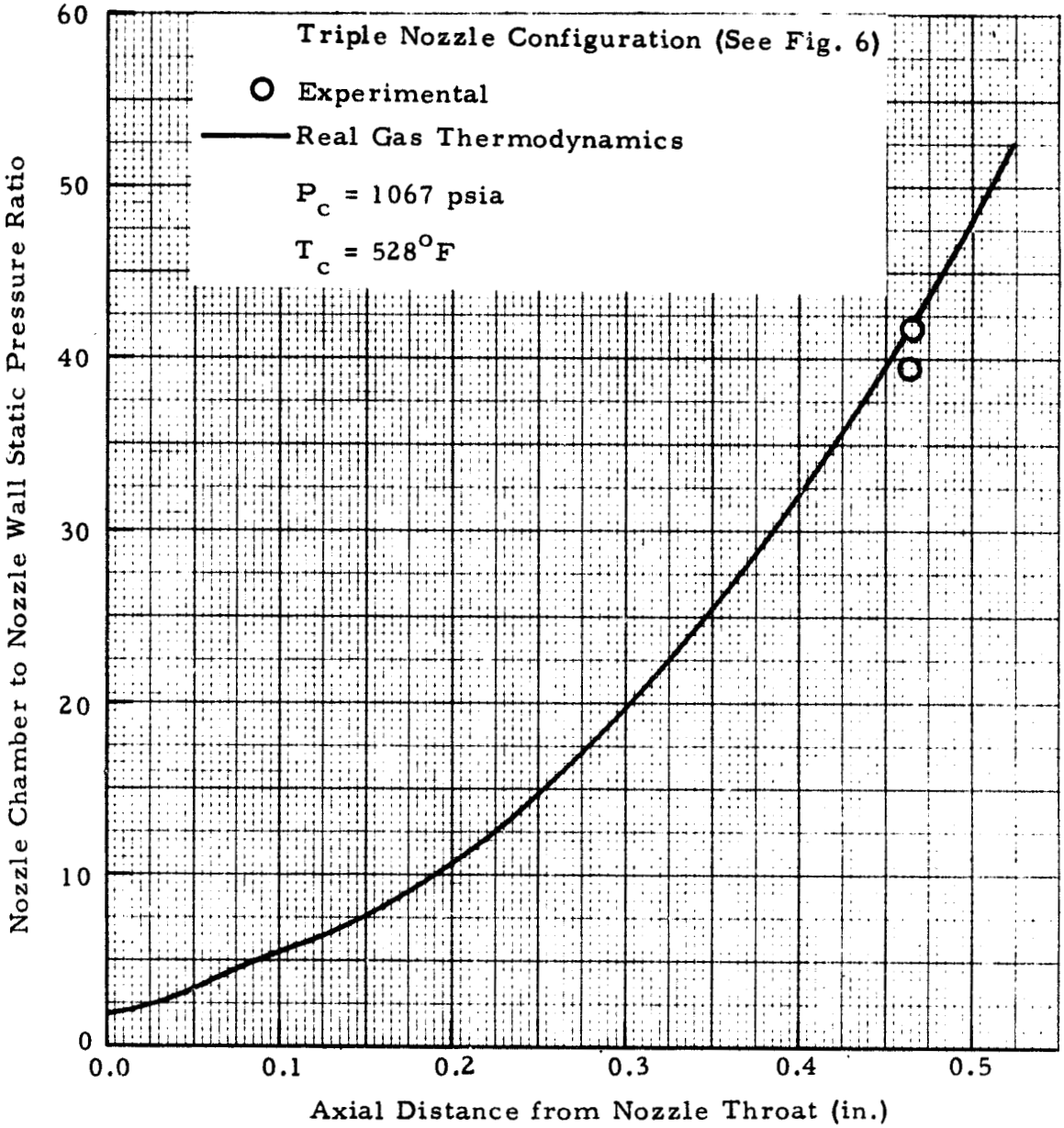

Fig. 18 - Non-Dimensional Nozzle Wall Static Pressure Distributions for Test Number TWT 575 and Nozzle 5A Flowing CF_4 at Test Point 604

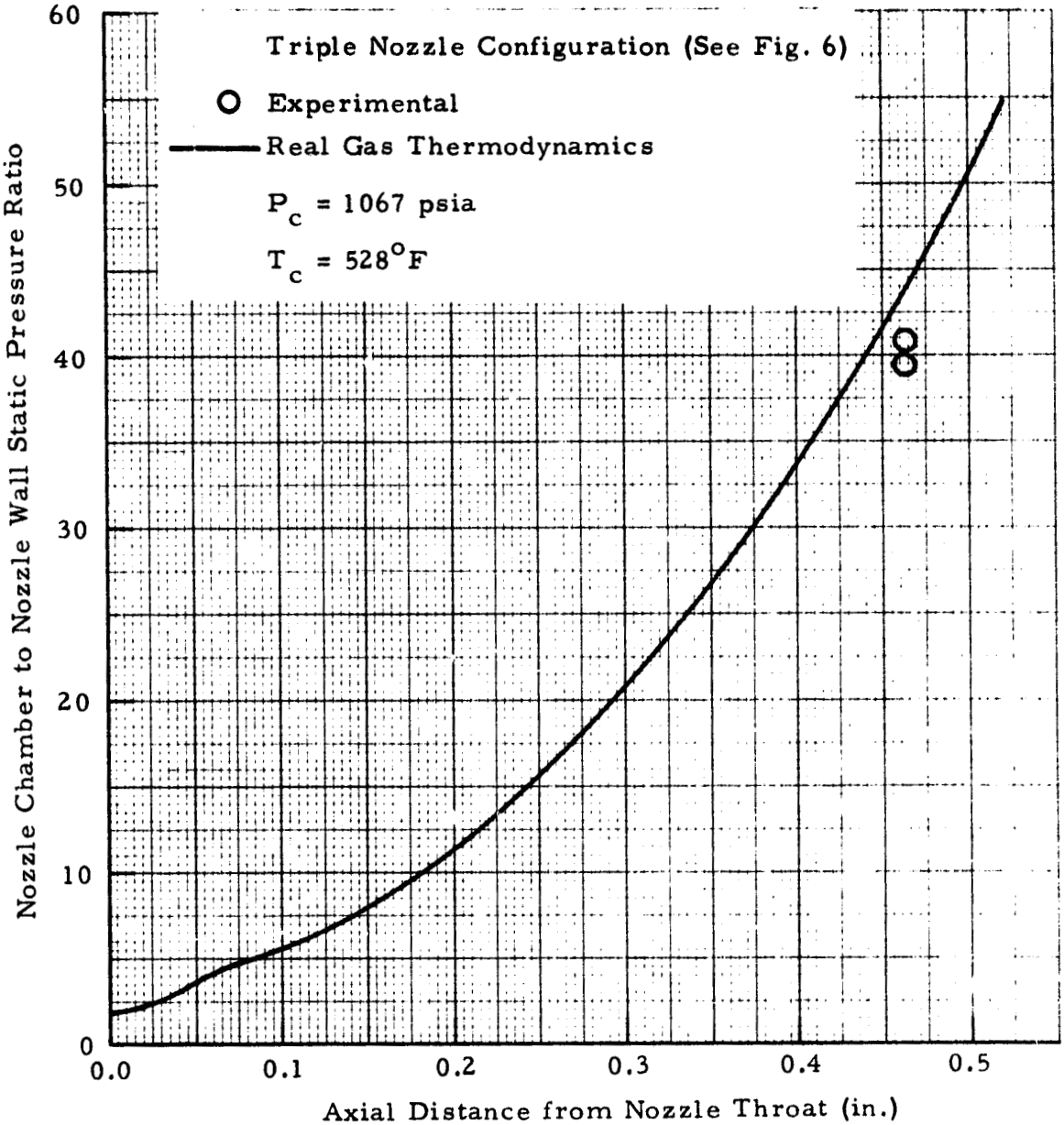

Fig. 19 - Non-Dimensional Nozzle Wall Static Pressure Distributions for Test Number TWT 575 and Nozzle 5B Flowing CF_4 at Test Point 604

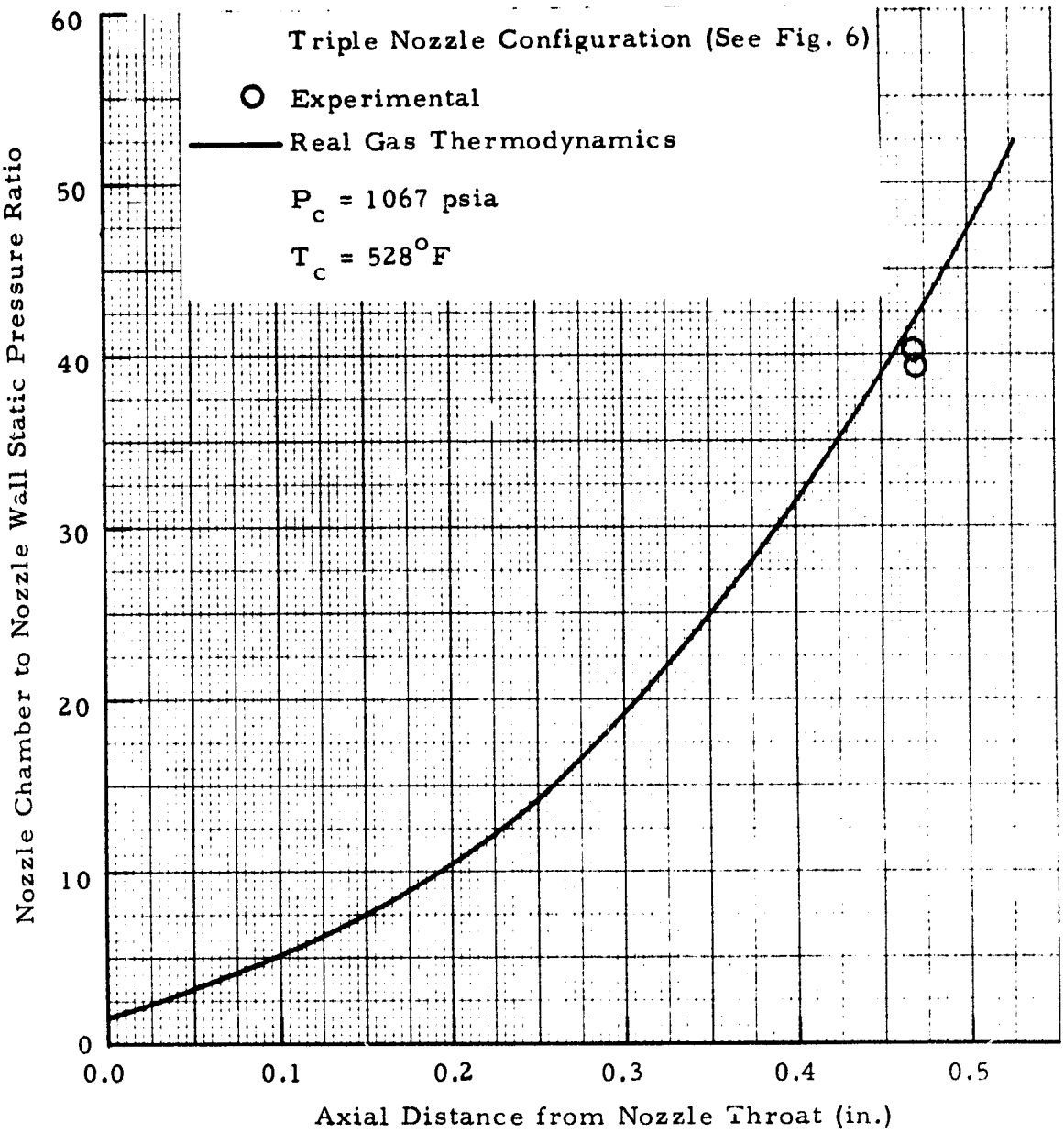

Fig. 20 - Non-Dimensional Nozzle Wall Static Pressure Distributions for Test Number TWT 575 and Nozzle 5C Flowing CF_4 at Test Point 604

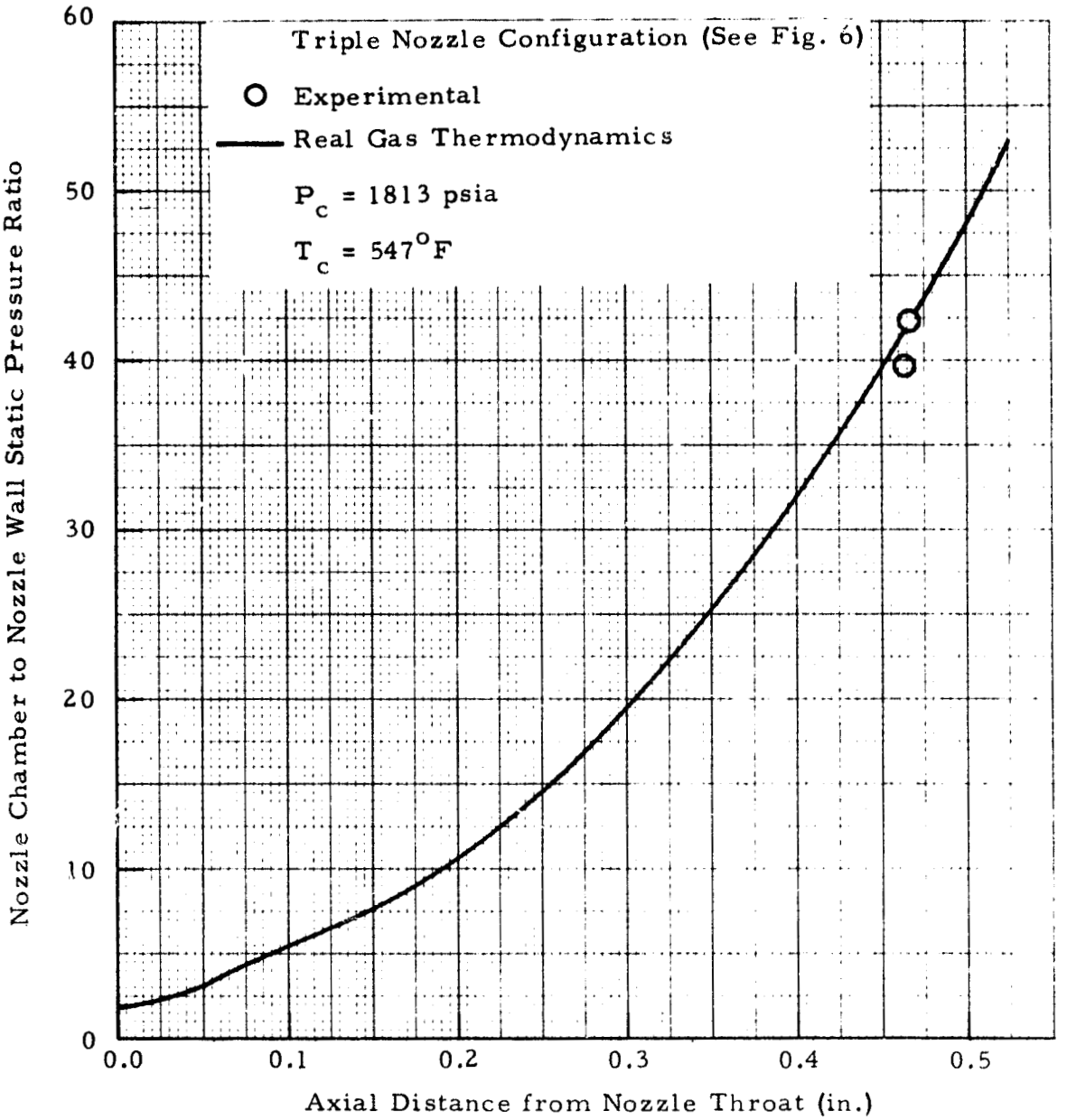

Fig. 21 - Non-Dimensional Nozzle Wall Static Pressure Distribution for Test Number TWT 575 and Nozzle 5A Flowing CF_4 at Test Point 606

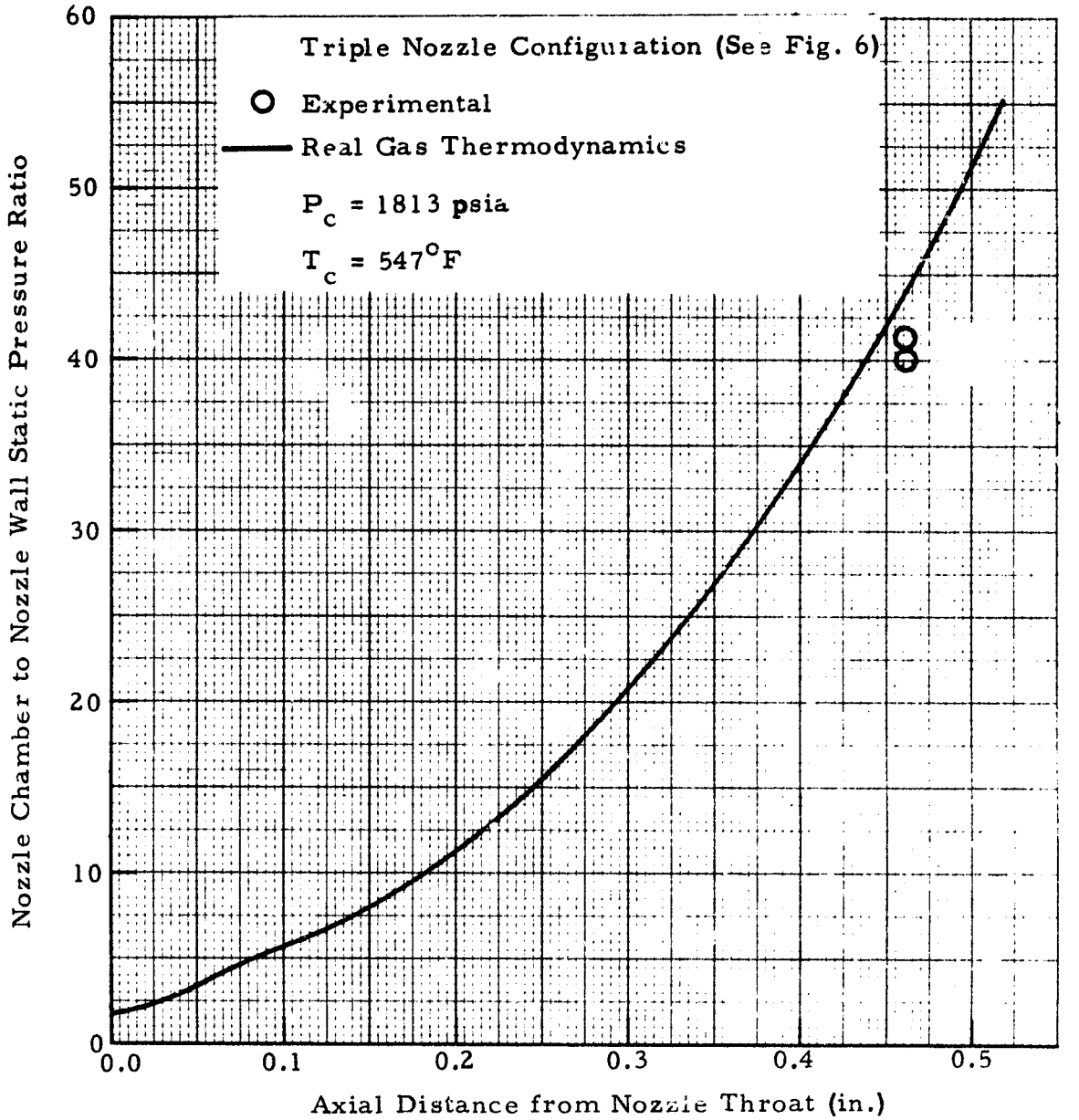

Fig. 22 - Non-Dimensional Nozzle Wall Static Pressure Distribution for Test Number TWT 575 and Nozzle 5B Flowing CF_4 at Test Point 606

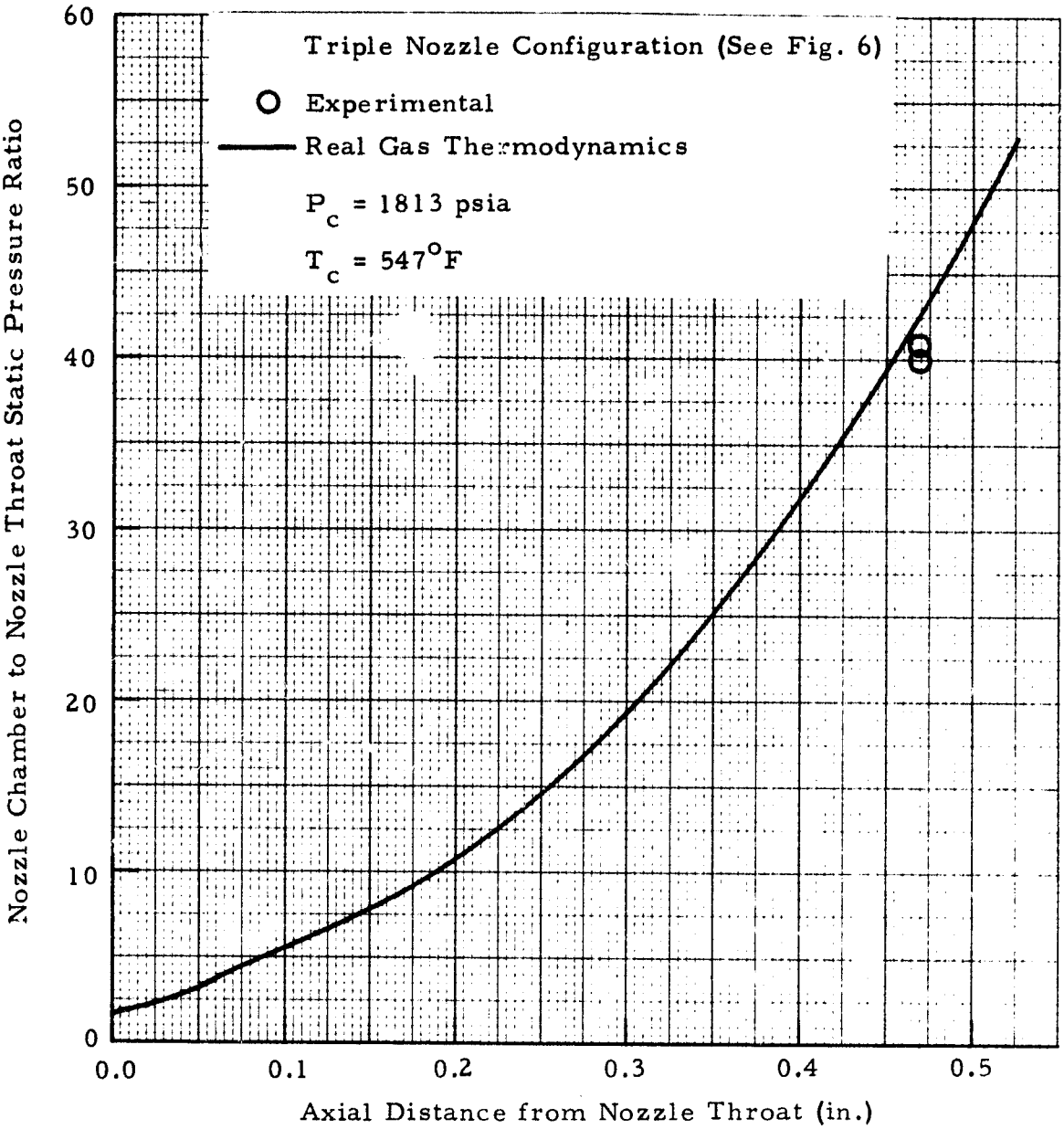

Fig. 23 - Non-Dimensional Nozzle Wall Static Pressure Distribution for Test Number TWT 575 and Nozzle 5C Flowing CF_4 at Test Point 606

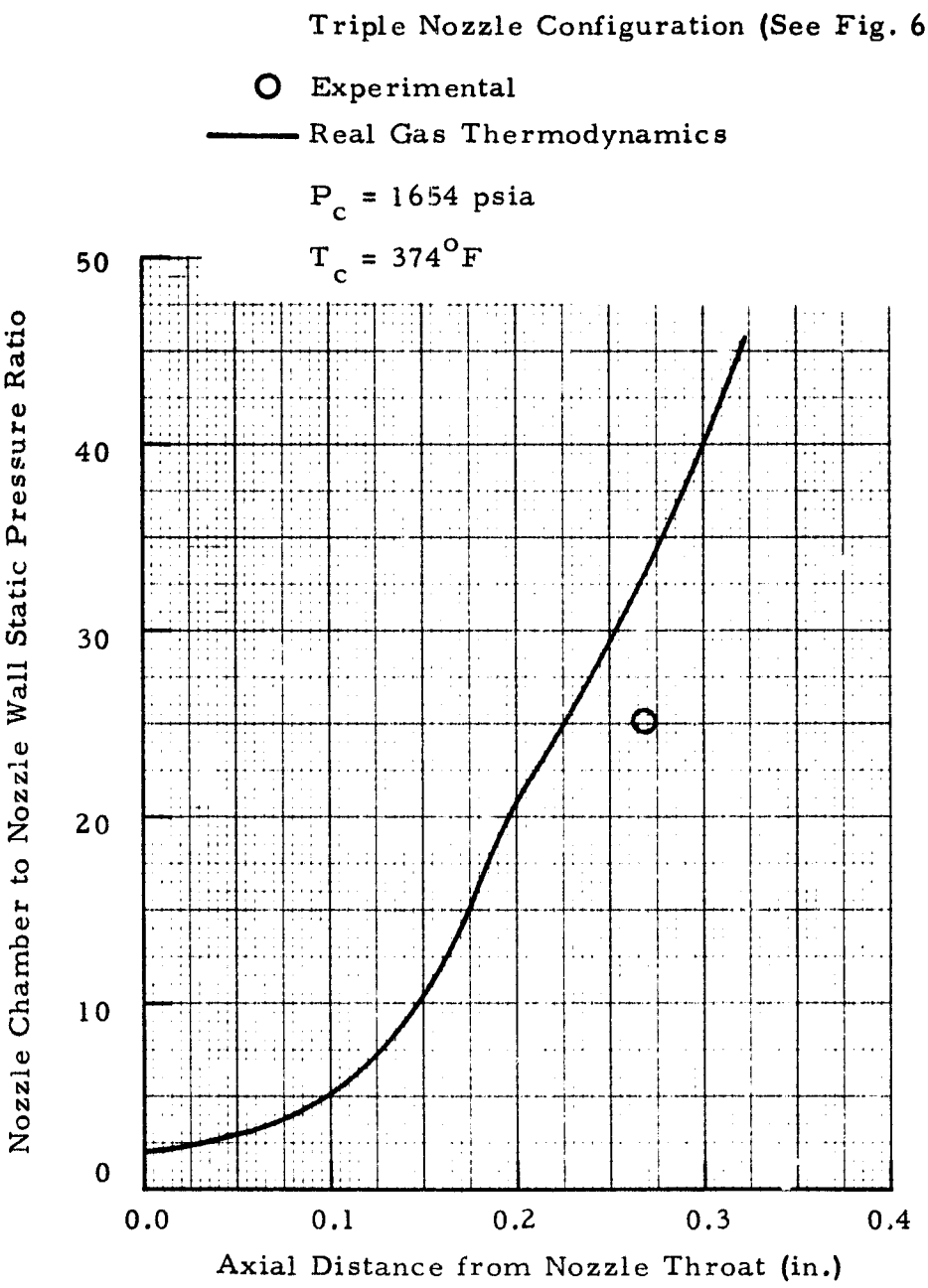

Fig. 24 - Non-Dimensional Nozzle Wall Static Pressure Distribution for Test Number TWT 575 and Nozzle 6A Flowing Air at Test Point 401

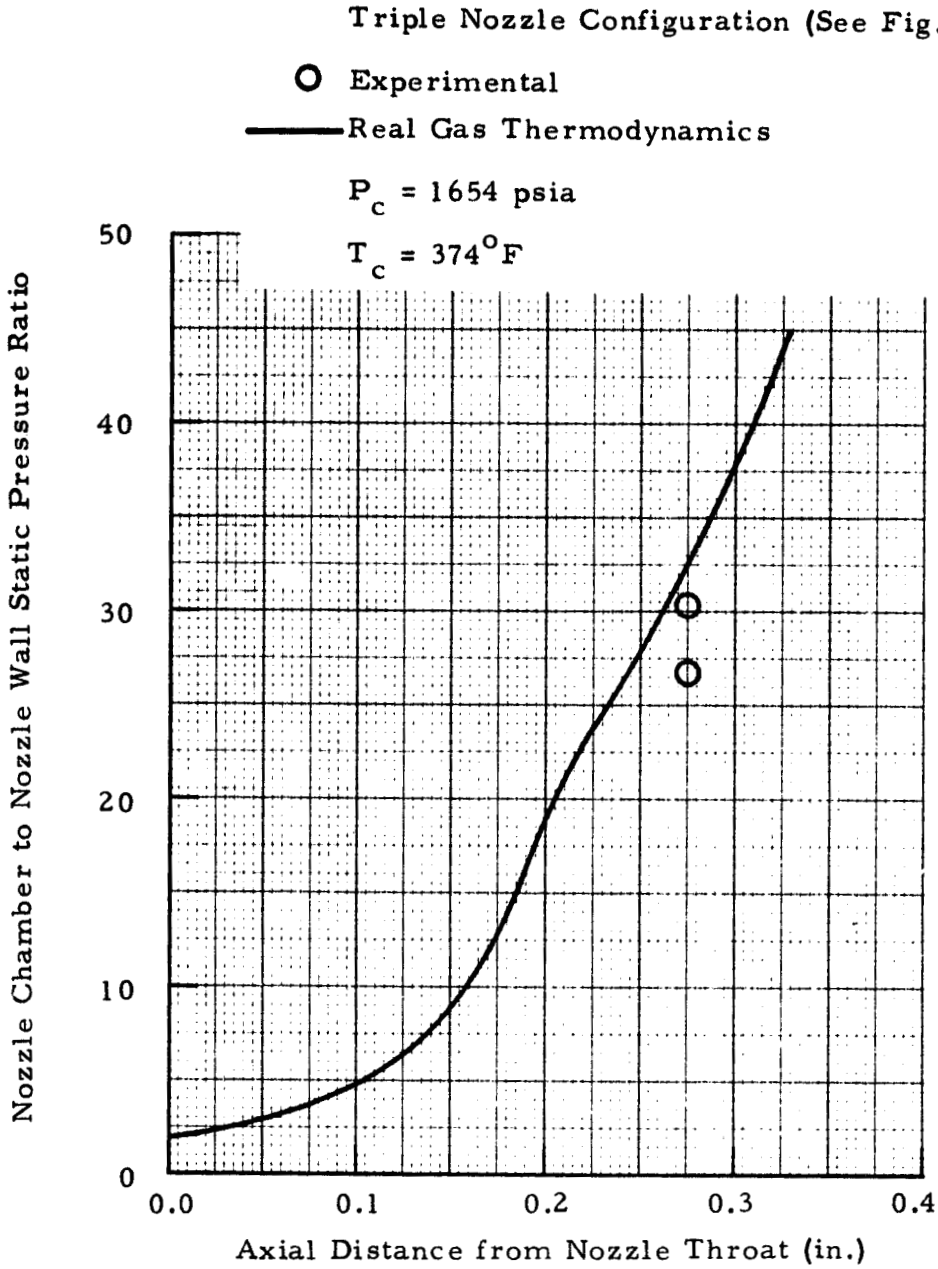

Fig. 25 - Non-Dimensional Nozzle Wall Static Pressure Distribution for Test Number TWT 575 and Nozzle 6B Flowing Air at Test Point 401

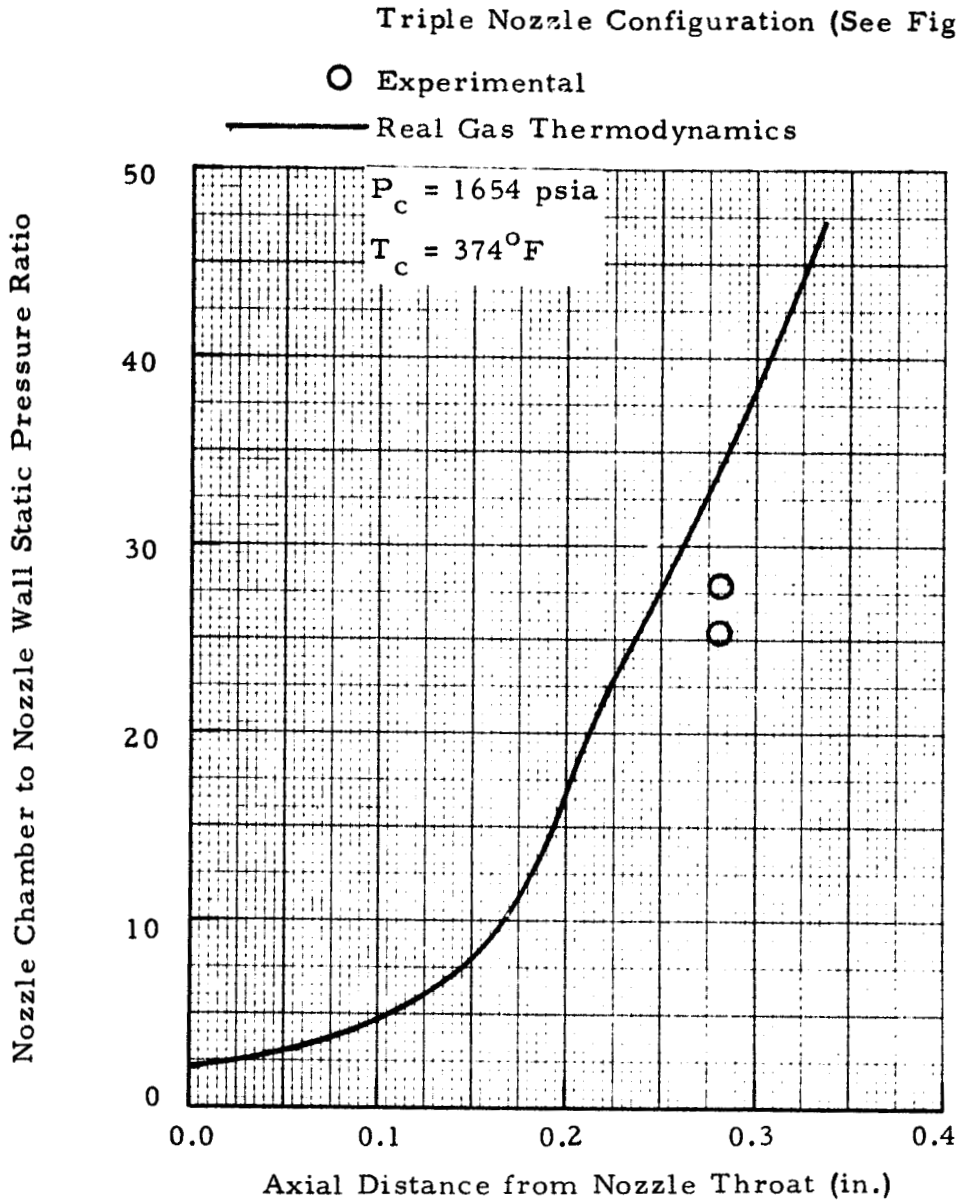

Fig. 26 - Non-Dimensional Nozzle Wall Static Pressure Distribution for Test Number TWT 575 and Nozzle 6C Flowing Air at Test Point 401

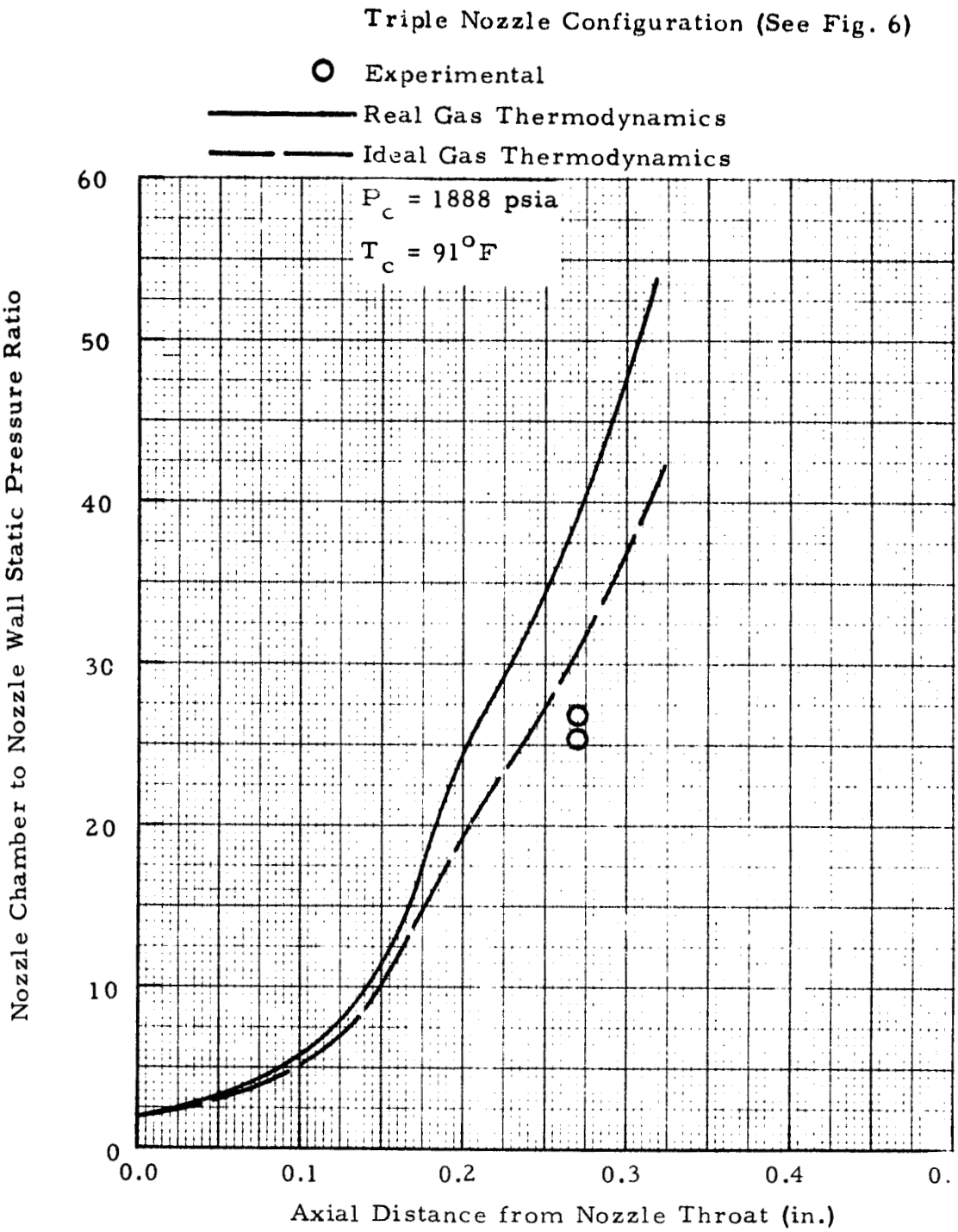

Fig. 27 - Non-Dimensional Nozzle Wall Static Pressure Distributions for Test Number TWT 575 and Nozzle 6A Flowing Air at Test Point 405

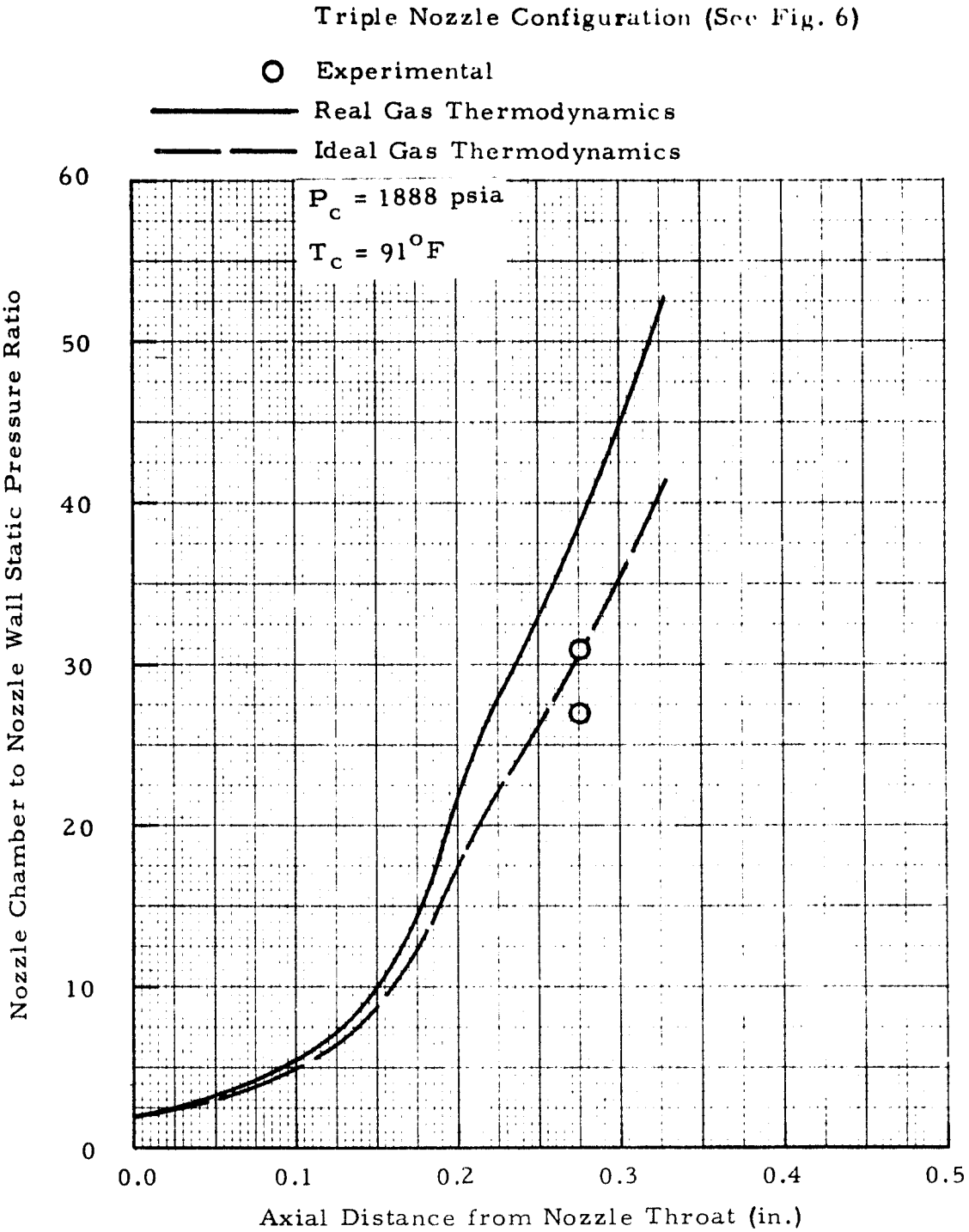

Fig. 28 - Non-Dimensional Nozzle Wall Static Pressure Distribution for Test Number TWT 575 and Nozzle 6B Flowing Air at Test Point 405

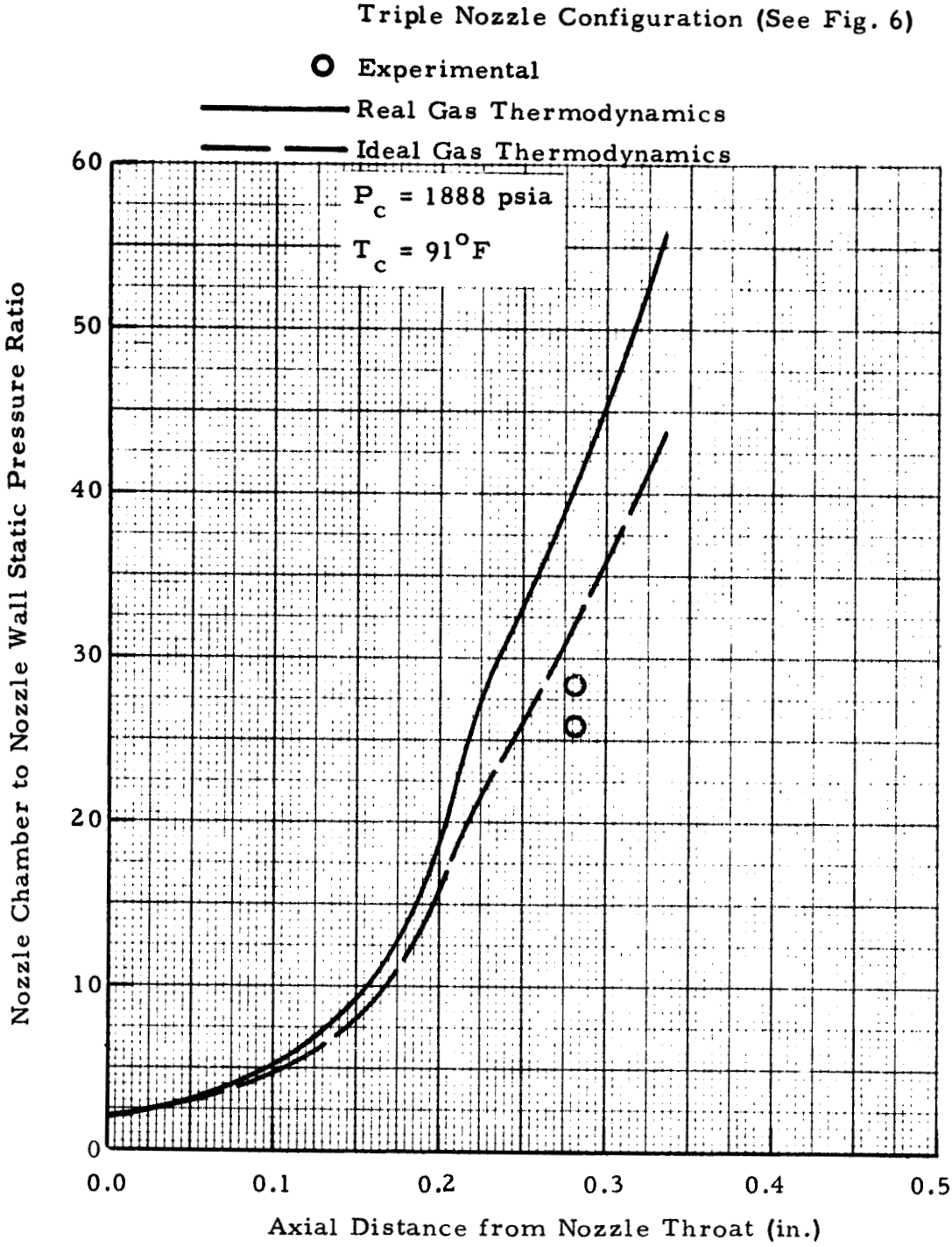

Fig. 29 - Non-Dimensional Nozzle Wall Static Pressure Distributions for Test Number TWT 575 and Nozzle 6C Flowing Air at Test Point 405

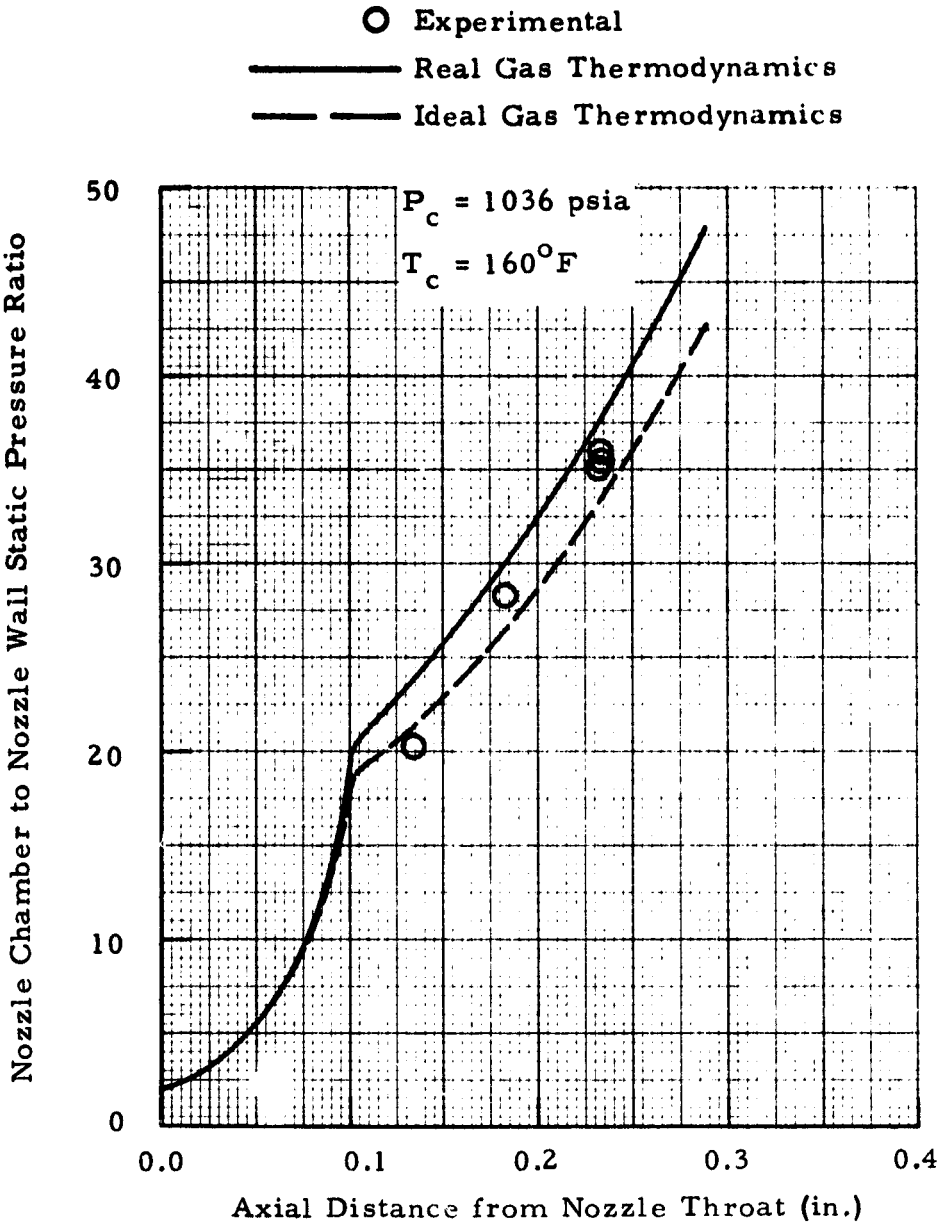

Fig. 30 - Non-Dimensional Nozzle Wall Static Pressure Distribution for Test Number TWT 593 and Nozzle 4A Flowing Air at Test Point 2

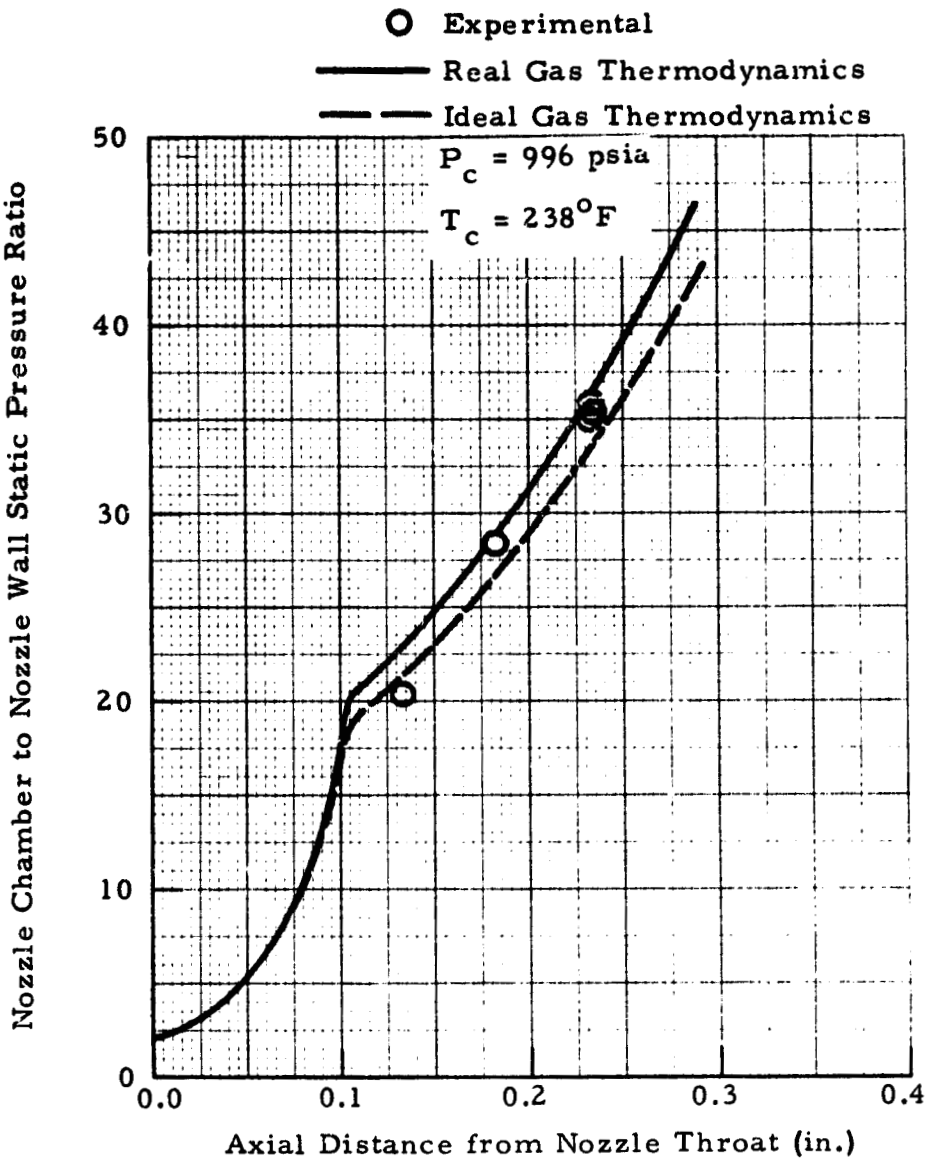

Fig. 31 - Non-Dimensional Nozzle Wall Static Pressure Distributions for Test Number TWT 593 and Nozzle 4A Flowing Air at Test Point 7

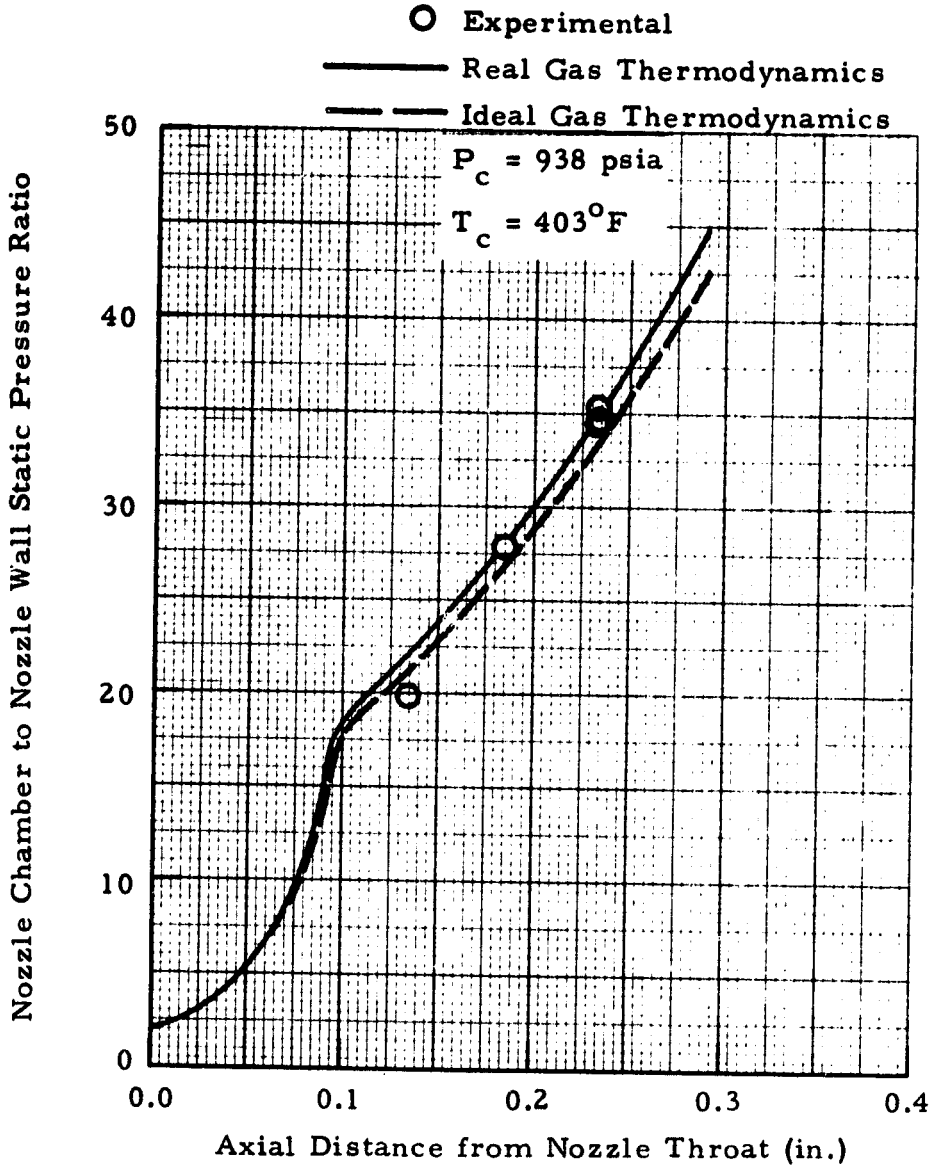

Fig. 32 - Non-Dimensional Nozzle Wall Static Pressure Distributions for Test Number TWT 593 and Nozzle 4A Flowing Air at Test Point 12

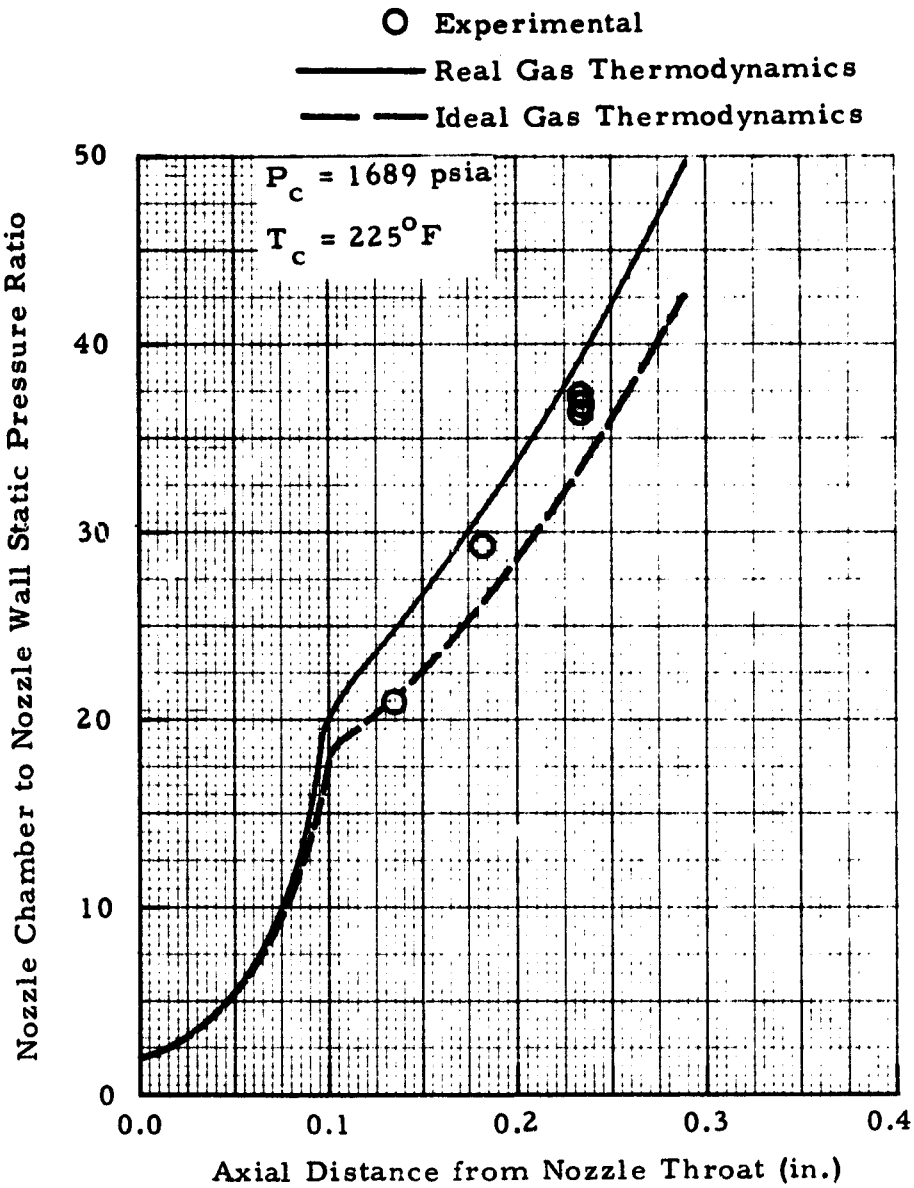

Fig. 33 - Non-Dimensional Nozzle Wall Static Pressure Distribution for Test Number TWT 593 and Nozzle 4A Flowing Air at Test Point 17

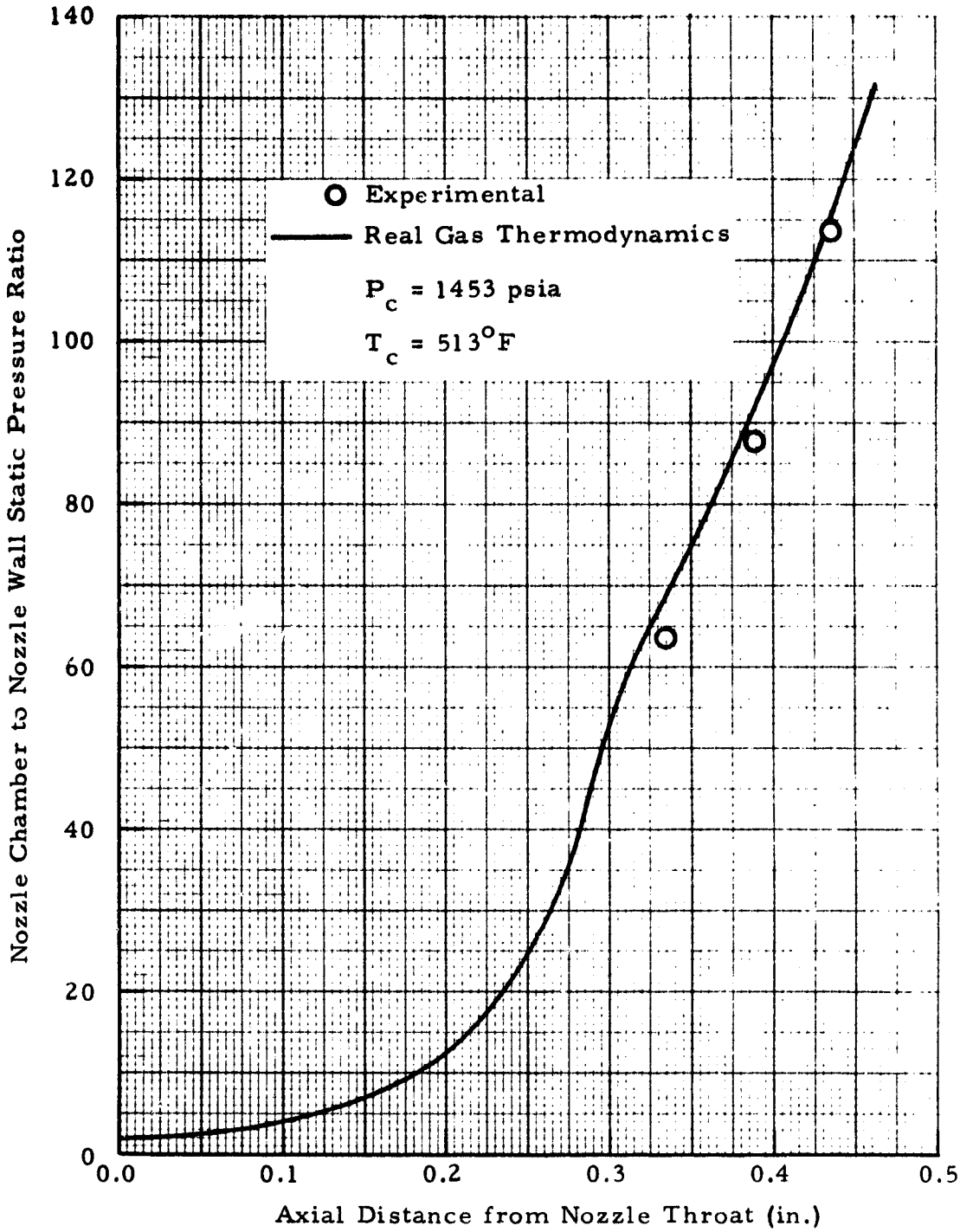

Fig. 34 - Non-Dimensional Nozzle Wall Static Pressure Distribution for Test Number TWT 593 and Nozzle 4 Flowing Air at Test Point 161

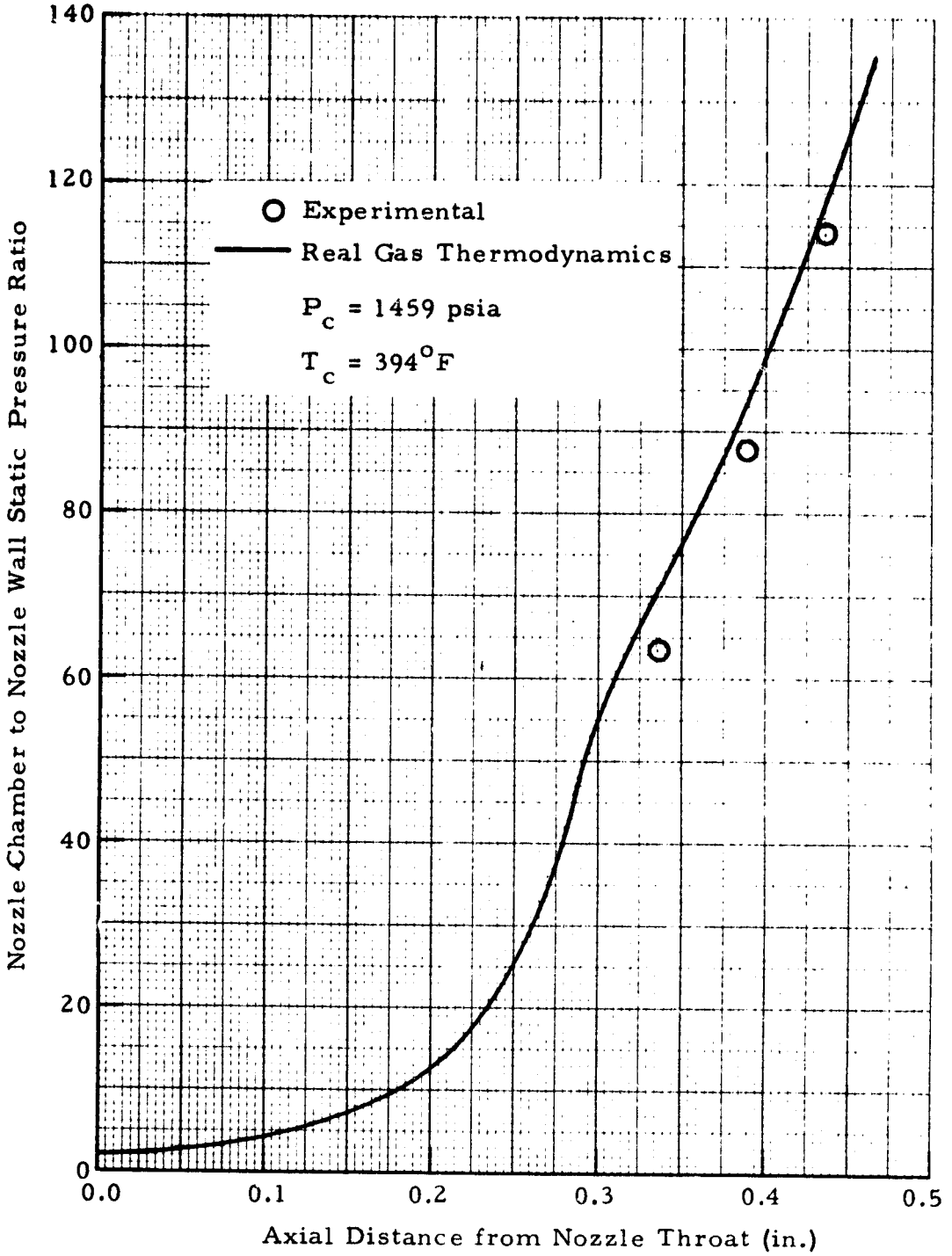

Fig. 35 - Non-Dimensional Nozzle Wall Static Pressure Distribution for Test Number TWT 593 and Nozzle 4 Flowing Air at Test Point 167

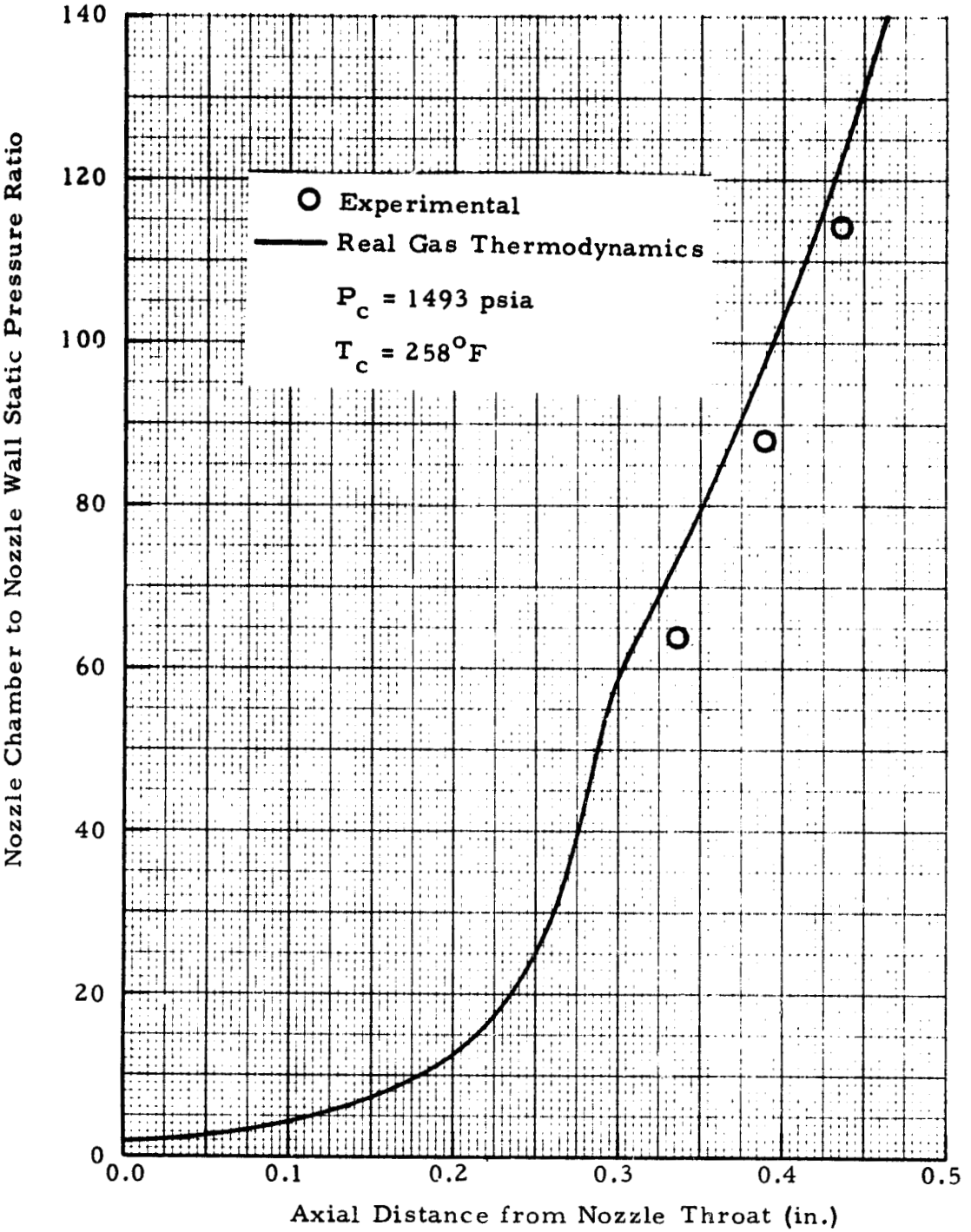

Fig. 36 - Non-Dimensional Nozzle Wall Static Pressure Distribution for Test Number TWT 593 and Nozzle 4 Flowing Air at Test Point 172

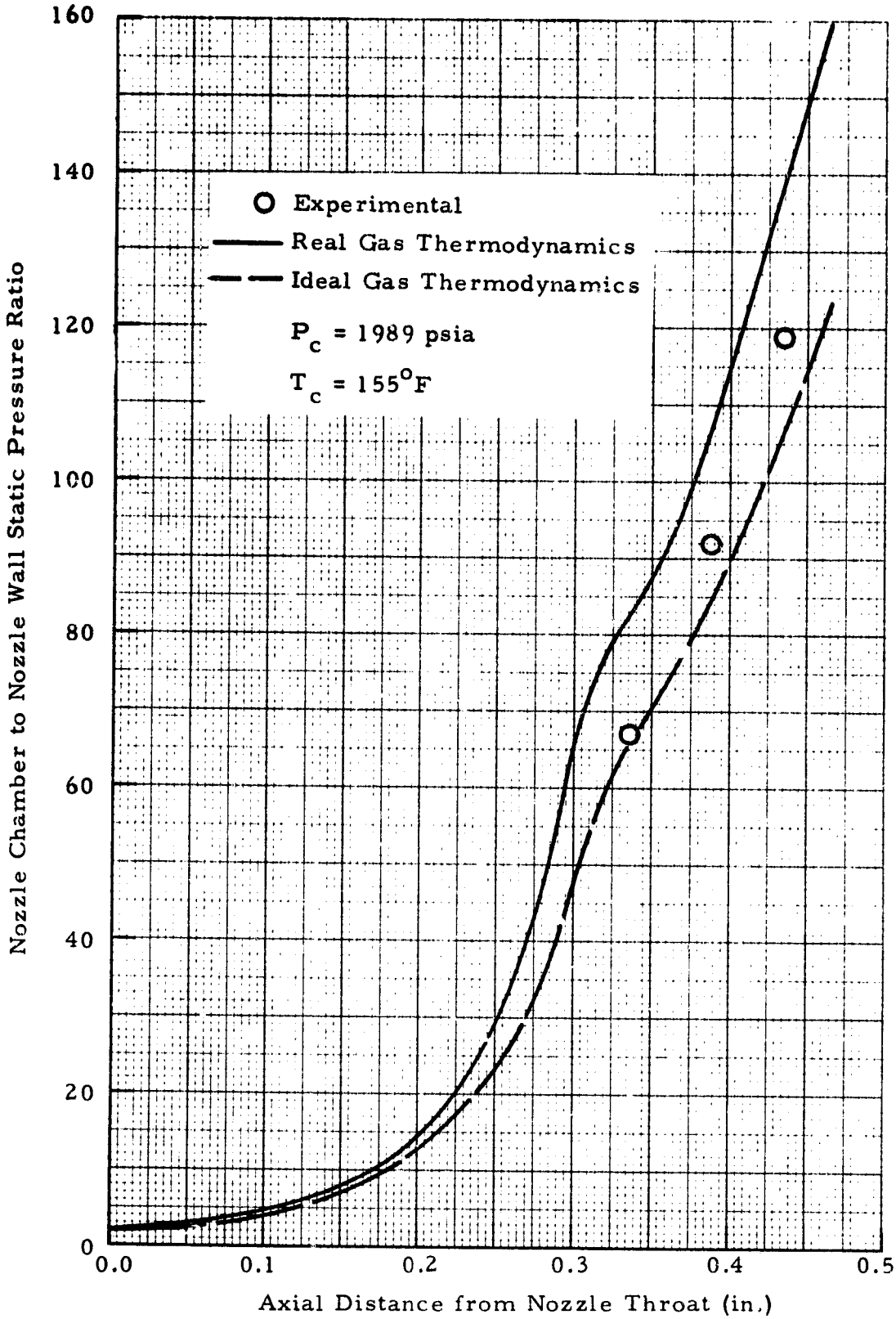

Fig. 37 - Non-Dimensional Nozzle Wall Static Pressure Distributions for Test Number TWT 593 and Nozzle 4 Flowing Air at Test Point 176

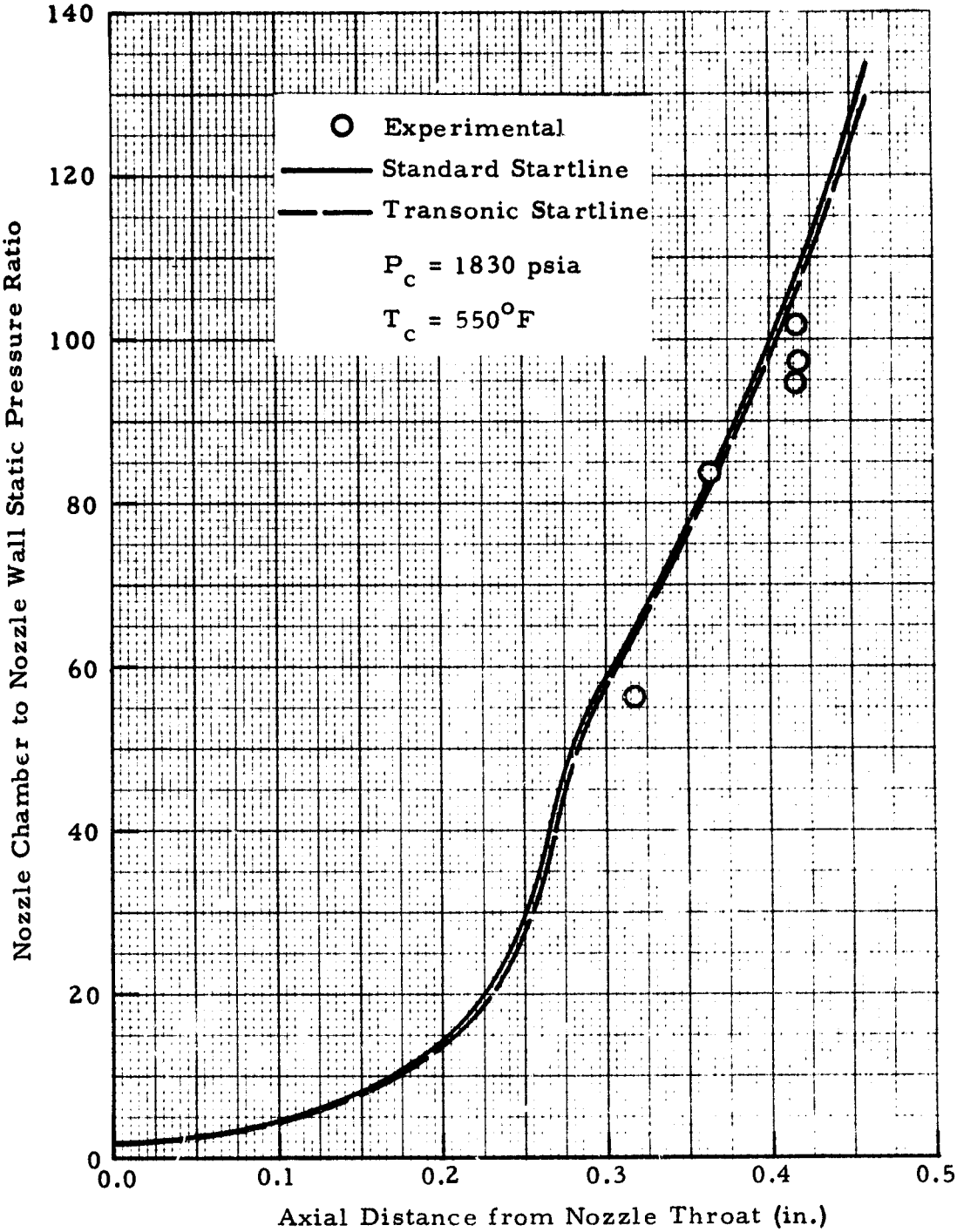

Fig. 38 - Non-Dimensional Nozzle Wall Static Pressure Distributions for Test Number TWT 575 and Nozzle 4 Flowing Air at Test Point 114

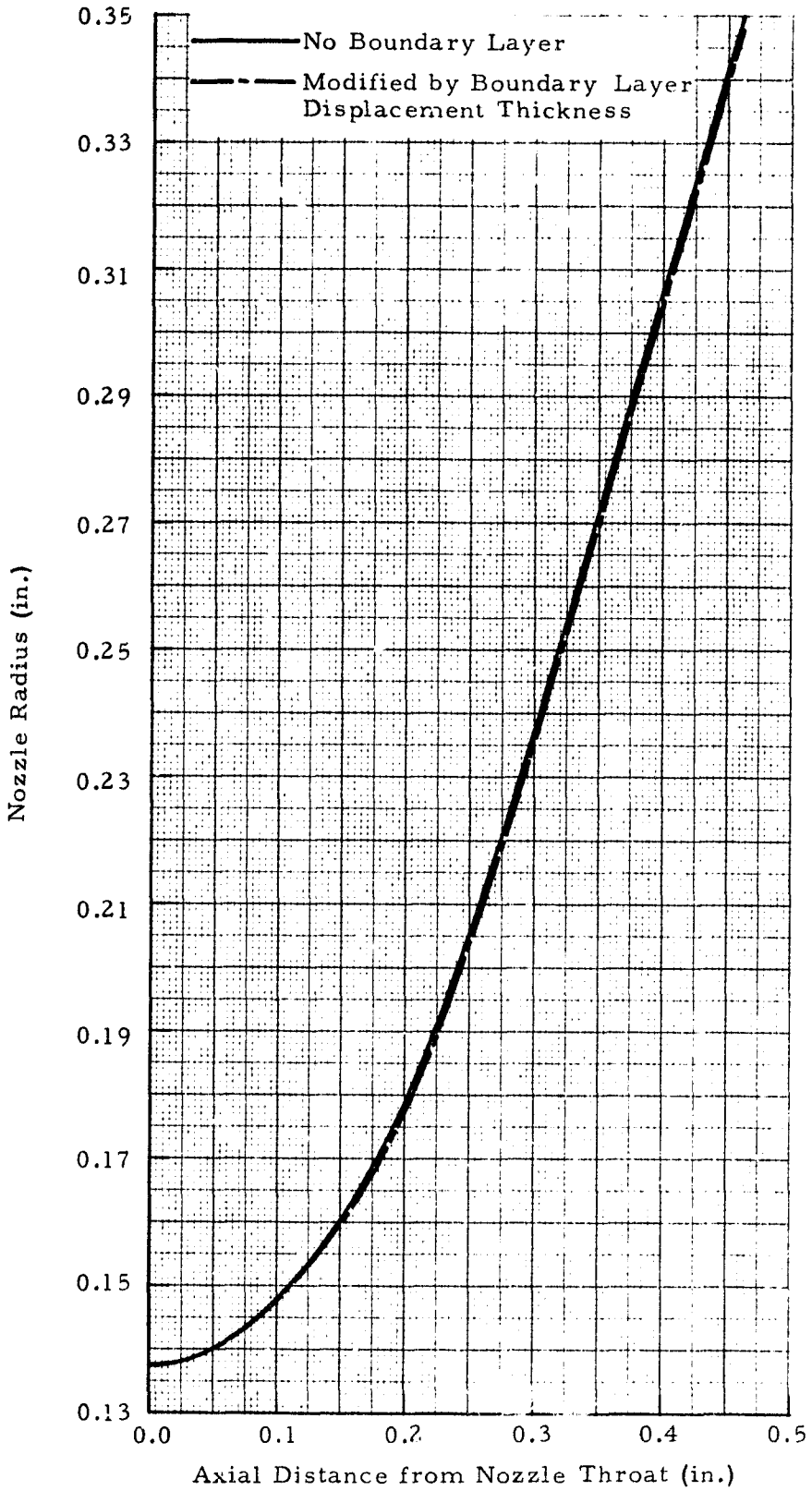

Fig. 39 - Nozzle Radius as a Function of Axial Distance from the Nozzle Throat of Nozzle 4 Test Number TWT 575

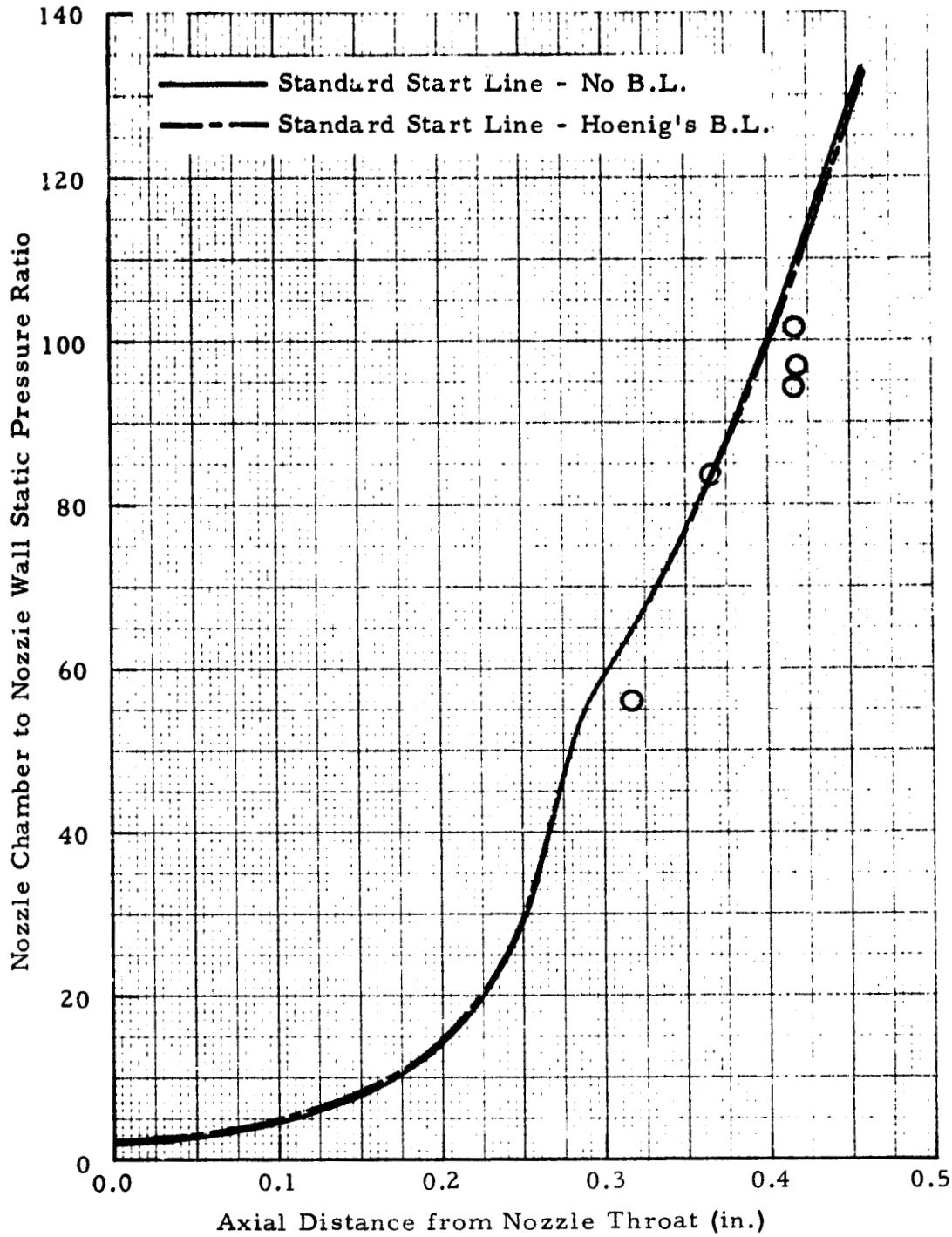

Fig. 40 - Non-Dimensional Nozzle Wall Static Pressure Distributions for Test Number TWT 575 and Nozzle 4 Flowing Air at Test Point 114

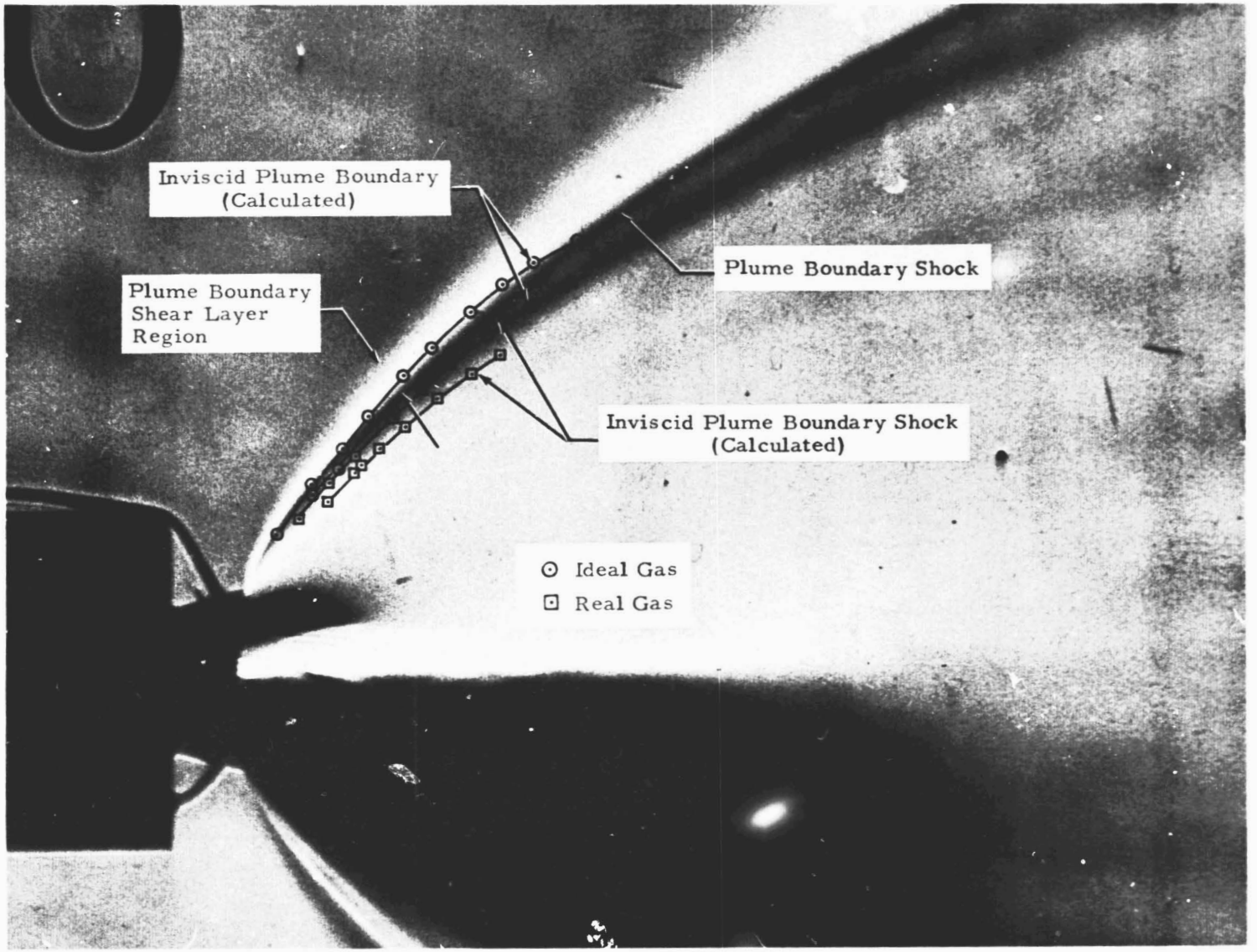

Fig. 41 - Comparison of Experimental and Analytical Exhaust Plume Boundary and Boundary Shock Locations for Test Number TWT 575, Nozzle 1 and Test Point 511

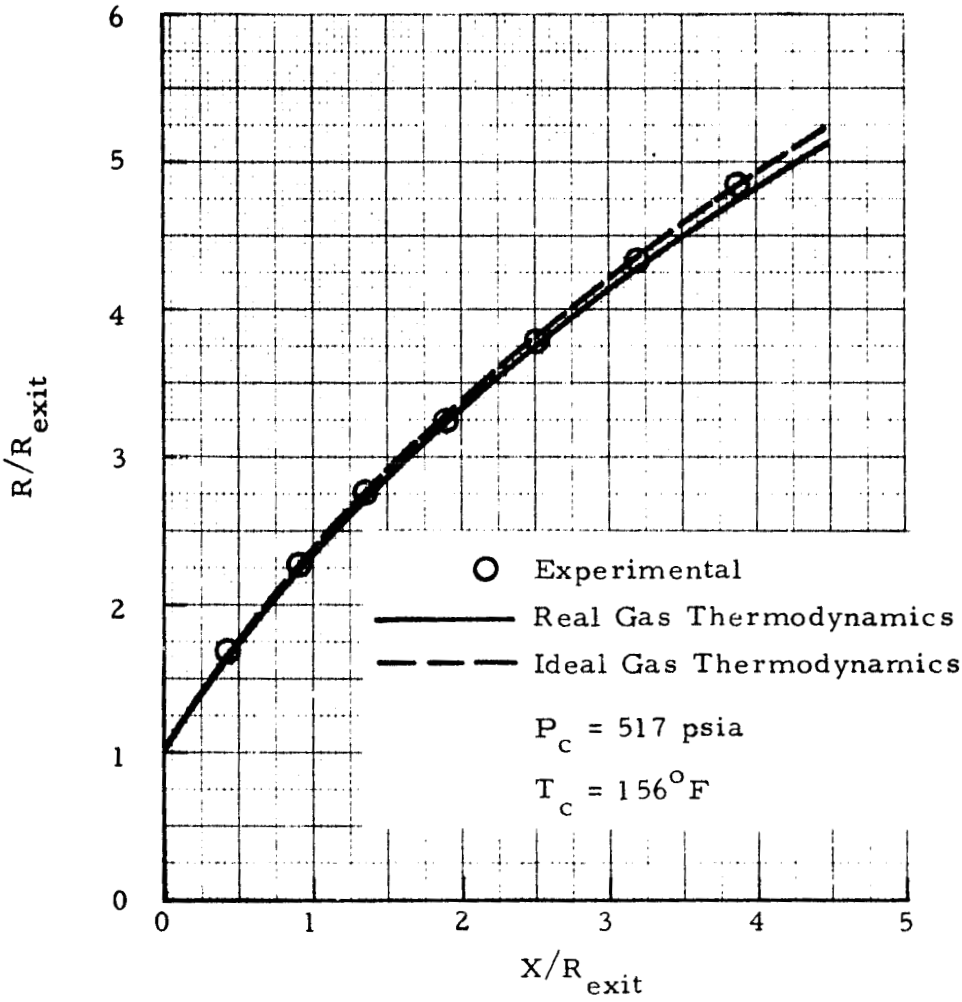

Fig. 42 - Comparison of Experimental and Analytical Exhaust Plume Boundaries for Test Number TWT 575, Nozzle 2 and Test Point 382

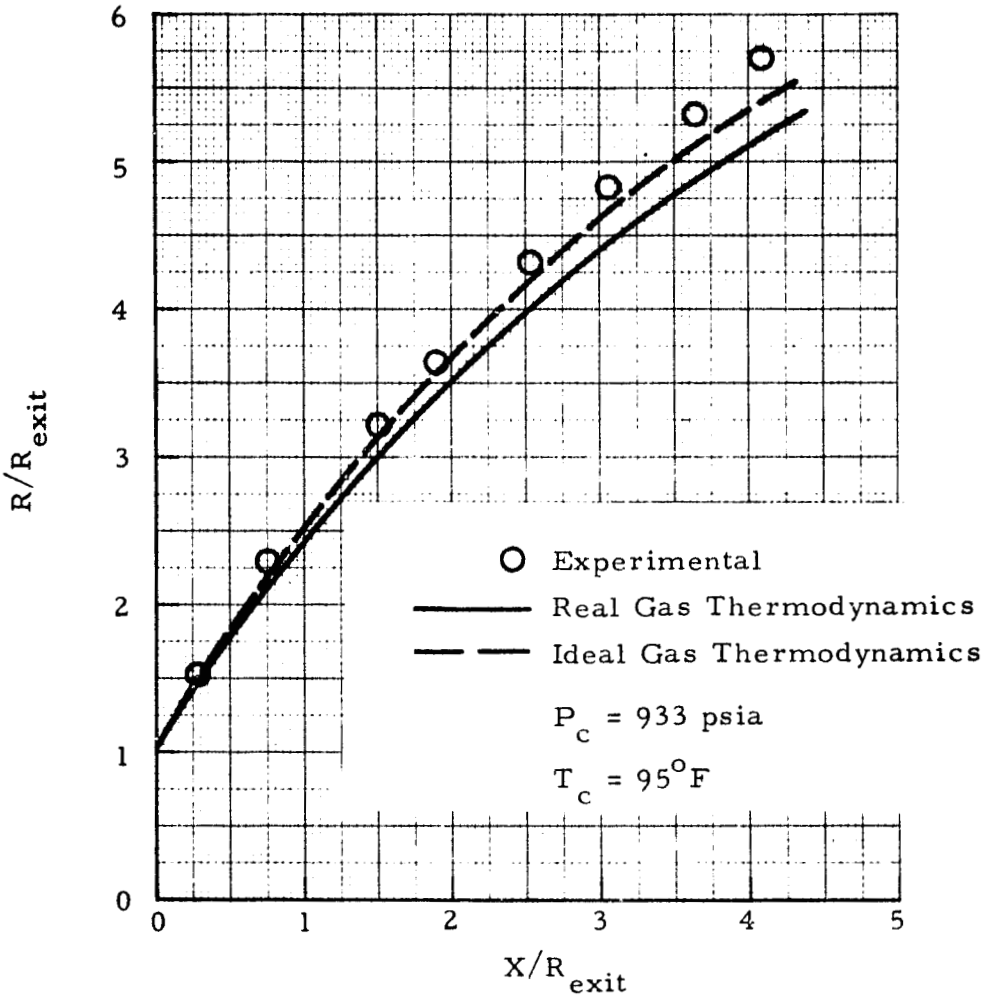

Fig. 43 - Comparison of Experimental and Analytical Exhaust Plume Boundaries for Test Number TWT 575, Nozzle 2 and Test Point 383

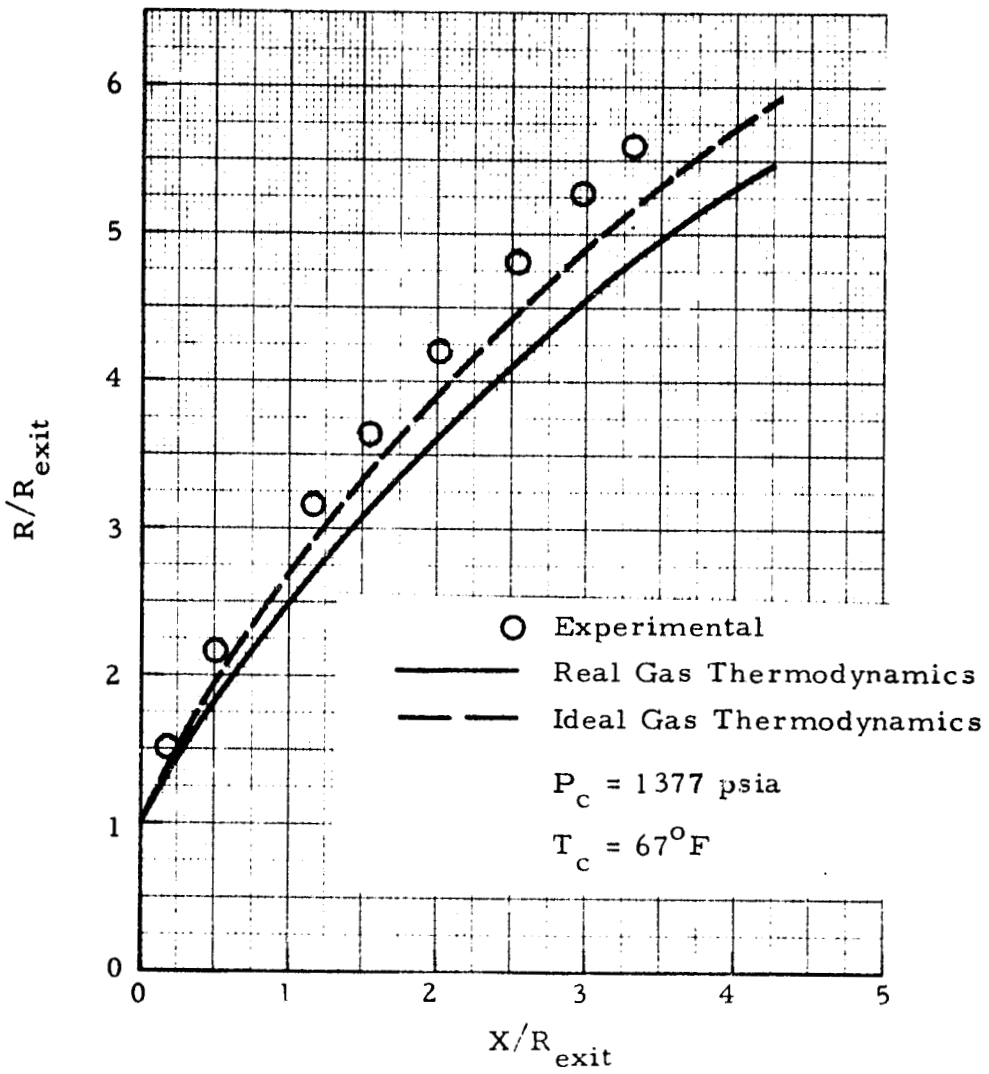

Fig. 44 - Comparison of Experimental and Analytical Exhaust Plume Boundaries for Test Number TWT 575, Nozzle 2 and Test Point 384

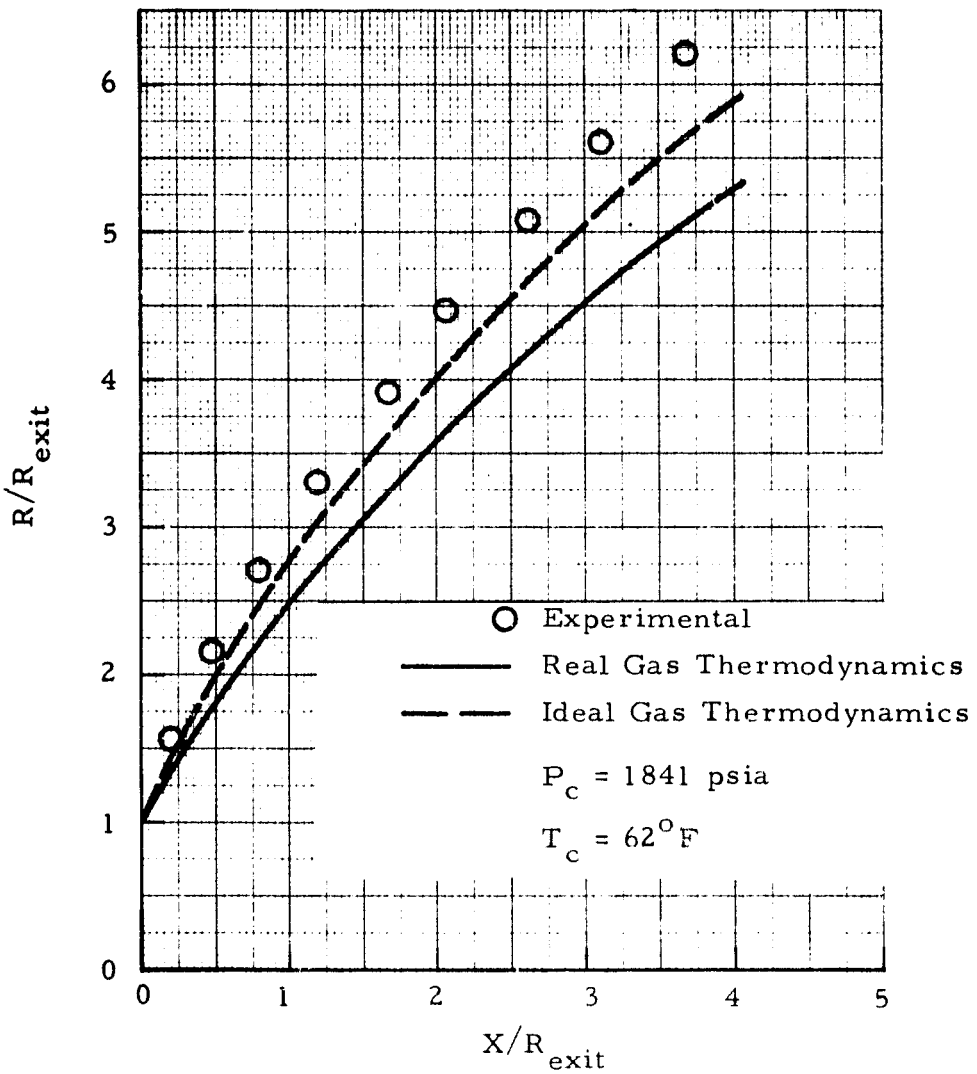

Fig. 45 - Comparison of Experimental and Analytical Exhaust Plume Boundaries for Test Number TWT 575, Nozzle 2 and Test Point 385

Fig. 46 - Comparison of Experimental Exhaust Plume Boundary and Boundary Shock Locations with Analytical Calculation using Real Gas Thermodynamics for Test Number TWT 575, Nozzle 2 and Test Point 382

Fig. 47 - Comparison of Experimental Exhaust Plume Boundary and Boundary Shock Locations with Analytical Calculation Using Real Gas Thermodynamics for Test Number TWT 575, Nozzle 2 and Test Point 383

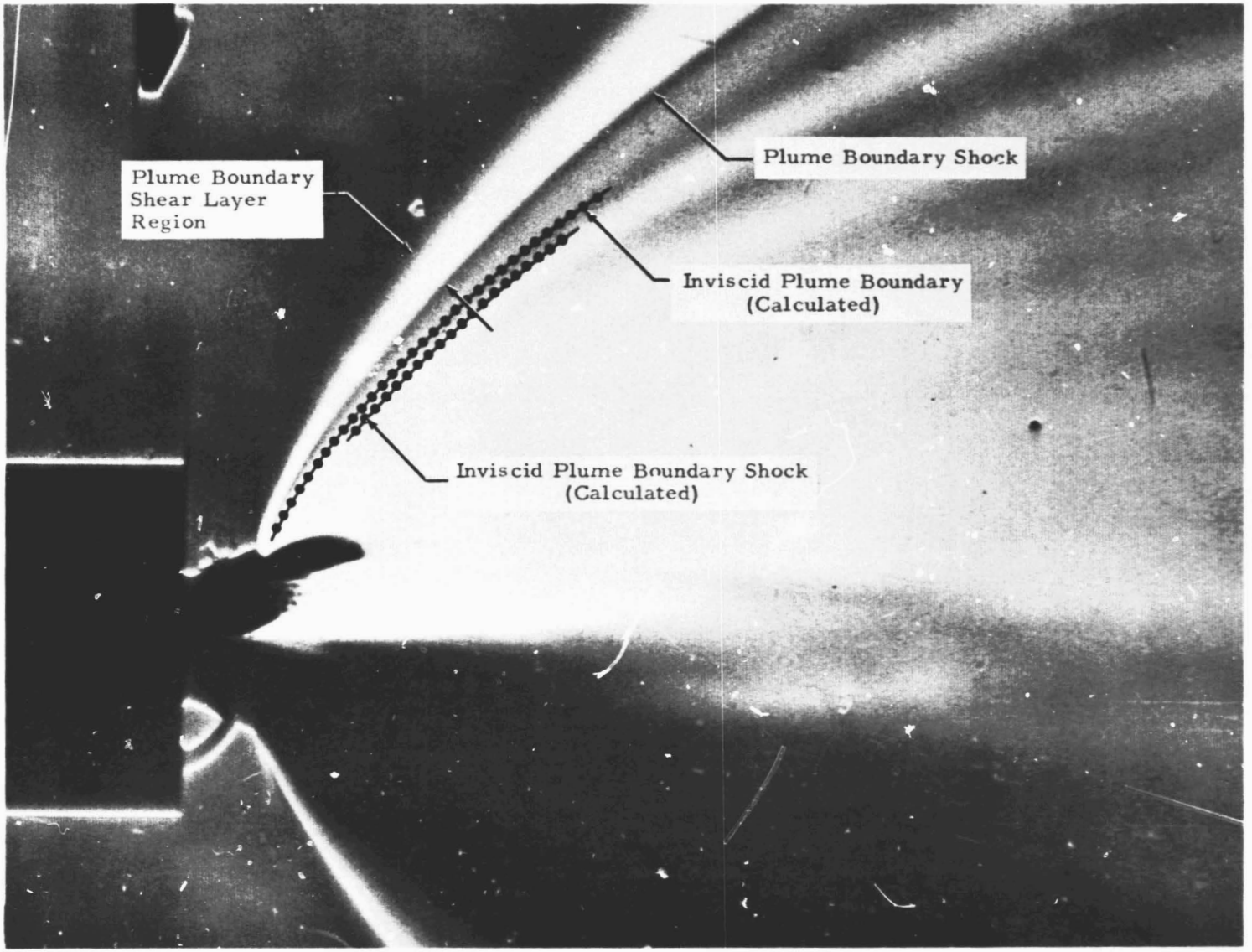

Fig. 48 - Comparison of Experimental Exhaust Plume Boundary and Boundary Shock Locations with Analytical Calculation using Real Gas Thermodynamics for Test Number TWT 575, Nozzle 2 and Test Point 384

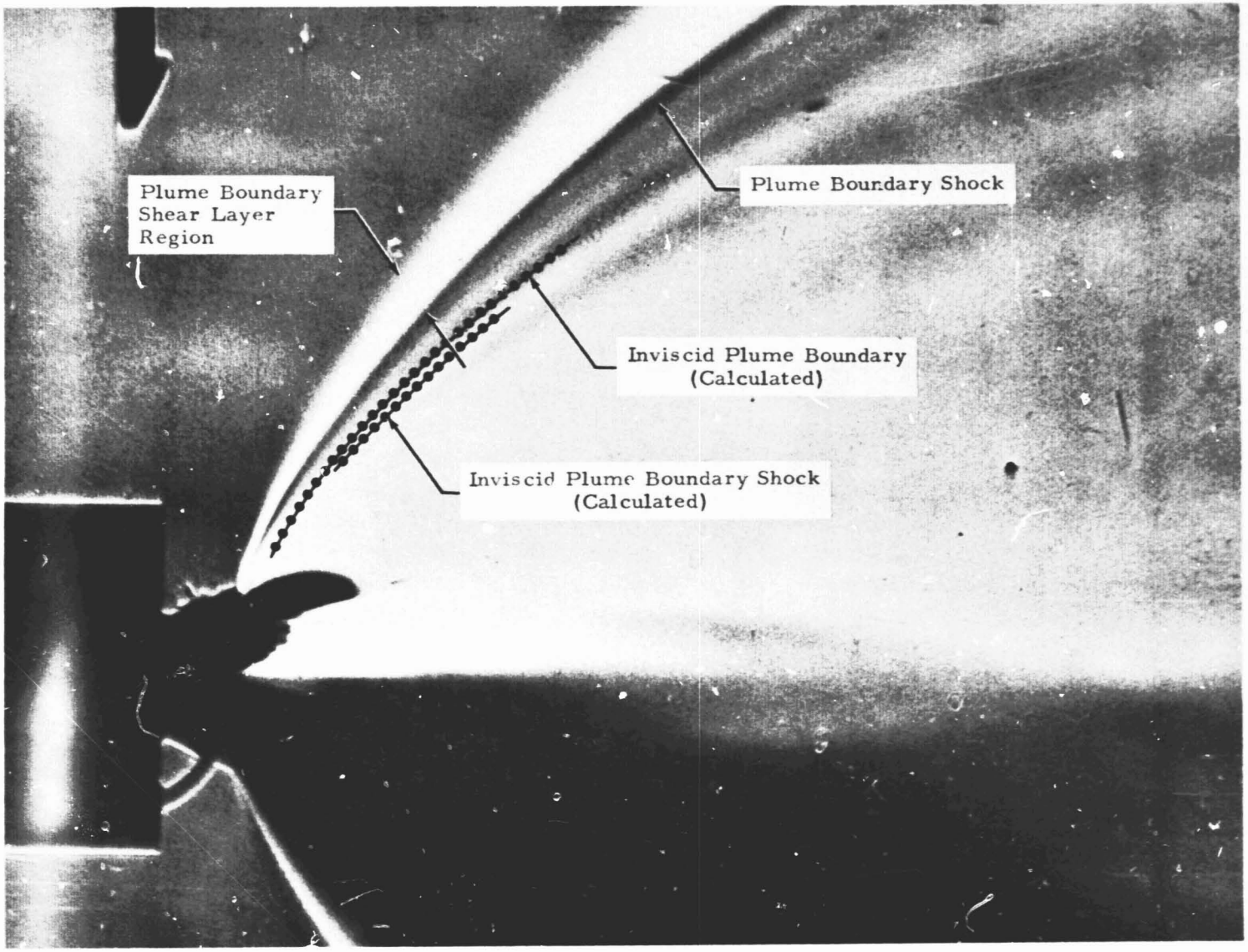

Fig. 49 - Comparison of Experimental Exhaust Plume Boundary and Boundary Shock Locations with Analytical Calculation using Thermodynamics for Test Number TWT 575, Nozzle 2 and Test Point 385

APPENDIX

METHOD FOR DETERMINING THE ABSOLUTE UNCERTAINTY OF A COMPUTED VALUE THAT IS A FUNCTION OF TWO MEASURED VALUES

Appendix

To determine the absolute uncertainty of a computed value that is a function of two measured values, the following procedure is followed.

Let z = the computed value

and $z = f(x,y)$ where x and y are the measured values.

$$dz = \frac{\partial f}{\partial x}\, dx + \frac{\partial f}{\partial y}\, dy$$

for our case $z = \frac{x}{y}$

$$\frac{\partial f}{\partial x} = \frac{1}{y} \; ; \; \frac{\partial f}{\partial y} = \frac{-x}{y^2}$$

$$\therefore\ dz = \frac{1}{y}\, dx - \frac{x}{y^2}\, dy$$

or $$\delta z = \frac{1}{y}\, \delta x - \frac{x}{y^2}\, \delta y \quad \Big\} \text{ absolute uncertainty}$$

the values of x and y are the measured values.

The maximum value of δz is obtained by using the negative value of δy.

Example calculation for our work

TWT 575 Nozzle 1 Pt 505

Let: $x = Pc$; $y = Pw$

$\delta x = 18.75$ $\delta y = 3.75)_{\text{tap } 44}$

$$\delta z)_{44} = \left[\frac{1}{236.68}\right] 18.75 + \left[\frac{1938}{236.68^2}\right] 3.75$$